RAPHAEL APARECIDO SANCHES NASCIMENTO

Quantificação de glicose intra e extra-celular por meio de biossensores micro e nanoestruturados

(Intra and extra-cellular glucose quantification by micro-nano-structured biosensors)

Tese apresentada ao Departamento de Física da Faculdade de Filosofia Ciências e Letras da Universidade de São Paulo para obtenção do título de Doutor em Ciências

Área de Concentração: Física da Matéria Concentrada

Orientador: Prof. Dr. Marcelo Mulato

Ribeirão Preto

2015

Catalogação da Publicação

Faculdade de Filosofia Ciências e Letras da Universidade de São Paulo

Nascimento, Raphael Aparecido Sanches.

Quantificação de glicose intra e extra-celular por meio de biossensores micro e nanoestruturados / Raphael Aparecido Sanches Nascimento; orientador Marcelo Mulato – São Paulo, 2015

p. 94;

1. Biossensor; 2. FTO; 3. EGFET; 4. Nanopipetas; 5. Glicose Oxidase; 6. Quitosana; 7. Glutaraldeído.

I. Biosensor; II. FTO; III. EGFET; IV. Nanopipettes; V. Glucose Oxidase; VI. Chitosan; VII. Glutaraldehyde

Nascimento, R. A. S. **Quantificação de glicose intra e extra-celular por meio de biossensores micro e nanoestruturados** *(Intra and extra-cellular glucose quantification by micro-nano-structured biosensors)*. Tese apresentada à Faculdade de Filosofia Ciências e Letras da Universidade de São Paulo para obtenção do título de Doutor em Ciências.

Aprovado em: _____

Banca Examinadora

Prof. Dr. _____ Instituição:_____

Julgamento:_____ Assinatura:_____

Prof. Dr. _____ Instituição:_____

Julgamento:_____ Assinatura:_____

Prof. Dr. _____ Instituição:_____

Julgamento:_____ Assinatura:_____

Prof. Dr. _____ Instituição:_____

Julgamento:_____ Assinatura:_____

Prof. Dr. _____ Instituição:_____

Julgamento:_____ Assinatura:_____

À minha família, com muita honra, dedico esse trabalho.

To my family, with honor, I dedicate this work.

Acknowledge

I will start thanking CAPES and CNPq Brazilian agencies for financial support all over my Ph.D.

Furthermore, I would like to thank very much all the friends and colleagues from both laboratories: here in Brazil and there in United States: Dr. Nilou, Dr. Wendy, Akshar, Parissa, Rahul, Assis, Dr. Boaz Vilozny, Michelle, Ace, Alex, John, Wai, Guilherme, Dr. Julio Ugucioni, Tobias, Jessica, Hugo, Marina, Amanda and Natália. I've learned a lot with these people and laughed a lot too.

I could not forget my two mentors on this journey: Prof. Dr. Marcelo Mulato and Prof. Dr. Nader Pourmand. To both of you, I simply cannot be grateful enough. Please, be aware of all of my respect and thankfulness to both of you.

And, of course, I must thank the most important part of my life as a human being, my family: Ofélia, Gabriel, Camila, Regina, Marcos, Lucas and Carolina. Without them I would just be a nobody, nothing.

Resumo

Segundo dados da Organização Mundial de Saúde, até o ano de 2030 a diabetes será a sétima enfermidade causadora de morte no mundo. A diabetes se caracteriza pela variação do nível de glicose no sangue dada ingestão de alimentos ou realização de certas tarefas. Além disso, já é sabido pela comunidade científica atual que células cancerígenas possuem metabolismo diferente quando comparadas a células normais, consumindo uma maior quantidade de açúcar devido a essa anormalidade.

No presente trabalho serão apresentados, basicamente, dois tipos de biossensores que possuem grande potencial para tornarem-se monitores contínuos de glicose. Ambos os biossensores utilizam a enzima glicose oxidase como catalisador específico da reação de oxidação do carboidrato.

O primeiro apresenta estrutura em escala micrométrica, tem por objetivo a quantificação de glicose em solução em ambiente extracelular e se baseia no sistema EGFET (Extended Gate Field Effect Transistor) com substrato de *Fluorine Tin Oxide* (FTO). Além do mais, foram utilizados dois protocolos de imobilização da glicose oxidase: quitosana (com uma janela de detecção de 1 a 5mM de glicose) e glutaraldeído (com janela de detecção de 0 a 15 mM de glicose).

O segundo apresenta estrutura em escala nanométrica, tem por objetivo a quantificação de glicose em ambiente intracelular e baseia-se no sistema de nanopipetas de quartzo. Com esse dispositivo foi possível estipular a concentração de glicose livre dentro de três linhas de células distintas: Fibroblastos humanos entre 0 e 2.8mM; MCF-7 maior que 4.7 mM; MDA-MB-231entre 3.6 e 4.5 mM.

Abstract

According to the World Health Organization, until 2030 diabetes will be the 7th cause of death worldwide. This disease is characterized by variation on blood glucose levels due to ingestion of specific food and tasks performing. Moreover, it is already known that cancer cells have a different metabolism when compared to normal cells and these abnormal cells have a higher sugar intake due to this abnormality.

This work will present, basically, two types of biosensors with great potential to become continuous glucose monitors. Both biosensors use the enzyme glucose oxidase as carbohydrate oxidation catalyzer.

The first one presents a micro-metric structure and its goal is to quantify glucose concentration in an extracellular solution. This device is based in EGFET (Extended Gate Field Effect Transistor) system and uses FTO as substrate. Furthermore, two immobilization protocols were used to fix the enzyme to the FTO: chitosan (with final range of 1~5mM of glucose) and glutaraldehyde (with final range of 0~15mM of glucose).

The second is a nano-structured biosensor based on nanopipette system and its goal is to quantify intracellular glucose concentration. With this device was possible to stipulate free glucose molecules inside different cell lines: between 0 and 2.8mM for human Fibroblasts; greater than 4.7 mM for MCF-7; and between 3.6 and 4.5 mM for MDA-MB-231.

FIGURE'S LIST

Abbreviations' list

$\vec{a}$	Area Vector
a_i	ion activity
ATP	adenosine triphosphate
Ca	Calcium
$CaCl_2$	Calcium Chloride
C_{dif}	differential capacitance
CO_2	Carbonic Dioxide
C_{ox}	capacitance of the gate oxide
E	electrochemical potential
$\vec{E}$	Electric Field Vector
e_0	elementary charge value
E_C	conduction band energy
E_F	Fermi level
E_{Fm}	metal Fermi level
E_{Fs}	semiconductor Fermi level
E_g	bandgap
EGFET	Extended Gate Field Effect Transistor
E_i	intrinsic semiconductor Fermi level
E_{ref}	reference electrode potential
E_V	valence band energy
F	Faraday Constant
FET	Field Effect Transistor
FTO	Fluorine Tin Oxide
GaN	gallium nitride
GCS	Gouy-Chapman-Stern model
GOx	Glucose Oxidase
GTA	Glutaraldehyde
H^+	Hydrogen ions
I_{DS}	current between the drain and source
IHP	*inner Helmholtz plane*
ISFET	**I**on **S**ensitive **F**ield **E**ffect **T**ransistor
k	Boltzmann constant
KCl	Potassium Chloride
L	length of the gate

MOS	Metal Oxide Semiconductor
MOSFET	**M**etal **O**xide **S**emiconductor **F**ield **E**ffect **T**ransisto
n	number of electrons transferred
n'^{0}	density of electrons
n^{0}	ion concentration at the bulk
O_2	Oxygen Gas
OFET	Organic Field Effect Transistor
OH^-	hydroxyl molecules
OHP	*outer Helmholtz plane*
p^{0}	density of holes
PBA	Phenylboronic acid
pH_B	Bulk pH
Q_B	interface states and the depletion charge respectively
$q\chi$	the electron affinity
$q\phi_m$	metal work function
$q\phi_s$	semiconductor work function
Q_{in}	total charge enclosed by the Gauss surface
Q_{ox}	charges located in the oxide
Q_{sc}	total space charge
Q_{ss}	charges located in surface states
R	gas constant
SnO_2	Tin Dioxide
T	temperature
TiO_2	Titanium Dioxide
V	voltage drop
V_{DS}	drain-source voltage
V_{GS}	Gate-source voltage
V_{ion}	Potential due to surface adsorbed ions
V_{Ref}	Reference Voltage
W	width of the gate
WHO	World Heal Organization
z	charge of the ion
ZnO	Zinc Oxide
$\beta_{\iota\nu\tau}$	intrinsic buffer capacity
$\chi^{\sigma o\lambda}$	surface dipole potential of the solution
ε	dielectric constant of the medium
ε_0	permittivity of free space

ϕ_ϕ	potential difference between the Fermi levels of doped and intrinsic silicon
ϕ^M	electrical potential at the surface of the electrode
ϕ^Σ	electrical potential at the electrolyte solution
ϕ_σ	potential at the surface of the semiconductor
$\Phi_{\Sigma\iota}$	silicon electron work function
κ	parameter responsible to characterize the potential due to holes or electrons inside the semiconductor
μ	average electron mobility in the channel
ρ	charge per unit of volume
σ^δ	charge density within diffuse layer
σ^ι	charge density from specifically adsorbed ions
σ^M	charge density in the surface of the sample
σ^Σ	charge density
ψ_0	electrostatic potential
ψ_B	potential difference between E_{Fs} and E_i

Summary

Chapter 1 -

General Introduction

Over the years, humanity has been seen huge changes the way medicine can diagnose and treat diseases. Faster diagnoses, smaller samples required, improved drug delivery etc… all those components are immediately or indirectly associated with size of new tools, fabrics and technical progress in vast research areas.

Thereby, the micro/nanotechnology age came pushed by this new trend. Devices had measurement power increased and became smaller in pretty much all areas. It is possible to see a true revolution towards miniaturization. Nowadays, big part of the technology applied to development in material science, works to bring up new materials or devices in micro-nanoscale or materials that have, at least, the potential to become miniaturized in near future. This technology is used with quite success in sensing area.

On health field the importance to make devices and sensors smaller consists in make less invasive procedures and taking very small and sufficient sample amounts. Moreover, it is possible to aim new horizons for the future: stop looking to organs or tissues and start to think about treating cells!

A key strategy in the health field is to discover and treat, as early as possible, any disease. This is especially true for very dangerous issues as degenerative or chronic disease and cancers.

There is an important molecule, normally ingested by humans, who can cause any of those three health issues: glucose. [1–5] Even though degenerative diseases and cancer are normally more worrying problems than the chronic disease linked to glucose (diabetes), this last one is the problem that calls more attention even from the World Heal Organization (WHO) when the subject is glucose.

Furthermore, the WHO concern is important and supported by statistical analysis of health documentation around the world. According to the WHO:

> *"Raised blood glucose was estimated to result in 3.4 million deaths in 2004, equivalent to 5.8% of all deaths. Impaired glucose tolerance and impaired fasting glycaemia are risk categories for future development of diabetes and cardiovascular disease. In some age groups, people with diabetes have a twofold increase in the risk of stroke. Diabetes is the leading cause of renal failure in many*

populations in both developed and developing countries. Lower limb amputations are at least 10 times more common in people with diabetes than in non-diabetic individuals in developed countries; more than half of all non-traumatic lower limb amputations are due to diabetes. Diabetes is one of the leading causes of visual impairment and blindness in developed countries. People with diabetes require at least 2-3 times the health care resources compared to people who do not have diabetes, and diabetes care may account for up to 15% of national healthcare budgets."[6]

When the WHO talks more specifically about diabetes, the picture is equally shocking:

"* *In 2014 the global prevalence of diabetes was estimated to be 9% among adults aged 18+ years.*
* *In 2012, an estimated 1.5 million deaths were directly caused by diabetes.*
* *More than 80% of diabetes deaths occur in low- and middle-income countries.*
* *WHO projects that diabetes will be the 7th leading cause of death in 2030.*"[7]

Diabetes is a health disease where people have problems in producing insulin or because the insulin produced is not able to act properly. Anyway, the glucose level for people with diabetes varies a lot during a normal day. Even in a few minutes, depending on the circumstances, glucose level can vary from very low to very high.

It would be of great interest to create a sensor to monitor glucose levels during a whole day or for several hours without changing it (continuous mode). Moreover, it should be part of a mobile system, improving the potential of point-of-care glucose monitoring.

With such a sensor it is possible to think ahead and picture an artificial pancreas capable of release insulin in the body as response to glucose level variation, just like a natural one.

Another interesting analysis of glucose molecule is about its cellular uptake. It is known that glucose uptake is quite different between normal and cancer cells. [8–11] There are even drugs/contrasts that use this characteristic as an advantage to drug intake by the cancer cell: they label the drug with a glucose molecule and it is

going to be preferentially uptake by the cancer cell once it naturally take more sugar than normal cells.

Regarding the sensor used to detect a biological signal, it is strategically named *biosensor*. Basically a biosensor is composed by coupling two parts: i) An immobilization matrix and ii) a transducer (see Figure 1).

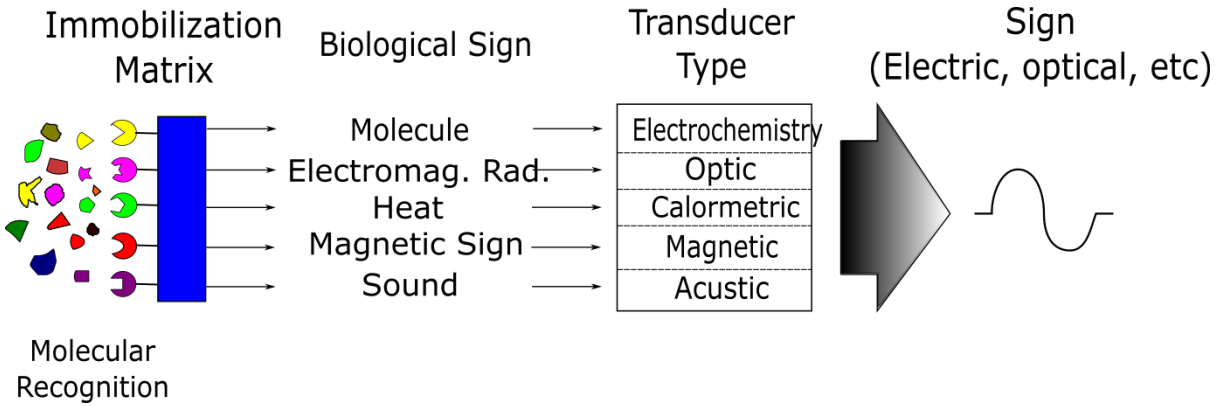

Figure 1 - Schematic biosensor's components.

The immobilization matrix is responsible to recognize the biological signal desired. According to the biological signal type, different physical transducers might be needed. The transducer will be responsible to change the biological signal to an electrical signal proportional to biological one. This electrical signal can then be processed, read, recorded, etc.

Glucose biosensors are already a reality nowadays. One can buy it even on neighbor pharmacies around the world. It is a necessary tool for people with diabetes. Unfortunately, the worldwide commercial available biosensors of this kind are not able to continuously monitor.

In this work, it is going to be presented two different ways to perform glucose sensing: intra and extra-cellular. Nevertheless, both sensors are based in the detection of a final product of glucose oxidation: the gluconic acid – even more specific, the proton ions released by gluconic acid. Hence, both types of biosensors are a Second-generation type of glucose biosensor. [12]

The first one is based on a thin film of Fluorine Tin Oxide (FTO) with characteristics of the micro-structured device to perform extracellular measurements. It is a highly specific glucose biosensor once its reaction is catalyzed by an enzyme named Glucose Oxidase and intended to become an alternative to continuously monitor glucose levels in solutions.

The second biosensor is as highly specific as the first one once it uses the same glucose reaction and Glucose Oxidase enzyme. This is a nano-structured device based on a nanopipette platform intended to perform intracellular measurements This type of measurement can help understand better cell physiology and differences between different cell types.

Chapter 2 –

Glucose sensing: extra-cellular measurement

2.1 Introduction

All the Physical Science research needs, somehow, to use sensors of any kind to acquire a signal. Sensors for a huge variety are used for this task.

A quite interesting and important development in this field was reached with the appearance of ISFET technology (that comes directly from **I**on **S**ensitive **F**ield **E**ffect **T**ransistor), introduced by Piet Bergveld in 1970. [13] ISFET is a solid state device which uses the gate of a field effect transistor as a sensitive membrane to detect ions. These devices were widely used through years to detect, for example, heavy metal ions [14], pH sensor [15] and bio-molecular sensor [16]. Unfortunately, the ISFET technology requires the production of the entire electronic component [17], and that is exactly the biggest disadvantage of this device.

Overcoming this main disadvantage, another device which can be considered an evolution of an ISFET, is the **E**xtended **G**ate **F**ield **E**ffect **T**ransistor (EGFET). This new device was first proposed by J. van der Spiegel in 1983. [18] It is basically composed by a Field Effect Transistor with the sensitive part separated and coupled through a wire that is further attached to the transistor's gate. [18]

Among the advantages of using EGFET technology instead of ISFET is possible to highlight: i) the field effect electronic part of this device does not enter in contact with the bulk solution to be probed, what means the electronic part is completely chemically sealed; [18] ii) the sensitive part can assume almost any shape; [18,19] iii) it is simpler to produce. [19]

An EGFET device couples a very high impedance active electronic device to a sensing structure. For this mean, it is advantageous to use a MOSFET (**M**etal **O**xide **S**emiconductor **F**ield **E**ffect **T**ransistor) as active electronic device. A MOSFET has a high entrance impedance due to its insulated gate. This allows the current flowing between drain and source of this component to be changed by a very small potential signal applied to its gate terminal.

The physical principle involved on EGFET sensing is essentially potentiometric. The surface of sensing structure suffers a potentiometric change. The potential is directly driven to the MOSFET's gate through the extended gate wire and this potential controls the current flowing between Drain and Source terminals of the MOSFET. So, there is a direct correspondence between potential applied to sensing structure and current read on the drain.

2.1.1 EGFET fabrication

To build an EGFET is necessary to link a sensible structure and an electronic component with high entrance impedance. EGFET is fabricated extending the distance between a sensing structure and the active electronics in a way that the last one doesn't get in contact with probed chemical solution.

There are few ways to perform this task. Figure 2 (a) shows the simplest way to build an EGFET device. On this figure is possible to see the MOSFET package at right. In this case it represents a commercial MOSFET. [19–28] At the same figure, it is possible to see a dashed line linking the gate terminal of a commercial MOSFET and the sensing structure already inside a beaker. This dashed line represents the wire that extends the MOSFET's gate.

Another electronic component capable to provide high input impedance to the device is an instrumental amplifier. [15,29–35] The schematic for use of such component is shown in Figure 2 (b). With an instrumental amplifier the response acquired is Voltage *vs.* Time. An alternative to instrumental amplifier is the operational amplifier. [19,36–39] The schematic to use this last component is slightly different than for the instrumental amplifier as shown in Figure 2 (c). Both amplifiers are normally set as a unitary gain buffer. The reason by which one of these components is chosen instead of a MOSFET is because the amplifier is capable to reduce hysteretic effect, a very common phenomenon to EGFET and ISFET sensors.

[40,41] As already alerted by Van der Spiegel, amplifier can reduce effects of input leakage and capacitance. [18]

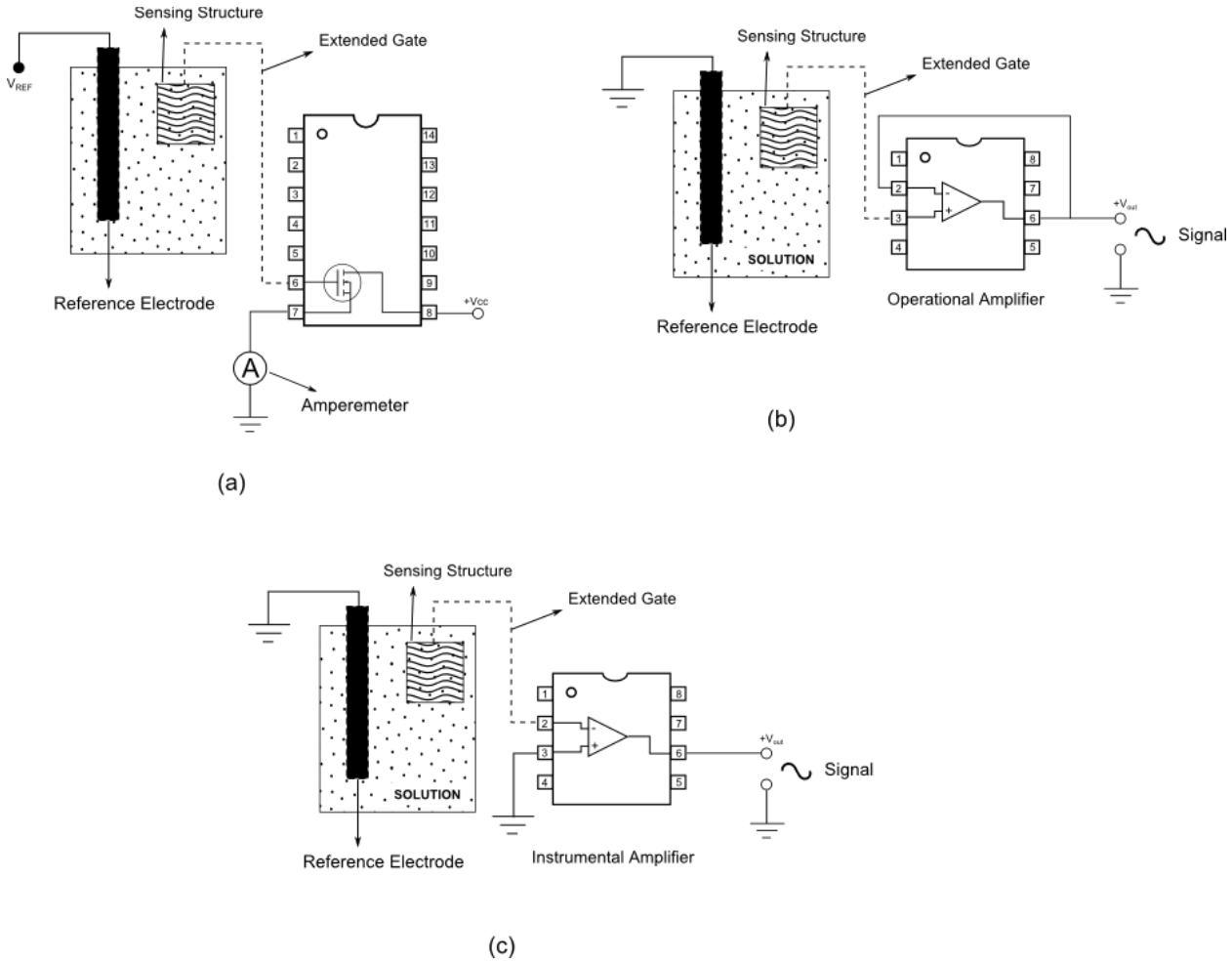

Figure 2 – EGFET Schematic. This is the simplest schematic to build an EGFET. It shows the MOSFET package on the right. By the left it is possible to visualize a beaker with a reference electrode and a sensing structure immersed in it. The dashed line coupled to the MOSFET gate represents a wire extending this component terminal. a) Classical EGFET schematic build with a MOSFET; b) Alternative EGFET schematic build with as Operational Amplifier; c) Alternative EGFET schematic build with an Instrumental Amplifier.

EGFET also can be entirely fabricated, including the MOSFET. There are a quite big number of authors that had fabricated even the field effect transistor from scratch. [18,42–66] It is a more complicated process that requires more steps to be accomplished too. Besides, this process requires more equipment and knowledge from researchers.

2.1.2 EGFET Physical Process

The fundamental process of an EGFET consists of modifying electrostatic potential at a sensitive membrane. To accomplish it is necessary a high input component that is able to "sense" low input voltages.

A MOSFET is an electronic component that can control an electronic channel width inside a semiconductor material by changing the electric field on which the electronic channel is immersed. The high input impedance of this component is provided by the oxide (insulator) between its semiconductor body (where electronic channel will be formed) and the metal gate (Figure 3).

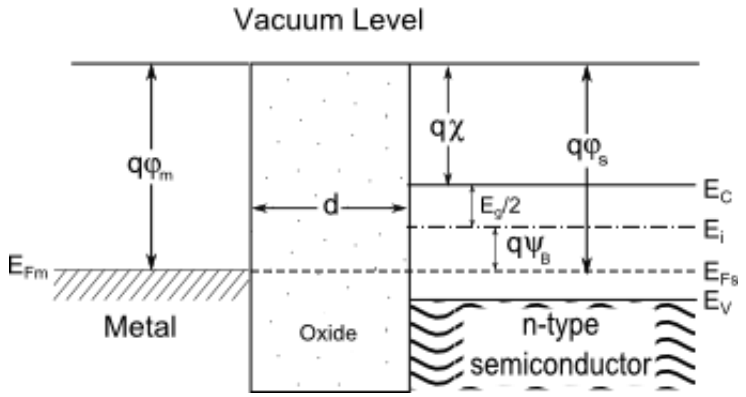

Figure 3 – Metal Oxide Semiconductor device type n. In this figure there is no bias applied to the device. In this figure: q (φ_m is the metal work function; q (φ_s is the semiconductor work function; q (χ is the electron affinity; E_C is the conduction band energy; EV is the valence band energy; E_{Fm} is the metal Fermi level; E_g is the bandgap; ψ_B is the potential difference between the semiconductor Fermi level E_{Fs} and the intrinsic Fermi level EI. [67]

Once the gate is insulated from the semiconductor's body, there is no current flowing through the gate. So, it is necessary just a sign of voltage, an electrostatic voltage, applied to the gate to control the current flowing through the semiconductor's body (between drain and source).

The physical fundament involved on current control is shown in Figure 4. At this figure is possible to see three different components that constitute the gate input of a MOSFET: a metal, an oxide (insulator) and a semiconductor body type n.

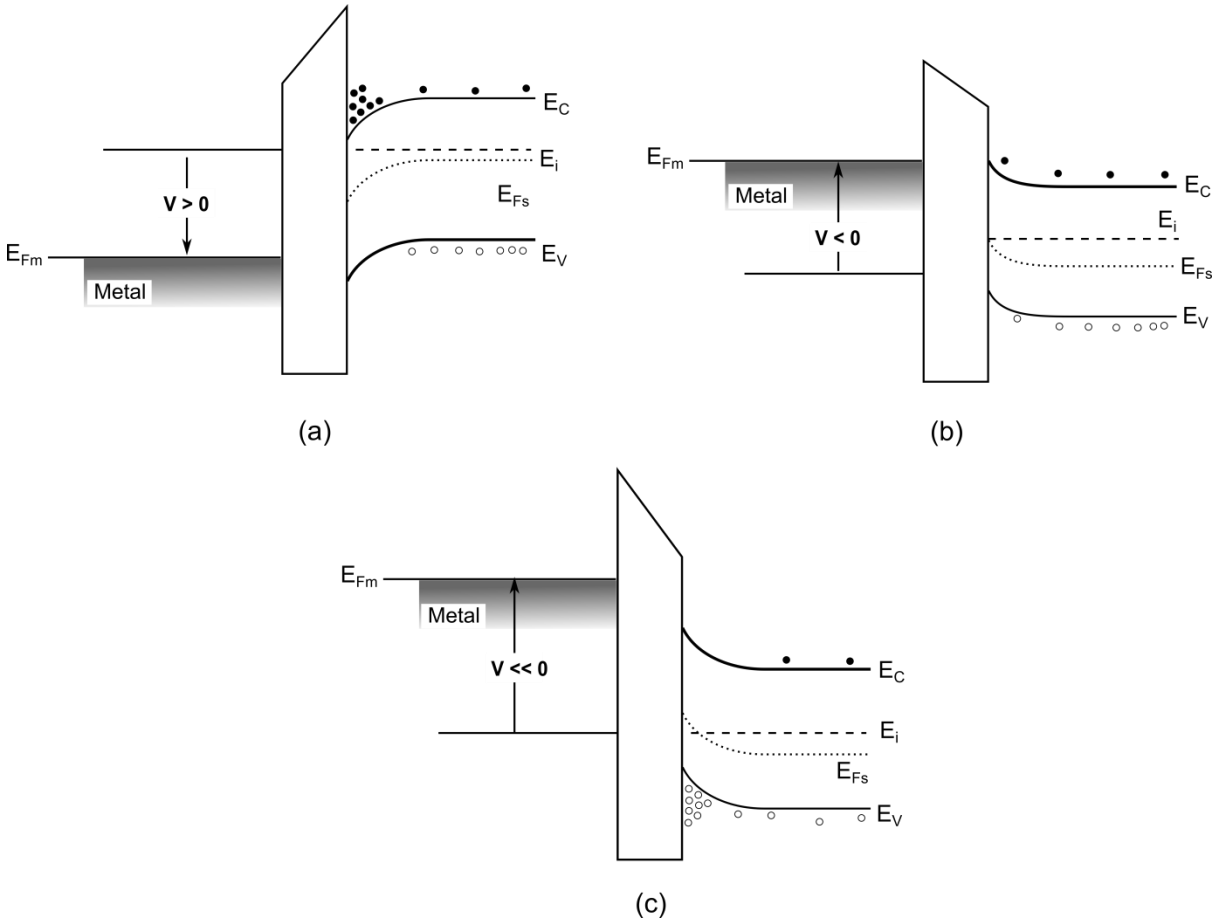

Figure 4 – Metal Oxide Semiconductor (MOS) type n band structures. In this figure is presented the three different possible diagrams according to the applied bias to a metal gate of a MOS device. a) Accumulation: a direct positive voltage is applied to the metal. At this case, the bands bend downward and electrons are accumulated in the semiconductor body nearby the oxide. If an electric field is applied to perpendicularly to this accumulation (between the drain and source of a MOSFET), a current can flow through this channel with a very low resistance. b) Depletion: a negative voltage is applied to the metal. In this case, the bands will bend slightly upwards, increasing the depletion layer on the semiconductor nearby the oxide. There is high impedance for the perpendicular channel (between drain and source). c) Inversion: if a high negative voltage is applied to the metal, this will make the bands to bend even more upward. Nearby oxide material, the semiconductor intrinsic Fermi level will cross over the Fermi level EF. The semiconductor on this region will perform like a semiconductor type p, with a high density of positive charge carriers. [67]

Basically, when a voltage is applied to the metal gate, three different cases can occur. Figure 4 shows those three cases for a semiconductor body type **n**. Figure 4 (a) demonstrated a negative bias (V<0) applied to metal gate. In this case the valence band bends downward, getting closer to the Fermi level of the semiconductor material type **n**. Conductance band and intrinsic Fermi level are downward bent as well at the same amount. Once no current flows through the oxide, the Fermi level does not bend. Then, the number of negative carriers accumulates near the oxide on the semiconductor side. This occurs thanks to the carrier density has a dependency on the difference between the Fermi level and the energy of valence layer (E_F-E_V).

If a small positive bias is applied to metal gate (V>0), the valence band is slightly bent upward relatively to the Fermi level. Conductance band and the intrinsic Fermi level are slightly upward bent too at the same amount. In this case, there is a more homogeneous distribution of negative and positive carriers on the whole semiconductor (see Figure 4 (b)).

If a high positive bias is applied to the metal gate (V>>0), the valence band, the conductance band and the intrinsic Fermi level are hardly bent upward relative to the Fermi level (see Figure 4 (c)). This hardness bending makes the Fermi level cross over the intrinsic Fermi level of the semiconductor. That means this region of the semiconductor, which is very close to the oxide material, will have characteristics of a semiconductor material type **p**. Thus, it is possible to see an accumulation of positive carriers at conductance band of **the n type semiconductor**, named as *inversion* cause.

2.1.3 EGFET: Electrochemical Process

All the electrochemical process by which an EGFET work can be explained based on a pH sensitive membrane. A different amount of different ions is adsorbed on membrane surface just exposing it to solutions with different pH values. Acid solutions have a great number of Hydrogen ions (H^+). When those ions are adsorbed

on the membrane surface, a positive bias is former in the membrane. Depending on ion concentration, a greater or smaller bias will be applied to the gate. Basically, the same idea explains how the electrochemistry works for alkaline solutions. Nevertheless, instead of applying a positive bias, the Hydroxyl group (OH^-) applies a negative bias. Once its concentration is increased, the bias voltage decreases (or, in other words, increases negatively).

Then, if those biases are applied to the gate of a MOSFET type **n on** a configuration like Figure 2 (a), the drain current flowing between drain and source can be modulated accordingly to the solution concentration and the voltage applied between drain and source (V_{DS}) as shown in Figure 5 (a).

If the reference voltage is kept constant and V_{DS} is varied, the current can be recorded as a function of pH too (see Figure 5 (b)). From the graphic of Figure 5 (b) is possible to extract the sensor sensibility, as shown in Figure 5(c). If the electronic component is an amplifier (instrumental or operational) the sensibility curve can be directly plotted from the measurements.

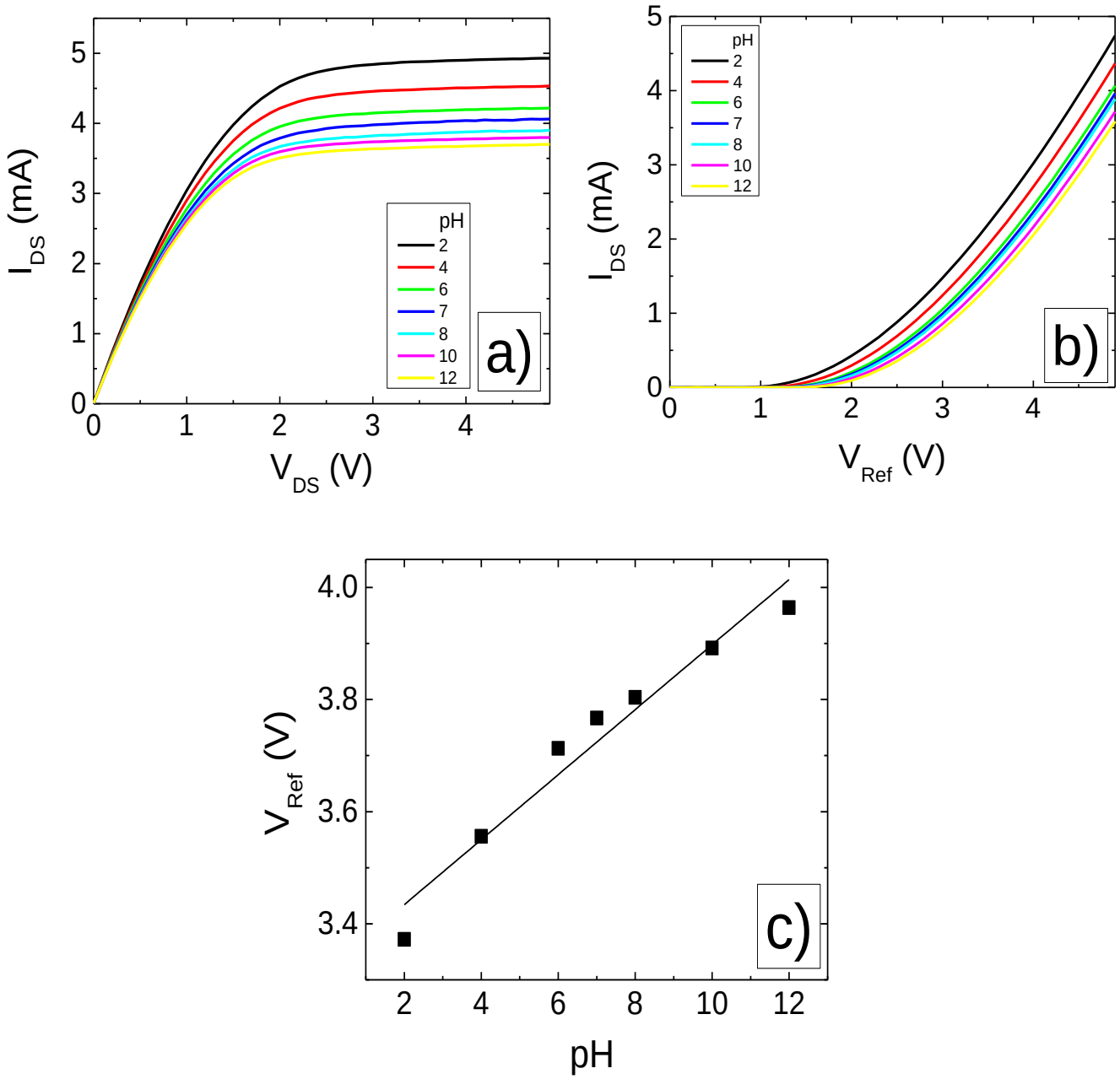

Figure 5 – a) Typical current dependence on the VDS voltage. In this case, V_{Ref} (Reference Voltage) was kept at a constant value of 5.0V. The lines above represent different pH values. At the saturation region is possible to distinguish all the pH values varying from 2 to 12 (top to bottom). b) Typical current dependence of the V_{Ref} voltage. In this case, VDS was kept at a constant value of 5.0V. The lines above represent different pH values. In the middle of the curve is possible to distinguish all the pH values varying from 2 to 12 (left to right). c) Typical sensibility curve. The pH meter sensibility is normally expressed in units of mV/pH. This kind of sensibility can be taken from this graphic by its slope. From a MOSFET EGFET this graphic is indirectly plot from graphic 4 b). If the component used is an amplifier, this graphic can be directly plotted of the data collected.

2.1.4 EGFET Biosensors

A biosensor is a device that recognizes a biological signal (protein, pH, heat, sound, etc.) through a sensing matrix and converts this signal to a physical signal (potential, current, charge etc.) on the transducer. Once EGFET recognizes a potential changes, it is known as a potentiometric biosensor.

2.1.5 Site binding model

The electrochemical interface between the sample and the electrolyte will show a very distinct configuration when compared to the bulk. The best way to explain the electrolyte model is by the Gouy-Chapman-Stern (GCS) model. [68]

In this model the electrolyte is thought to be composed of several layers. The first layer to be seen near the sample electrode is the inner layer. This layer is composed of two planes and can be directly compared to a parallel-plate capacitor. The first plane of this capacitor is considered the place where the center of *specifically adsorbed* ions is founded. This plane is at a certain distance from the surface of the sample and can be called *an inner Helmholtz plane (IHP)*. The second plane is composed of solvated ions which can approach sample by a molecular distance x_2 (see Figure 6). The place where the centers of solvated ions are founded is called *outer Helmholtz plane (OHP)*. [68,69]

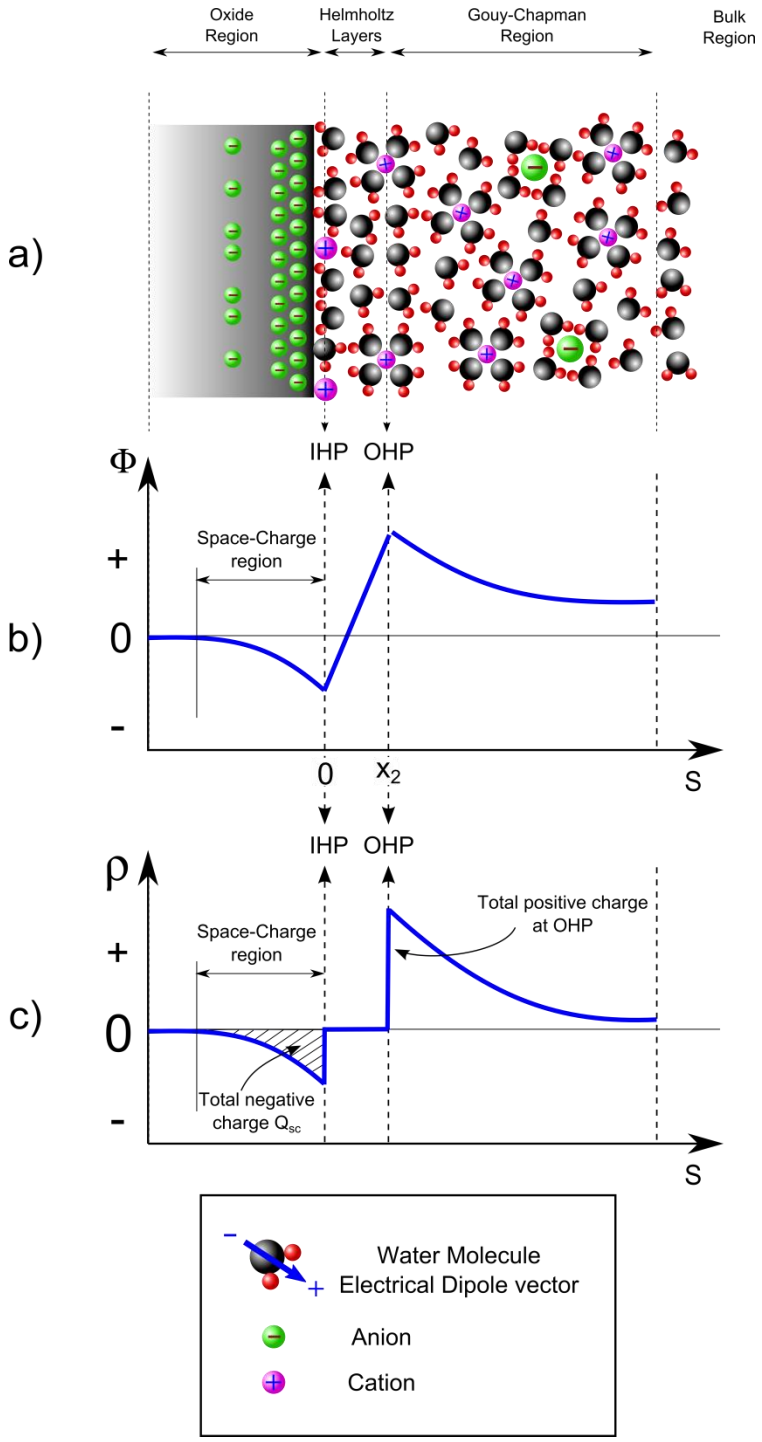

Figure 6 – Qualitative scheme of Gouy-Chapman-Stern model. a) Ionic distribution over space; b) Spatial electrical potential distribution; c) electric charge density distribution.

Solvated ions out of this first capacitor are called *nonspecifically adsorbed* ions. Because of the thermal agitation, these ions are distributed in a three-

dimensional region called *a diffuse layer.* The diffuse layer extends from the OHP until the bulk region (see Figure 6).

The whole combination of ions and solvent oriented dipoles existing between the IHP until the bulk region is named the *double layer.* Its charge density (σ^S) is described by equation 1.

$$\sigma^S = \sigma^i + \sigma^d = -\sigma^M \quad (1)$$

Where: σ^i is the charge density from specifically adsorbed ions in the inner layer; σ^d is the charge density in the diffuse layer; σ^M is the charge density on the surface of the sample.

The entire thickness of the double layer depends on the ionic concentration on the electrolyte solution. The greater this concentration is, the smaller the double layer thickness. For ionic concentrations greater than 10^{-2}M for the electrolyte solution, the double layer thickness is less than 100Å. The potential drop across the double layer region is presented in Figure 6 (b).

The difference between electrical potential at the surface of electrode in contact with the solution (ϕ^M) and the electrical potential of the electrolyte solution (ϕ^S) is called *interfacial potential difference*. This potential difference depends clearly on charge density at the interface. Nevertheless, a change of this potential requires fairly large alterations on charge density at the surface.

The potential profile presented by the Helmholtz layer in Figure 6 dropping shows the potential dropping linearly through this layer. This linearity can be explained because there is no charge between the two Helmholtz planes. So, once the potential of this region can be expressed by Poisson, it should be strategically shown as follows in Equation 2.

$$-\frac{1}{\varepsilon\varepsilon_0}\rho = \nabla^2 V = 0 \qquad (2)$$

Equation 2 is the Poisson Equation for Potential across the Helmholtz layer. ε is the dielectric constant of the medium, ε_0 is the permittivity of free space, ρ *is* charge per unit of volume, V the voltage drop.

NOTE: In equation 2 the dielectric constant is given by ε. This notation follows the electrochemistry notation as found in university books. [68] It is valid to remember this notation is quite different from physics notation where dielectric constant is given by K. [70] Once this little section is based in an electrochemical basis, dielectric constant will be assumed to be ε.

The solution for this Poisson equation is a first degree equation for potential. So, the potential across Helmholtz layer varies linearly.

For the diffuse layer ($x \geq x_2$ in Figure 6), the potential will be explained by the Poisson-Boltzmann equation as follows in equation 3. [68,69]

$$\int_{\phi_2}^{\phi} \frac{d\phi}{\sinh\left(\frac{ze_0\phi}{2kT}\right)} = -\left(\frac{8kTn^0}{\varepsilon\varepsilon_0}\right)^{1/2} \int_{x_2}^{x} dx \qquad (3)$$

Equation 3 is the Poisson-Boltzmann equation. T is the temperature; z is the charge of the ion; k is the Boltzmann constant; e_0 is the elementary charge value; n^0 is the ion concentration in the bulk.

The electric field at the OHP is given by the divergent of the potential.

$$\vec{E} = -\vec{\nabla}V \qquad (4)$$

Equation 4 is the divergent of an electrical potential for the electrostatic. This equation can be rewritten as follows:

$$E = -\left(\frac{d\phi}{dx}\right)_{x=x_2} = \left(\frac{8kTn^0}{\varepsilon\varepsilon_0}\right)^{1/2} \sinh\left(\frac{ze_0\phi_2}{2kT}\right) \quad (5)$$

Equation 5 is the electrical field at the OHP. So, the potential across the entire double layer is given by Equation 6 bellow.

$$\phi_0 = \phi_2 - \left(\frac{d\phi}{dx}\right)_{x=x_2} x_2 \quad (6)$$

Equation 6 is the potential across the double layer. ϕ_0 is the potential at x=0. The pattern graphic describing this solution is found in Figure 6 (b) as well.

2.1.6 Semiconductor-Electrolyte Interface

Now, let's describe what happens inside an oxide used as a sensing structure for an EGFET. More specifically, let's describe semiconductor oxides. At this point is important to remember that, as in an electrolyte solution, the number of positive and negative carrier inside an intrinsic semiconductor is equal. Then, there is no excess-charge inside any volume of a semiconductor. Hence, for the semiconductor bulk is possible to write the Equation 7 bellow. [69]

$$n'^0 = p^0 \quad (7)$$

Equation 7 represents the equality between carriers inside an intrinsic semiconductor bulk. n'^0 and p^0 are the density of electrons and holes respectively. For the bulk is then possible to write the charge density as follows in Equation 8:

$$\rho_{bulk} = e_0 p^0 - e_0 n'^0 = 0 \qquad (8)$$

Equation 8 is the charge density at the bulk of the semiconductor. The OHP is charged as shown above. This charged plane exerts an electric field on semiconductor. This electric field is strong nearby interface and decreases as it goes toward the semiconductor bulk. The charge density ρ_x for intrinsic semiconductor can be obtained by solving the Poisson equation too as follows.

$$\nabla^2 V = -\frac{1}{\varepsilon\varepsilon_0}\rho_x \neq 0 \qquad (9)$$

Equation 9 is the Poisson equation for inside the oxide when in contact with the electrolyte. Using Boltzmann distribution to solve the Poisson equation and the relation shown in equation 7 is possible to find the charge density inside the semiconductor as follows in equation 10.

$$\rho_x = -e_0 n'^0 \left(e^{\frac{e_0\phi_x}{kT}} - e^{-\frac{e_0\phi_x}{kT}} \right) = -2e_0 n^0 sinh\frac{e_0\phi_x}{kT} \qquad (10)$$

Equation 10 represents the charge distribution inside the intrinsic semiconductor under influence of the electrolyte electric field. Combining equation 9 and equation 10 the Poisson-Boltzmann equation is reached again in the following form:

$$\nabla^2 V = -\frac{2e_0 n'^0}{\varepsilon\varepsilon_0} sinh\frac{e_0\phi_x}{kT} \qquad (11)$$

Equation 11 is the Poisson-Boltzmann equation in the differential form. Its solution will be the same as shown in equation 5. The Gauss law of electrostatic is:

$$\oint_S \vec{E} d\vec{a} = \frac{Q_{in}}{\varepsilon\varepsilon_0} \qquad (12)$$

Equation 12 is the Gauss Law. $\vec{E}$ is the electric field; $\vec{a}$ is the area vector, Q_{in} is the total charge enclosed by the Gauss surface. If the Electric field is constant on the entire surface and the area around the charge is assumed to be unitary and combining equation 4 and equation 12, it is possible to rewrite the result as follows.

$$Q = \varepsilon\varepsilon_0 \frac{d\phi_S}{dx} \qquad (13)$$

Equation 13 represents the total charge inside a unitary surface. ϕ_s is the potential at the surface of the semiconductor. Combining equation 5 and equation 13 is possible to reach:

$$Q_{sc} = 2(\varepsilon\varepsilon_0 n^0)^{1/2} sinh \frac{e_0\phi_s}{kT} \qquad (14)$$

In equation 14, Q_{sc} is the total space charge. Equation 11 has a very important and interesting consequence. Linearizing its hyperbolic sine it is possible to find:

$$sinh \frac{e_0\phi_x}{kT} \approx \frac{e_0\phi_x}{kT} \qquad (15)$$

Equation 15 is the hyperbolic sine linearization. Combining equation 15 and equation 5 it is possible to write the following equation in one dimension:

$$\left(\frac{d\phi}{dx}\right)_{x=x_2} = -\left(\frac{2{e_0}^2 n'^0}{\varepsilon\varepsilon_0 kT}\right)^{\frac{1}{2}} \phi_x = -\kappa\phi_x \qquad (16)$$

Rearranging the two right terms of equation 16, is possible to write an equation for potential anywhere inside the semiconductor material as a function of electrical potential on its surface. See equation 17.

$$\phi_x = {\phi_s}^{-\kappa x} \qquad (17)$$

In equation 17, ϕ_s is the electrical potential at the surface of the semiconductor.

$$\kappa = \left(\frac{2{e_0}^2 n^0}{\varepsilon\varepsilon_0 kT}\right)^{\frac{1}{2}} \qquad (18)$$

Equation 18 shows κ. This parameter is responsible to characterize potential due to holes or electrons inside the semiconductor.

According to equation 17, there is an exponential decay of potential inside the semiconductor material according to space. There is an electric field applied to material (due to OHP). This electric field tends to zero far away from the interface oxide - electrolyte. Hence, there is an electrical distribution inside the semiconductor material too. The carrier density distribution inside the semiconductor is similar to the ion distribution inside an electrolyte solution around an electrode applying a potential. This excess charge-density decay to zero far from interface semiconductor-electrolyte.

The term κ^{-1} is responsible to describe the charge-density thickness inside the semiconductor. This thickness, as an example of what happens with the double layer inside the electrolyte, is changed as bulk charge carrier density is changed. As concentration increases, this thickness decreases.

2.1.7 pH Sensors

A very important biological signal comes from pH. It is a quite important biological signal to be monitored and that is a good reason to keep researching in this area to improve the big number of articles dedicated to develop new EGFET pH sensors. [29,34,35,39,55,71–90]

The development of new pH sensors is done, basically, changing the sensing structure of EGFET. Different materials are used for this purpose, normally oxides like as: ZnO [20,74–77,86,87], SnO_2 [15,19,21,24,71], V_2O_5 [22,23,25–27], TiO_2 [26,29,34,73], PdO [81], CuO [85] and Ga_2O_3. [91] Other materials were already used too, as example of Boron Carbon Nitride [82], Carbon Nanotubes [72,79,88], Graphene [47],Titanium Nitride [34] and Silicon Nanowires. [83]

It was already explained by Bergveld that potential electrochemically generated at the sensitive part of an ISFET should be a response to Nernst equation (equation 19Equation). [13]

$$E = A + \frac{RT}{nF} lna_i \qquad (19)$$

Equation 19 is the Nernst equation. In the equation: *E* is the electrochemical potential; *A* is a constant; *R* is the gas constant; *T* is the temperature; *n* is the number of electrons transferred; *F* is the Faraday Constant; *AI* is the ion activity.

EGFET is an evolution of an ISFET. Basically an EGFET is an ISFET with an extended gate. The field effect transistor material changed by the electrochemical potential applied to the sensor membrane is essentially the same. Thus, in an absence of an exclusive theory for EGFET devices, they should be well explained by the same Nernst equation too.

A more detailed theory involving Nernst potential and Field Effect Transistor theory is shown by van Hal et al. [92] which shows the explanation of the expression

found by Bergveld and Sibbald [93] of the drain current of a Field Effect Transistor (FET) due to chemical potential changing on its sensing surface (equation 20).

$$I_D = \mu C_{ox} \frac{W}{L} \left\{ \left[V_{GS} - \left(E_{ref} - \psi_0 + \chi^{sol} - \frac{\Phi_{Si}}{q} - \frac{Q_{ox}+Q_{ss}}{C_{ox}} - \frac{Q_B}{C_{ox}} + 2\phi_f \right) \right] V_{DS} - \frac{V_{DS}^2}{2} \right\} \qquad (20)$$

Equation 20 is the Bergveld and Sibbald expression. At this equation: μ is the average electron mobility in the channel; W and L are respectively the width and the length of the gate; E_{ref} is the reference electrode potential; V_{DS} is the drain source voltage; V_{GS} is the gate source voltage; Φ_{Si} is the silicon electron work function; q is the elementary charge; C_{ox} is the capacitance of the gate oxide; Q_{ox}, Q_{ss} and Q_B are the charges located in the oxide, charges located in surface states and interface states and the depletion charge respectively; χ^{sol} is the surface dipole potential of the solution; ϕ_f is the potential difference between the Fermi levels of doped and intrinsic silicon; ψ_0 is the electrostatic potential

After rearrangements and the combination of this equation and Nernst equation, van Hal et al. could find an equation for the sensitivity of electrostatic potential due to changes in the bulk pH as shown in equation 21. [92]

$$\frac{\delta \psi_0}{\delta pH_B} = -2.3 \frac{kT}{q} \cdot \frac{1}{\left(\frac{2.3kTC_{dif}}{q^2 \beta_{int}} \right) + 1} \qquad (21)$$

Equation 21 is the van Hal expression of sensitivity of electrostatic potential to changes in the bulk pH. In this equation: pH_B is the Bulk pH; C_{dif} is the differential capacitance; β_{int} is the intrinsic buffer capacity.

The last term of the equation 21 is dimensionless and can vary between 0 and 1. For sensitivity close to the theoretical maximum this term approaches to 1. This term can go to zero when the intrinsic buffer capacity goes to zero. [92] The main idea for an EGFET sensitive to pH variation is the number of proton ions (H^+) or hydroxyl molecules (OH^-) adsorbed in sensing surface. These ions will change the electrochemical potential of sensing surface. This potential will be directly driven to

the gate of a high input electronic component (a MOSFET for example) which will control a current or a potential proportional to electrochemical potential.

During the redox reaction of some biomolecules different products can be generated and further alter local pH. With the appropriate use of different techniques is possible to detect the pH variance, as an example: glucose detection [30,33] and urea [89,94,95] detection.

2.1.8 Non-Enzymatic

Other biomolecules and ions were already investigated by EGFET technology. It is very interesting to highlight a few of those other molecules or ions such as:

Calcium ions (Ca^{++})→ were detected by two different ways by current [96] and by potential. [32]. Although, both ways used $CaCl_2$ as Calcium source. The potential method (instrumental amplifier) found sensibility of 27.71mV/decade of Ca^{++}. Its detection range was $1M \sim 10^{-4}M$. The current method (through a MOSFET) found sensibility of -113.92nA/mM of Ca^{++}. Its detection range was $1\mu M \sim 10^{3}\mu M$.

DNA molecules → As an example of a technique to detect DNA, an EGFET was used to detect different DNA concentration due to its hybridization on: gold electrode probes deposited in fabricated FET (Field Effect Transistor) device [60,63,65] and GaN nanowire probes using commercial MOSFET [97].

Acetylcholine → Due to release of H^+ in the media as a product of its hydrolysis, acetylcholine can be detected with a commercial operational amplifier [37].

Saccharide → Phenylboronic acid (PBA) is a molecule that can form reversible complexes with saccharides. These complexes change the molecule charge potential. For the detection, the PBA was immobilized in gold substrate and a commercial

MOSFET [98] or a home-made organic FET (OFET) [42] were reported to be used as high impedance input component.

Proteins → The detection of protein can be done by immobilization of an antibody on EGFET sensing structure. The target molecule is then labeled with another tiny molecule which the antibody can recognize or is a molecule that naturally has the tiny molecule incorporated in its structure. For example, streptavidin is known to be an antibody that recognizes biotin or biotinylated molecules. This fact helped to produce EGFET biosensors with home-made OFET [44,46] or FET [62,64] devices and commercial MOSFET [99]. Another example is the detection of microalbumin by its antibody and a commercial MOSFET platform [100].

Aptamers are another alternative to protein detection. In this case, aptamers are immobilized on the EGFET sensing structure and could detect specifically Thrombin Lysozyme (home-made FET and detection limit of 28.2 nM) [101], Lysozyme (home-made FET and detection limit of 17.8 nM) [101] and protein CDK2 (home-made MOSFET and range detection between 21fM~1.9nM) [58].

CO_2 → CO_2 was successfully monitored solved in solution. [67] To accomplish this task, authors report the fabrication of a home-made FET device and its sensitive structure. The sensitivity reported is of 44.4mV/decade of CO_2 in concentrations varying from 0.25~50mM.

Uric Acid → Uric acid can be detected by ferrocene immobilized on the sensing structure of a EGFET biosensor [102] made with a commercial MOSFET.

Chloride → A home-made FET device and a polyvinyl chloride ion sensitive membrane are the main components to detect this ion. [53] The reported sensitivity is 45mV/decade of chloride ions.

Cancer Cells → A gold metal EGFET was used as a platform for culture and detection of pancreatic cancer cells. [103] A home-made MOSFET was used on this device. The study present differences between signal of a bare and cultured electrode. Another interesting test was the introduction of drugs on cell medium to kill the cancer cells that presented readable signal.

ATP molecule → In this work is presented ATP detection due reaction of this molecule with a hairpin ATP-binding aptamer. [104] Once ATP molecule is detected, the hairpin releases DNA binders that are charged. This changes the gate potential in the gate of an EGFET producing the signal through a commercial FET device. The detection range goes from 10^{-8} to 10^{-6} M.

Sodium and Potassium → A detection platform for detection of Sodium and Potassium was described. [105] It consists on an commercial instrumental amplifier and oxides as sensitive structure. The detection limit ranges between 10^{-7}M ~ 1M for Sodium and between 10^{-6}M ~ 1M for Potassium.

Among a huge variety of sensors, electrochemical ones and specially *Extended Gate Field Effect Transistor* (EGFET) sensors can be highlighted as really promising devices because of their properties (possible miniaturization, high entrance impedance, low cost, simple equipment required and big variety of materials including biocompatible materials). These sensors are used as biosensor's transducers. Such transducer can be made by oxides such as: TiO_2[106], SnO_2[24] and ZnO[86]. The biocompatibility of these materials have already been demonstrated by other groups [107–111]. These materials have been used as part of various bio sensors of all types.

Some groups have reported interesting works describing the usage of EGFET as a biosensor to detect, for example: DNA [97,112], CO_2 [113], O_2 [110], Urea [89,95], Protein [114], Uric Acid [115] and Glucose [116]. Therefore, the majority of works using EGFET as a biosensor describes it as a pH-sensor [20,21,34,76,77,80,83,88,117,118]. pH control is quite important. The human body needs to keep blood pH on a very narrow window of value to keep the homeostasis. In addition, reactions of other important biomolecules as urea [119], glucose [120] can be monitored through indirect pH detection.

Our group has a vast history using the EGFET system to sense mainly H+ ions. [20-28]. So, it is very convenient to continue performing experiments in this system. Moreover, the results already reached allied to the versatility of this system (as mentioned) makes the EGFET an interesting device to be used to glucose sensing.

Among the transducer oxide types is possible to highlight the *Fluorine Tin Oxide (FTO).* This material, when produced by spray pyrolysis method, presents interesting, very promising and useful physical-chemistry characteristics such as: potential to be miniaturized; high transparence on visible spectrum region; high surface area; high or relatively low conductivity; mechanically hardness; thermal stability for biosensing; biocompatibility; it is a n-type semiconductor; and large band gap (4.21eV).[121–123]

The transducer could be made by almost any conductive oxide which can sense H+ ions. The choice of this author to FTO is mainly related to the relative low price to acquire FTO from a manufactory besides the fact our group has a history using this material. [24,125]

Although all these biosensors are claimed to work, as far as this author is concerned, none of the articles presented until today describes a very important step to make these devices useable: the cleaning process between consecutive measurements.

Oxide transducers, generally, have porous surface. Within these surfaces, ions are adsorbed from bulk solution and can mask the biosensor response when some cares are not taken. The cleaning method used in this work is based on water only as explained further.

2.2 Material and Method

A thin film of *Fluorine Tin Oxide (FTO)* purchased from *Sigma* was used as a transducer. This film was deposited on glass by spray pyrolysis technique. This technique enables better control of the films' sheet resistivity besides a production of crystalline and heterogeneous grain sizes and grain distribution.

The grain sizes were already measured elsewhere for this same material and is, in average, around 150nm in diameter. [125]

FTO samples with sheet resistance of 10Ω/□. All samples were cut in pattern size of 26mm x 10mm. A copper wire, connected to the FTO surface by conductive silver epoxy glue, attach the thin film to the gate of a commercial N-channel type MOSFET, model *CD4007* from *Texas Instruments*. The contact was then encapsulated with epoxy resin. This encapsulation always took the same amount of sample's area of 3mm width and 10mm length.

As cleaning solution, it was used DI water – with resistivity ≥ 1MΩ.cm. 100mM Phosphate Buffer solution with 100mM KCl at pH 7 was used to prepare the enzyme solution and for reference measurements as well. *Glucose Oxidase (GOx)* from *Aspergillus niger, Acetic Acid* and *Glutaraldehyde (GTA)* 25% in water were purchased from *Sigma*. D-glucose was purchased from *Synth* and KCl was purchased from *CINETICA*. All cited chemicals were used without further purification. *Chitosan* was acquired from *Ultrafarma* as a diet supplement and used as acquired.

GTA is a classic material used in immobilization of molecules presenting lysine groups. It is a molecule widely used for this purpose and works very fine. However, it has some toxicity and should be avoided its contact with a human being. Chitosan, in the other hand, has low toxicity. It is freely protein found in nature and is very cheap. It will be studied as an alternative to GTA use on GOx immobilization.

To digitize the data a *Data Acquisition HP 34970* was used. Potential and current were provided through an *Agilent E3646A Dual Output DC Power Supplies*. To control the power supply and record the data, a homemade software (written in *LabView 8.5*) was used. To analyze all data we used *OriginPro 8.* As an electrolyte solution, 100mM KCl with different glucose concentrations was used. Its pH is around 5.6.

On its reaction with GOx, D-glucose releases proton H^+ as a final product, as seen in Figure 7 bellow. The released protons change the potential on surface of the sensor that is further transmitted to the MOSFET by a wire, as shown in the scheme of Figure 8.

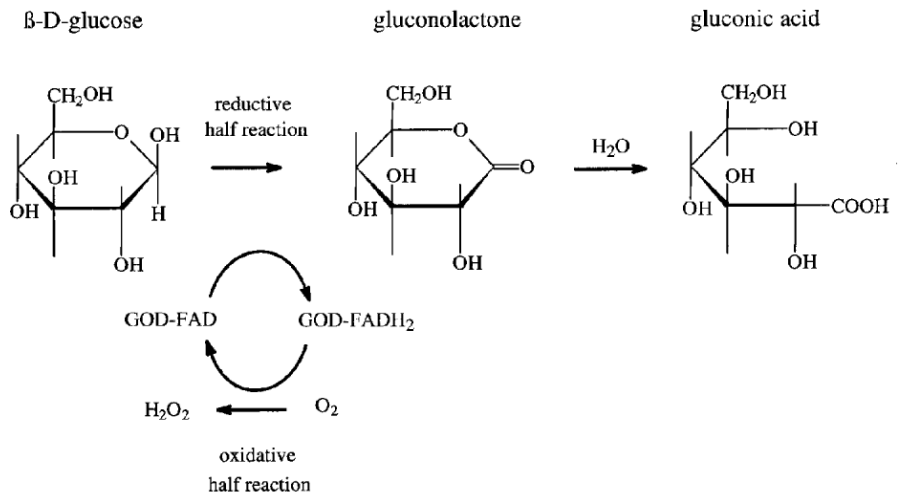

Figure 7 – D-glucose oxidation reaction scheme catalyzed by GOx

Figure 8 shows an electronic scheme of an ion sensor transducer based on EGFET. In that scheme, one can see an ion sensor totally submerged in electrolyte solution. This sensor is linked by wire to the gate of the N-channel MOSFET. Hence, as higher the gate potential gets, higher will be the current flowing through the drain towards the source. In the same scheme, is possible to see a reference electrode into the solution too. This electrode will apply in solution a constant potential V_{Ref}. The ions that eventually attach to the sensor's surface, will apply for it a variable potential V_{ion} (that depends on how many and what kind of ions are attached to it). So, the potential applied to the gate of transistor is $V_{GS} = V_{Ref} + V_{ion}$. This V_{GS} potential will control the size of the ion channel inside the transistor, and consequently, current between the drain and source of the transistor (I_{DS}). In other words, current I_{DS} will be controlled by the number of ions attached to the sensor.

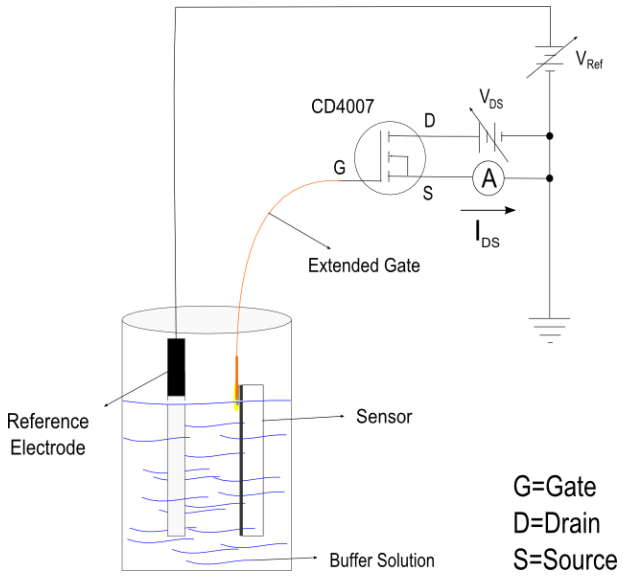

Figure 8 – The whole apparatus to use an EGFET as a biosensor.

When the scheme of Figure 8 is used, V_{DS} and V_{Ref} are fixed in 5V. There is another variation of this scheme used in this study. The other scheme is enhanced with a commercial junction transistor (type **BC338**) to make an amplification of current I_{DS} provided by the MOSFET (see Figure 9).

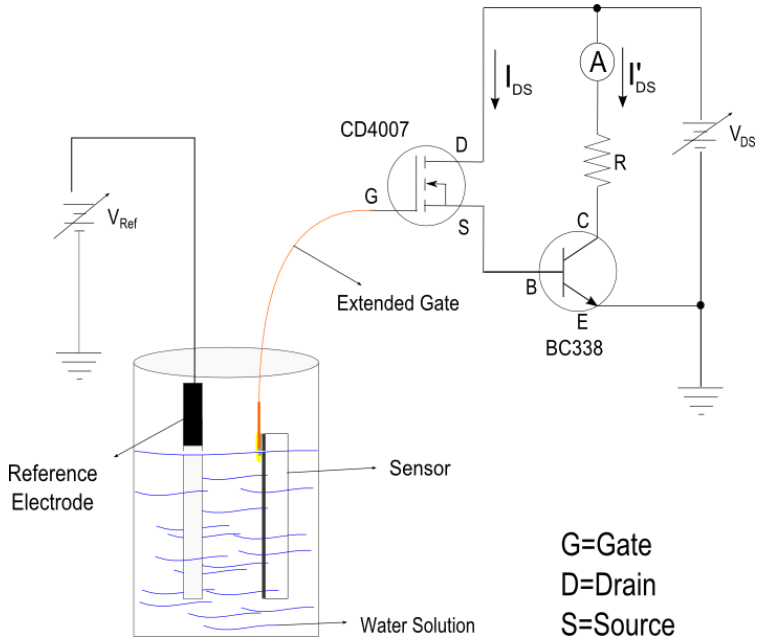

Figure 9 – Amplified EGFET Scheme.

In Figure 9 is present a resistor R that is placed on the circuit to keep a smaller potential applied to the transistor. This resistor was calculated in a way I_{DS} was amplified 100 times. Its value is 13Ω. Such circuit adopts a different set of voltages to its sources as follows: V_{Ref} = 4.0 V and V_{DS} = 3.0 V. The use of different values of these sources is explained by setting the sample's blank line in the middle of the active transistor curve. [124]

The amplifier circuit was made with the intention of becoming easier to see tiny differences between signal (increase the measurement's resolution). So, to make any experiment comparable with each other independently of adopted circuit, big part of graphs are plotted in Current Percentage Variation (ΔI) – normalization – always adopting as reference the value of measurements for 0mM of glucose solution.

If a sensor is reused for any reason in different measures it needs to be cleaned. As already shown before[123], to clean the samples, water procedure was adopted. At this procedure, before each measurement, the sample is cleaned with DI water. This cleaning consists of just squeezing the water on sample for approximately three seconds. After this simple procedure, another measurement was allowed to start if this is the case.

2.2.1 – Immobilization Protocols and Sensor Production

The most interesting characteristic of an enzymatic biosensor is related to the enzyme itself. An enzyme is highly specific as a catalyzer.

I) Glutaraldehyde

There are some different protocols already described in literature about glucose oxidase immobilization through glutaraldehyde (GTA) on various materials. However, as far as the author is concerned, there is no specific protocol designed to GOx immobilization in FTO substrate. Hence, after testing few protocols designed to oxide substrates without success, it was decided that for this work a new immobilization protocol should be developed.

The following steps presented in this section were used to build a glucose sensor with GOx immobilized in FTO substrate via GTA (GTA sensor). These steps contain the immobilization protocol as well:

a) **Clean the electrical contact area with acetone. Use a swab to gently scratch the area for better cleaning.**
b) **Make the electrical contact between FTO thin film and copper wire using epoxy conductive glue. Leave the glue to dry at room temperature.**
c) **Cover the entire area where the electrical contact was made with epoxy insulator glue (normal epoxy glue). Let the epoxy glue dry overnight.**
d) **Clean the FTO thin film with acetone. Use a swab to gently scratch the area for better cleaning.**
e) **Immerse the entire area on 10% GTA V/V water solution for 3 hours.**
f) **Rinse the sensor, gently, with DI water.**
g) **Dry the sensor with inert gas.**
h) **Immerse the entire area on 100mM KCl solution containing 4mg/ml of Glucose Oxidase for 4 hours.**
i) **Rinse the sensor, gently, with DI water.**
j) **Dry the sensor with inert gas.**

II) Chitosan

Once more, no protocol was found in literature describing GOx immobilization in FTO via Chitosan. The following sensor production steps contain an immobilization protocol developed in our lab to immobilization of GOx in Chitosan (Chitosan sensor).

a) **Clean the electrical contact area with acetone. Use a swab to gently scratch the area for better cleaning.**

b) Make the electrical contact between FTO thin film and copper wire using epoxy conductive glue. Leave the glue to dry on room temperature.

c) Cover the entire area where the electrical contact was made with epoxy insulator glue (normal epoxy glue). Let the epoxy glue dry overnight.

d) Clean the FTO thin film with acetone. Use a swab to gently scratch the area for better cleaning.

e) Spread, equally, through the entire sensor area 75μl of chitosan solution for every 1cm². This solution is made by dissolving 50mg of chitosan in 5ml of 2% V/V Acetic Acid. Let the sensor dry inside a fume hood in room temperature.

f) Rinse the sensor, gently, with DI water.

g) Dry the sensor with inert gas.

h) Spread, equally, through the entire sensor area 50μl of 100mM KCl solution containing 4mg/ml of Glucose Oxidase solution for every 1cm² 100mM KCl solution containing 4mg/ml of Glucose Oxidase. Let the sensor dry in room temperature.

i) Rinse the sensor, gently, with DI water.

j) Dry the sensor with inert gas.

2.3 – Results of EGFET GOx Biosensor

A sensor used in point-of-care analysis needs to be able to take measurements on continuous mode. To test this ability of a sensor is necessary to introduce glucose in the system during measurement. Such introduction of new specie in the media can generate noise in the signal. The new specie is introduced to the system by a micropipette as illustrated in Figure 10. So, the turbulence and any other factor that can generate noise to data were tested by the introduction of solvent and glucose solution, as shown in Figure 11.

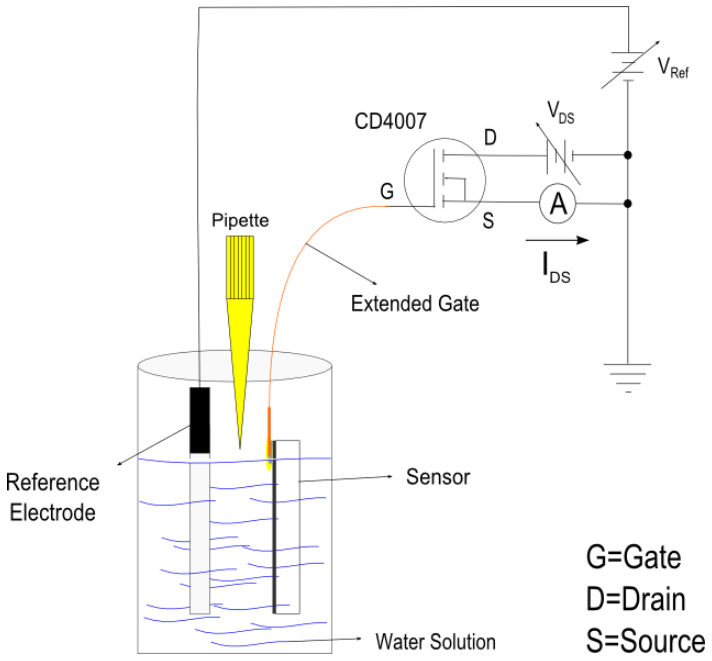

Figure 10 – EGFET scheme for glucose sensing.

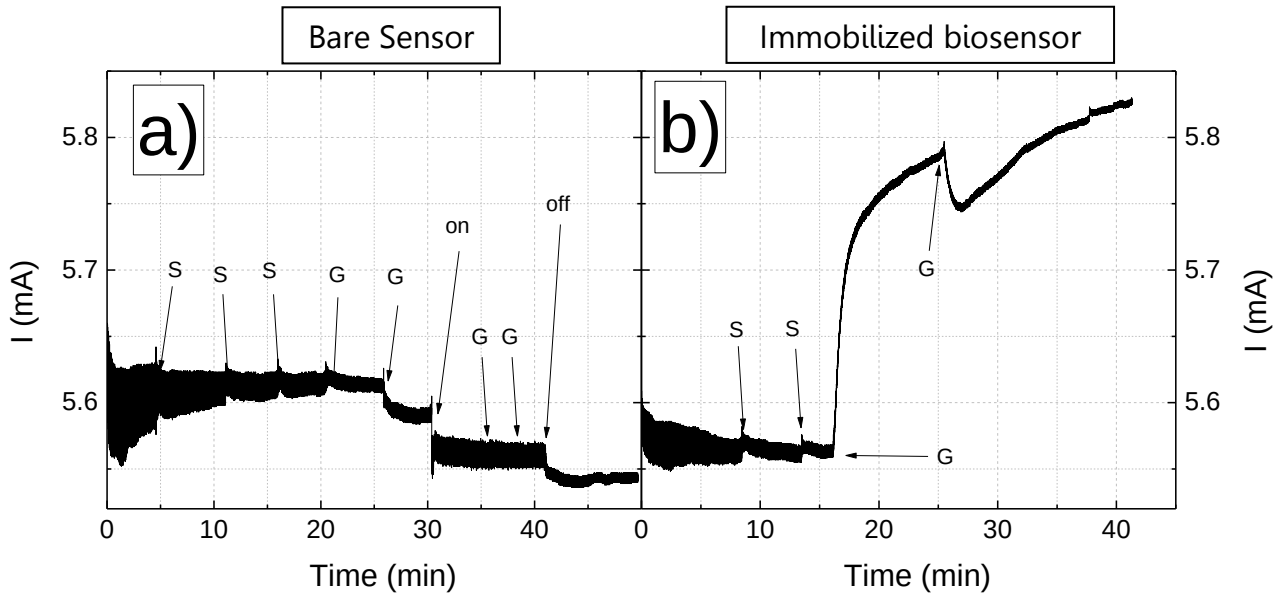

Figure 11 – Proof of concept for a glucose sensing. The labels at the graphic are representing the exact moment where some change is applied to the system. The labels are: S = Solvent; G = Glucose Solution; on = Magnetic shaker turned on; off = Magnetic shaker turned off In a) is presented the data of a FTO film without functionalization. In b) is the data of a functionalized FTO film.

The solvent used is DI water. A FTO thin film without functionalization is used to test how sensitive the transducer is to the introduction of new species as shown in

Figure 11 (a). At this figure, is possible to see arrows indicating the moment when an event happens. The labels describe the event itself like: **S**olvent introduction (S); **G**lucose solution introduction (G); magnetic shaker turned **ON** (on); magnetic shaker turned **OFF** (off). Moreover, is possible to notice in

Figure 11 (a) that there is almost no influence to introduction of new species (glucose solution until concentration of 136mM or solvent) to the system. However, turning the magnetic shaker on or off showed a significant influence to signal.

Figure 11 (b) shows the response of a FTO thin film functionalized with GOx submitted to the same experiment. Although, once magnetic shaker had a high influence on sensor's response (Figure 11 (a)), the magnetic shaker was then eliminated from the experiment. It is pronounce that the introduction of solvent (DI water) to system does not affect the signal significantly again. Nevertheless, the very first introduction of Glucose solution (34mM of glucose) caused an abrupt response from the sensor. This abrupt response only for functionalized film means three things: 1) The GOx was successfully attached to the FTO surface and is sensitive; 2) This film has a potential to become a point-of-care sensor; 3) The magnetic shaker is really not necessary for experiments.

A more detailed and careful experiment was performed with the main goal to find a sensor's calibration curve. Hence, seven different solutions with seven different glucose concentrations were prepared. Each one of those solutions was measured each time by same sensor. After each measurement, the sensor was cleaned with 15ml of DI water squeezed on it. Figure 12 (a) shows the result of this experiment. At this figure is possible to observe the wide detectable range sensor has. Besides, it is important to see that, between the concentrations that embrace the human body glucose concentration values (3.9mM to 10.0mM – accordingly to the *American Diabetes Association*)[23], sensor' sensibility is almost linear.

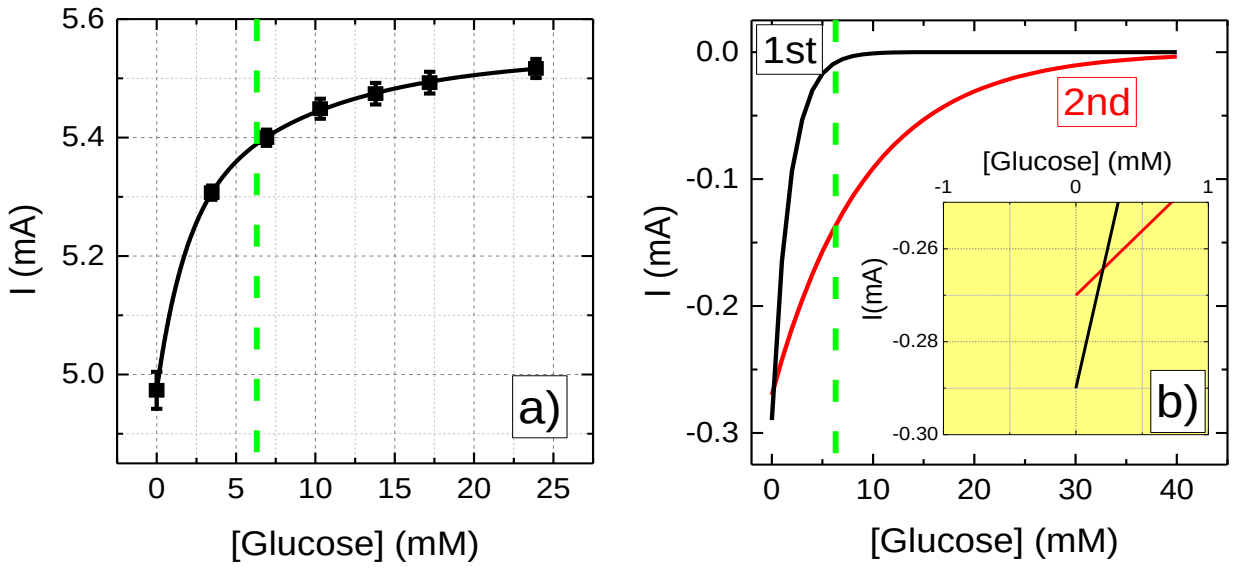

Figure 12 – Response of Glutaraldehyde Sensor to different glucose concentrations. a) Calibration curve for the FTO sensor. The line represents the Exponential Decay of 2nd order with R^2 of 0.99959. b) Two components of 2nd order fitting of the calibration curve. The inset graph is a zoom of the region around 0mM of glucose for both 2nd order components. Green dashed lines, on both graphs, represent the knee of the 1st component curve.

The curve fitting all data points in Figure 12 (a) is given by 2nd degree decay equation (see equation 22 below). The two dependent terms of this equation are plotted in Figure 12 (b). The dash line represents the curve's knee for the first term. The concentration for this knee is around 6.3mM.

$$I = -0.00029e^{\left(-\frac{x}{1.768}\right)} - 0.00027e^{\left(-\frac{x}{9.237}\right)} + 0.00554 \quad (22)$$

For concentrations above knee concentraion, there will be, practically, only the second term is responsible for current change (see Figure 12 (b)). For a glucose concentration below 6.3mM, both (first and second) terms compete and are responsible for changes in electrical current.

First and second terms of equation 22 are responsible for two distinguished mechanisms that change the final current of this glucose sensor. For a better

understanding of both mechanisms it is interesting to explain Figure 12 from big concentration to small glucose concentration.

Figure 12 (a) is almost completely saturated in solution with concentration of 25mM of glucose. For any small glucose concentration, the sensor response decreases.

In Figure 12 (b) is possible to see both, first and second, components of equation 22 plotted separately. Going from high glucose concentration to low, it is possible to notice both components go to higher negative current values, which means both components reduce the final sensor response for small glucose concentration.

Yet in Figure 12 (b), the first component (in black line) does not affect the signal for concentration higher than 12mM. Below this threshold value, and especially below 6.3 mM, its influence increases dramatically. The low value necessary for its influence suggests this mechanism might be mass dependent. The most common and probable mechanism responsible for it is the enzyme usage.

For glucose concentration below 12mM not all GOx enzymes are being used in their full capacity or at the same time. There is no glucose enough to make use of all the immobilized enzymes.

The second component of equation 22 plotted in Figure 12 (b) (red line) is always playing an important role for almost all concentration value. However, for high glucose concentration its influence is smaller. Decreasing glucose concentration its influence becomes bigger. This curve might represent the microenvironment pH influence on GOx.

The pH is one of the main mechanism which influences the catalytic activity [127]. GOx optimum pH is 5.5, as indicated by the producer. The KCl solution used in the experiments has pH around 7.0. Once immersed within a high glucose concentration solution, a lot of oxidative reactions of glucose molecules are performed. In the end of such reaction H+ is released from gluconic acid (see Figure 7). The pH of the microenvironment around the immobilized enzymes is then

changed towards a smaller value than the bulk pH. So, the pH around the enzymes becomes acidic. If the glucose concentration is big enough, this acidic microenvironment pH might reach the optimum value for GOx catalytic activity (pH 5.5).

For low glucose concentration, there will be a small quantity of oxidative reactions happening in a given time. It means that a small number of gluconic acid will be generated and, consequently, a small change in microenvironment pH will happen. So, the tendency of microenvironment pH is continuing being around 7. In this value the GOx activity is low. Hence, the final current response will be greatly affected by this mechanism in small glucose concentration.

In the inset graph of Figure 12 (b) is possible to see a zoom of low glucose concentration of both components of calibration curve. It is interesting to notice that second component of equation 22 (in red) is slightly modified by the glucose presence in low concentrations if compared to the first component (black curve). Moreover, the second component is dominant in current changes for glucose concentration bellow 0.2mM. Also, from Figure 12 (a) is possible to ensure that the sensor has an upper limit for glucose detection around 15mM.

This inversion in dominant current changer seen in the inset graph is completely understandable and corroborates previous discussion. Notice that for very small glucose concentration the main factor dominating current suppression is the GOx use. There is a very small number of enzymes being used at this point. The GOx use changes very rapidly and above 0.2mM it is not the main current suppressor anymore. Keep in mind that if no GOx catalyze the reactions there would be no change in enzyme activity because no change in microenvironment pH would be noticed.

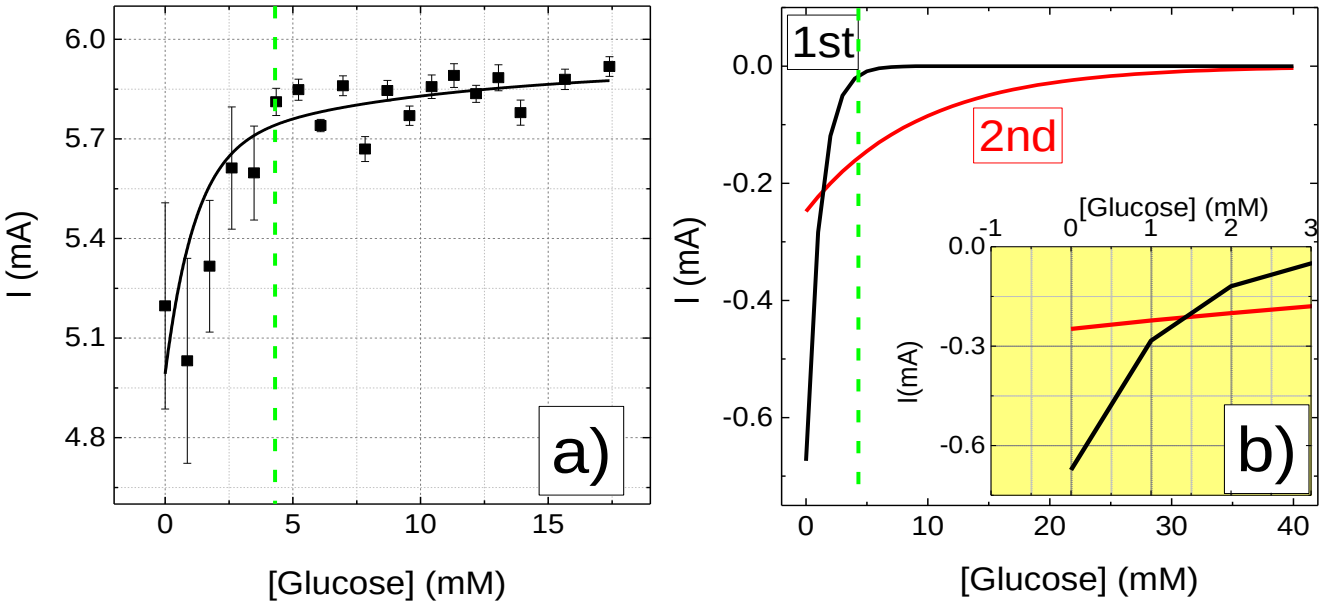

Figure 13 – Response of Chitosan Sensor to different glucose concentrations. a) Calibration curve for the FTO sensor. The line represents the Exponential Decay of 2nd order with R^2 of 0.23162. b) Two components of 2nd order fitting of the calibration curve. The inset graph is a zoom of the region around 0mM of glucose for both 2nd order components. Green dashed lines, on both graphs, represent the knee of the 1st component curve.

Figure 13 (a) shows the calibration curve for a glucose sensor immobilized by chitosan. This calibration curve is an exponential curve of second degree decay, shown in equation 23 below. Its two components were plot separated in Figure 13 (b). The green dashed line in both graphs represents the concentration for the knee of 1st exponential component of Figure 13 (b). The concentration for this knee is 4.3mM.

The same discussion addressed to Figure 12 can be extended to Figure 13. Moreover, in the inset of Figure 13 (b) is possible to see that the main mechanism suppressing the biosensor current response until 1.4mM belongs to GOx use. Above this concentration, the microenvironment pH becomes the main suppressor mechanism. Besides, notice the total use of GOx is reached around 7.5mM. The explanation for both phenomes cited is how the GOx is immobilized on the FTO thin film.

The discussion above suggests that a smaller number of enzymes is immobilized in chitosan process than in GTA process. So, with a smaller number of enzymes on the surface of chitosan glucose biosensor, the saturation of GOx use is reached in a smaller concentration (~7.5mM) when compared to the GTA glucose sensor (~10mM).

$$I = -0.00067e^{\left(-\frac{x}{1.15519}\right)} - 0.00025e^{\left(-\frac{x}{9.33169}\right)} + 0.00591 \qquad (23)$$

Equation 23 represents the calibration curve for chitosan sensor. The analyses addressed to equation 22 can be extended to equation 23 as well: the first term represents the GOx use, the second term represents GOx activity and the third term is just a constant.

In the beginning of the curve is possible to verify the error bars are bigger than for the rest of the same curve of 13(a). Actually there are two different possible explanations for that: **1)** the sensor can be achieving its equilibrium once the chitosan fibers are not soluble in pH 7 (as the buffer used in this experiment). So, the first points would be noisier than the rest of the curve. **2)** Maybe the sensor is a good sensor only for high glucose concentrations. As we can observe in Figure 13, for higher glucose concentrations the error bars decrease drastically.

Both arguments given above for the error bars in Figure 13 are speculative. It need more experiments to assure the real reason of the error bars distribution in Figure 13.

An important detail can be highlighted now, the similarity between equation 22 and equation 23. Notice that even the factors dividing ***"x"*** are very similar in these equations (see table 1). Consequently, there is similarity in the behavior of curves of first and second components of Figure 12 and Figure 13. This detail suggests both sensors are driven by the same detection mechanisms.

Table 1 – Comparative table of equations 22 and 23 terms

	1st term	2nd term
Equation 22 (GTA sensor)	1.768	9.237
Equation 23 (Chitosan sensor	1.155	9.332

Assuming both sensors are driven by same detection mechanisms, is possible to conclude that the reason biosensor immobilized via chitosan has a smaller detection range than biosensor immobilized via glutaraldehyde (GTA) is the smallest quantity of GOx on the surface. The chitosan biosensor has a low number of GOx immobilized on its surface when compared to the GTA biosensor. The explanation for that relies on the steps of its building (section 2.2.1). But a modest number of GOx can diffuse to inside chitosan matrix. There is no covalent bond between GOx and chitosan matrix. There is just an enzyme entrapment inside chitosan matrix.

GTA molecules can bind covalently to GOx molecules. However, it cannot covalently bind to FTO. The experiments shown this biosensor responds correctly and as expected in the glucose presence in the media. Nevertheless, as can be seen in Figure 14, this enzymatic sensor is well stable.

The experiment shown in Figure 14 was performed during two different days. During these two days, thirty-nine measurements were performed (thirty in the first day and another nine in the second). During the first day, it is pronounced the way signal decay after forth measurement. After this first decay, biosensor demonstrated to be well stable.

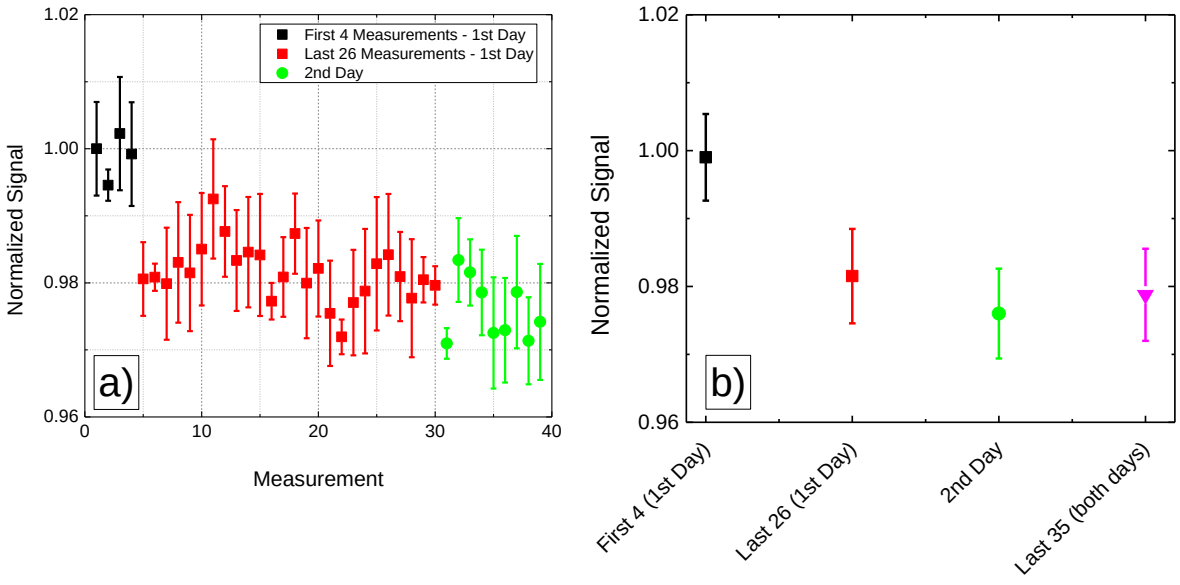

Figure 14 – GOx biosensor (Glutaraldehyde) stability. The stability was tested during two days and on totally 40 different measurements. a) All the discrete data of stability tests; b) Average data grouped by day and similarity.

Figure 14 (a) shows each measurement made and its evolution with time while Figure 14 (b) shows the average of first 4 measurements of first day, last 26 measurements of first day, 9 measurements of second day and the sum of the last 26 measurements of the first day plus the 9 measurements of second day.

The percentage difference between the average of first 4 measurements from the first day and the average of last 26 measurements from same day is about 1.8% (see Figure 14 (b). The percentage difference between average of last 26 measurements from the first day and the average of 9 measurements from second day drops to only 0.5% (see Figure 14 (b)). This experiment shows how robust and accurate the biosensor with GOx immobilized with GTA is during 39 measurements in two days. Even the biggest difference in measurements (1.8%) is considerably small for a glucose biosensor.

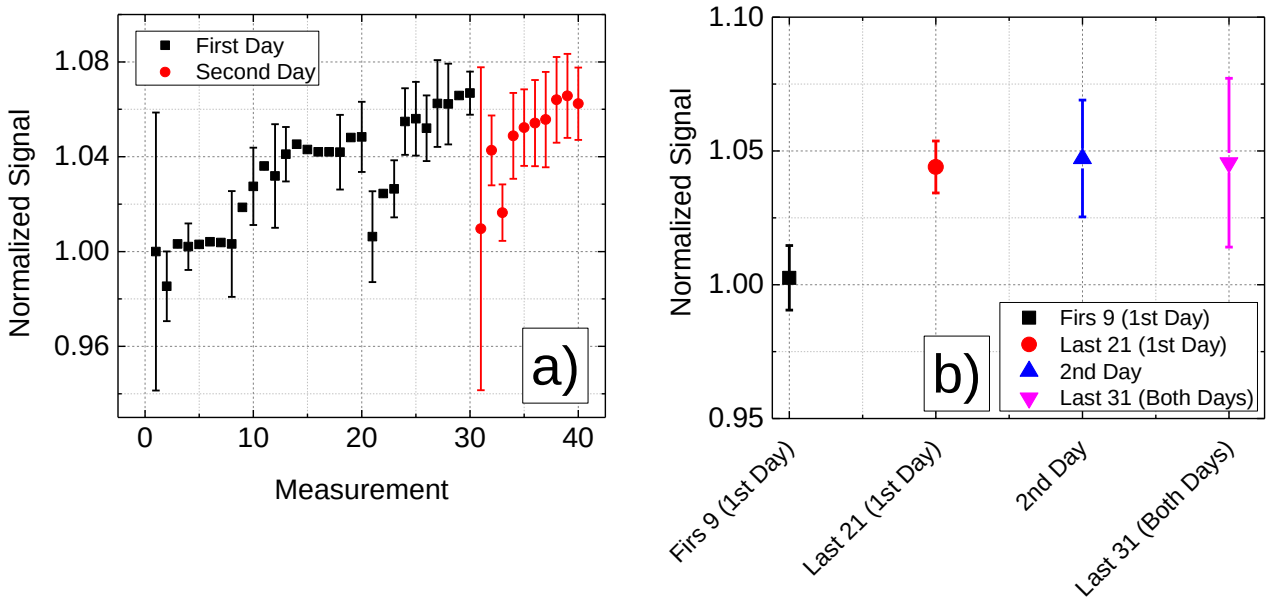

Figure 15 - GOx biosensor (Chitosan) stability. The stability was tested during two days and on totally 40 different measurements. a) All the discrete data of stability tests; b) Average data grouped by day and similarity

Figure 15 shows a case similar to that of Figure 14 but this time for GOx immobilized by chitosan. In this figure is clear the chitosan sensor is not as stable as GTA sensor. Through error bars in Figure 15 (a) is possible to see big variations among data. Thirty measurements were made on the first day and another ten measurements were made on the second day. Again, for a better discussion of these results, normalization was done with reference to the very first data collected.

Once more, if the error bars of Figure 15 (a) were disregarded, it becomes possible to group few data by signal similarity. The first nine points of Figure 15 (a) are similar. The other 21 points of the first day were grouped together as well as all the points of the second day. Doing these groups is possible to build the graphic of Figure 15 (b). It is very clear in Figure 15 (b) the cited signal similarity. After the first 9 points on the first day, the sensor changes its signal about 5%. However, this analysis is not accurate and should be considered just qualitatively. It is quite clear in Figure 15 (a) the big fluctuation among data points.

So, by comparison between Figure 15 and Figure 14 it become clear the sensor made by immobilizing GOx via GTA is more stable than the one made via chitosan. It is possible to go even further, saying the sensor immobilized via GTA is, at least, twice more stable than the sensor immobilized via chitosan.

It is important to notice to the first measurements for the day for the chitosan immobilization in Figure 15(a). The first measurement of the first day as well as the first measurement of the second day have, both, big error bars. In this case the glucose concentration was kept constant. The only difference between these measurements and the rest of the other measurements is the condition of the sensor previously to its use.

The sensor was stored in fridge. So, previously to the first use of the day it was totally dried. The first measurement helps to support the idea of the biosensor achieving the equilibrium state, just as discussed for the error bars in Figure13(a) above. However it is important to be clear that this is just a possibility and its confirmation needs more careful experiments to be done.

The characteristics of both biosensors (GTA and chitosan) presented above lead to two different possible methods of GOx immobilization on FTO thin film (see Figure 16).

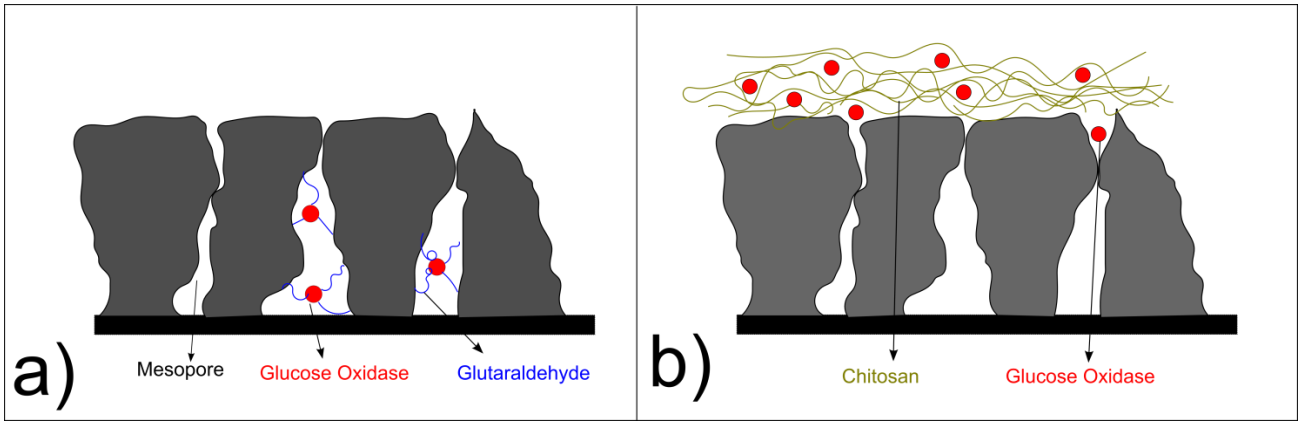

Figure 16 – The main GOx Immobilization processes. a) Via glutaraldehyde; b) via chitosan.

The use of GTA molecule as an immobilization molecule is because this molecule is very reactive. It can polymerize itself and can the aldehyde end of it can covalently bind to amine groups (present in GOx molecules). It is a very know reaction and it is widely used. [128, 129]

Figure 16 shows a schematic draw of possible process for GOx immobilization at both processes: in (a) for GTA and in (b) for chitosan. As known, GOx can easily bind itself to GTA molecule. Several GTA molecules can attach to a single GOx once the binding is made through a peptide bond between the aldehyde end of the GTA and a lysine group of GOx.

First the GTA penetrates on FTO mesopores (for IUPAC pores between 2 and 50nm – see immobilization process in section 2.2.1). Great part of GTA is still inside mesopores even after a fast water rinsing. Part of the residual GTA inside mesopores will then suffer polymerization. Once the FTO is immersed in GOx solution, it will penetrate inside mesopores and attach to residual aldehyde ends of a chain of polymerized GTA molecules. This is a covalently bound and GOx will now be stably attached to the FTO film (see Figure 16 (a)).

The GTA polymerization prevents its leakage to outside. This polymerization doesn't happen on FTO grains surface because there is no covalent bond between GTA and FTO. On the surface, GTA is in constant contact with bulk solvent which prevents the polymer to weekly bind to FTO surface. Otherwise, any polymer weekly adsorbed to FTO surface would be washed out from the surface by the rinsing procedure.

As seen in Figure 16 (b), the chitosan immobilization process is quite different than GTA. Chitosan is known to form a polymer as well. Its use is justified because chitosan is a very cheap biocompatible material and it can form a massive chain of fibers which will entrap the GOx molecule.

A viscous chitosan solution deposit the polymer on FTO surface. By diffusion GOx penetrates the chitosan matrix and fixes there. Deeper the penetration, more stable the immobilization will be. Unfortunately, GOx solution cannot penetrate as

deep as desired into chitosan matrix. Chitosan is hydrophobic and consequently GOx immobilization is superficial. During the sensing time few GOx molecules can be released from chitosan matrix. This generates instability in signal. Moreover, glucose molecule needs to diffuse inside chitosan matrix as well to reach the GOx enzyme. This diffusion process takes time once chitosan matrix is very low permeable to water.

Chitosan does not covalent bind to FTO. This sensor is built by casting process. In this process the chitosan solution is left to dry on the top of FTO surface. Chitosan polymer and FTO surface are weakly bonded by physiosorption. The same physiosorption will bond the GOx to the chitosan polymer matrix.

Figure 17 shows the response of a new experiment. On this experiment a sample runs three cycles. On each cycle the sample measures, for 30 minutes, KCl solution without glucose. The sampling rate is 2Hz. V_{DS} and V_{Ref} are fixed in 3 and 5 volts respectively. After this step solution is changed to KCl solution and a fixed sugar concentration that for GTA could be 3mM, 6mM, 9 mM, 12 mM or 15 mM. For Chitosan sensor the glucose concentrations could be 1 mM, 2 mM, 3 mM, 4 mM or 5mM. These concentration values are represented in Figure 17 (a) by ***"X mM"***. Its measurement had same sampling rate (2Hz) and same amount of time (30 minutes). Both measurements (0mM followed by XmM) complete one single cycle.

The same cycle was repeated 3 times for each sample. Moreover, a different new sample was used to measure different sugar concentration. So, each sample measured only one specific glucose concentration (see Figure 17 (a)).

An average value for the 90 minutes of measurement at a KCl solution with no glucose was then established for each sample. An average value for the 90 minutes of measurement on KCl with a specific glucose concentration was established for each sample as well. So, the average value for a specific glucose concentration was normalized by average value of KCl solution with no glucose. Adopting the same procedure for all samples was possible to build Figure 17 (b) for biosensor immobilized by GTA and Figure 17 (c) for biosensor immobilized by chitosan. These

two graphics can be considered as another form of building calibration curves for both immobilization methods.

It is interesting to compare Figure 17 (b) to Figure 12 (a) and Figure 17 (c) to Figure 13 (a). It is quite clear the linearity of Figure 17 (b) and Figure 17 (c) when compared to Figure 12 (a) to Figure 13 (a) respectively. The linear calibration curve is convenient once there is just one multiplication factor by which the response of biosensor should be multiplied to reach a corresponding glucose concentration as an answer.

Besides, it is possible to conclude from Figure 17 that GTA samples are more sensitive to glucose than Chitosan samples. This can be easily seen through the linear fitting slope value. For GTA samples it is 0.63 and for Chitosan it is 0.29.

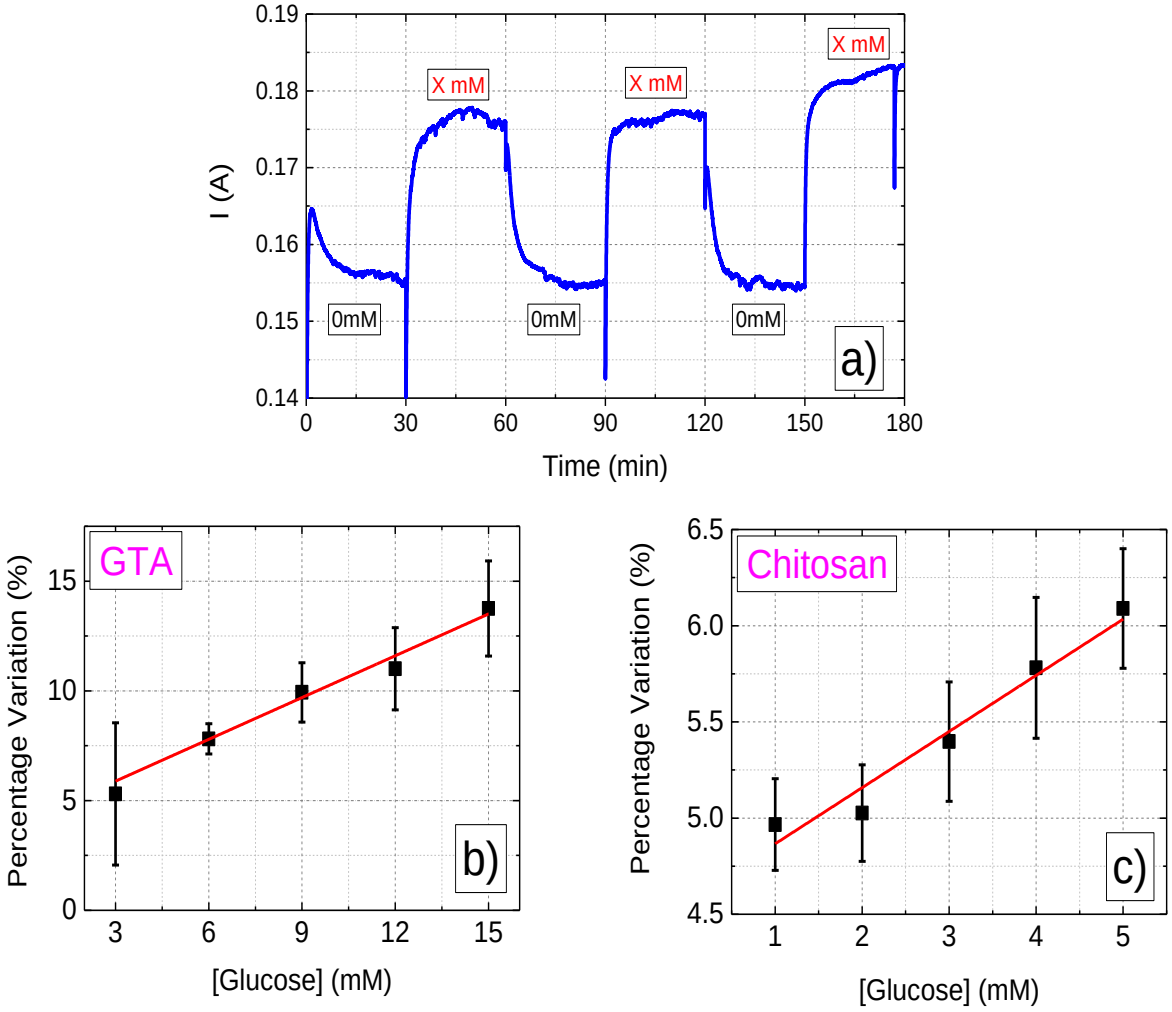

Figure 17 – Continuous measurement of fixed glucose concentration. a) Typical sign of this experimentation. Glucose concentration was varied always between 0mM and another different value. Each glucose concentration was measured by a different sample. b) GTA calibration curve for this experimentation. The slope of the linear fitting is 0.63. c) Chitosan calibration curve for this experiment. The slope of the linear fitting is 0.29.

It is of interest to know how the sensor would respond to a fixed glucose concentration value while the pH of electrolyte solution changes. With this experiment is possible to better understand pH dependence of the immobilized enzymes. The result of such experiment is shown in Figure 18. It is a complementary experiment.

One sample was used to measure all the pH values with a fixed glucose concentration of 8mM each. Three acidic pH values (4, 5 and 6) and 3 alkaline pH

values (8, 9 and 10) were used. Each one of the responses for any pH value was normalized by the reaction of the sensor to neutral KCl solution (pH 7) with the same glucose concentration of 8mM.

Both Figures 12 and 17 for Glutaraldehyde immobilization can be used as calibration curve. However the calibration curve of Figure 17 can be considered a more general and desired curve once it is normalized and consequently is immune to any triggering current variation. Moreover, its range is bigger and comprehends the human body glucose concentration range (between 3.9 and 10mM [23]).

Each pH value was measured for 30 minutes with V_{DS} and V_{Ref} of 3 and 5 volts respectively. The sampling rate for this acquisition was 2Hz. The data presented in Figure 18 correspond to the average normalized value of 3 different samples. The error bars correspond to the standard deviation of these values.

Figure 18 the GTA immobilization method GTA immobilization method. The red star point corresponds to the KCl solution response (normalization reference). Notice that in acidic electrolyte solution data is quite stable and, basically, all of these acidic pHs presented the same positive signal variation (around 20%). This suggests the signal is already saturated even for slightly acidic electrolyte solutions at pH 6.

The positive variation for acidic pHs was expected once for these pH values the number of free H^+ ions is greater than on pH 7 KCl solution. This ion is the main responsible for varying potential on the surface of FTO sample. Improving this number, surface potential improves as well.

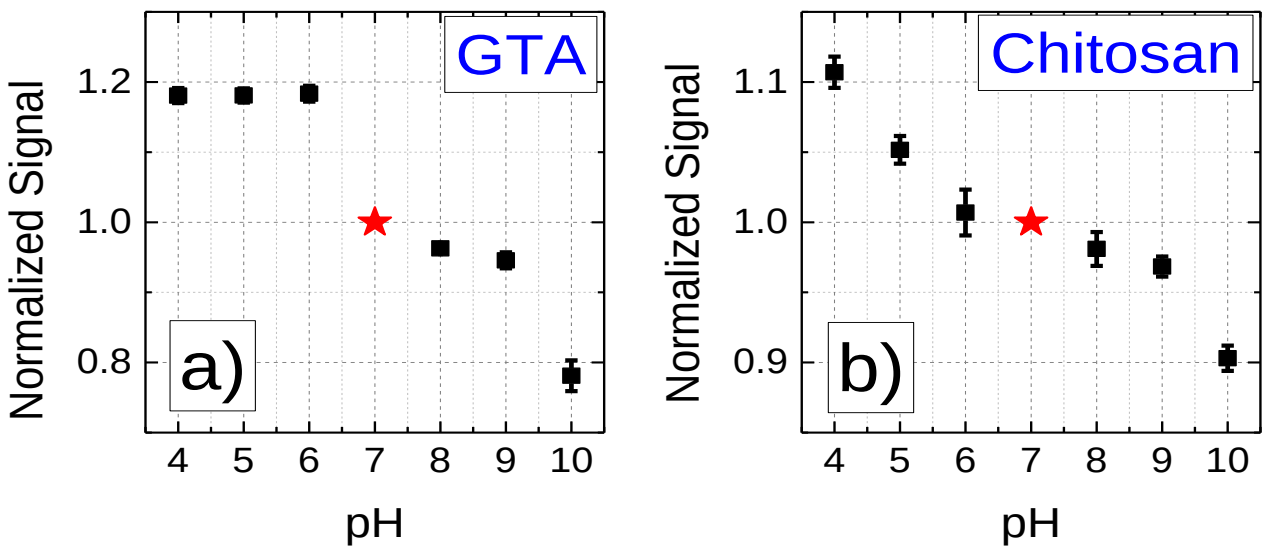

Figure 18 – pH variance experiment. At this experiment the pH of electrolyte solution was varied and the glucose concentration was kept constant in 8mM. All the data are normalized taking as reference the measurement of KCl solution pH 7. a) Response to the pH variance experiment for GTA immobilization method. b) Response to the pH variance experiment for the Chitosan immobilization method.

For alkaline electrolyte solutions signal is not completely saturated for pH values slightly alkaline like 8 or 9. For this type of electrolyte solution the potential variation is always negative, suppressing the signal if compared to KCl pH 7. This characteristic is expected once for alkaline solutions there is a smaller number of H^+ free ions in solution and, consequently, electrical potential decreases. Besides, alkaline pHs can alter enzyme activity as well. At those value GOx activity decreases. Figure 18 (b) shows signal variation changes for the Chitosan immobilization method. Once more, the red star on this figure represents a KCl solution pH 7. For alkaline pHs signal is suppressed when compared to neutral solution and for acidic pHs signal is raised. The explanation is exactly the same as for biosensor with the GTA immobilization method.

The interesting aspect to be noticed in Figure 18 (b) when compared to Figure 18 (a) is that Chitosan immobilized sample variation for acidic pHs doesn't achieve the same levels as GTA immobilization method samples. The maximum variation for chitosan samples at pH 4 is around 10%, just a half of the variation of GTA sample

for pH value of 6. This corroborates the idea that GTA sample is more sensitive to glucose than Chitosan sample.

Qualitatively, Chitosan samples have the same behavior as GTA samples for alkaline solutions. However, the variation values (and consequently its sensitivity) still smaller for Chitosan samples.

A final analysis can be obtained by calculating the apparent Michaelis-Menten [127,130–133] constant (K_m^{app}) which can be calculated from Lineweaver-Burk equation [130–133], shown below:

$$\frac{1}{i_{ss}} = \left(\frac{{k_m}^{app}}{i_{max}}\right)\frac{1}{C} + \frac{1}{i_{max}} \qquad (24)$$

In equation 24, i_{ss} represents the steady-state current after the addition of substrate, C represents the bulk concentration of glucose and i_{max} represents the saturation current. K_m^{app} indicates the kinetics for the biosensor. This equation can be linearized by $y = a + bx$, where $\frac{1}{i_{ss}} = y$, $\left(\frac{{k_m}^{app}}{i_{max}}\right) = b$, $\frac{1}{C} = x$ and $\frac{1}{i_{max}} = a$. The linearization can be analyzed by graphic as in Figure 19.

According to the linearization shown in Figure 19, K_m^{app} for chitosan is 0.16 ± 0.01 mM and for GTA is 0.16 ± 0.01 mM. The values found in this analysis are much lower than others already found in previous works (4.58mM for Wang et al. [130], 14.4mM for Zou et al. [133],10.73mM for Chu et al. [134] and 1.91mM for Lee and Chiu [131]). Besides, it is comparable to other value found by Kouassi et al [135] of 0.208 mM. The Product Information sheet (from Sigma) notifies that the solution Km for this enzyme is between 33~110mM. As reported the litereature, small K_m^{app} values represent a high biological affinity to glucose by enzymes.

The value found for GOx Km in solution is much higher than any other value presented for immobilized GOx. This is not alarming at all once is widely known immobilization can improve some characteristics of the enzyme. It is acceptable the immobilization processes performed in all works cited from literature and specially the ones demonstrated here could improve this characteristic of the enzyme.

Notice that the K_m^{app} values found in this work seems to be very small. However it should be kept in mind that this constant represents the enzyme affinity to glucose in the range the biosensor works. So, the main message transmitted by this constant is that the biosensor has a high affinity by glucose within the range it is supposed to work.

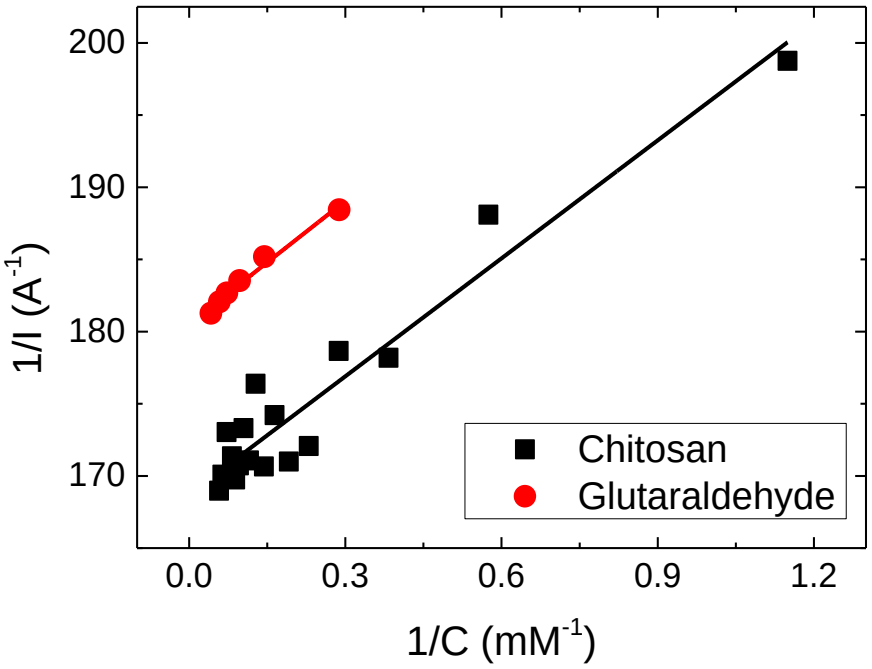

Figure 19 – Lineweaver-Burk linearization for apparent Michaelis-Menten constant calculation. In black, glucose biosensor immobilized by chitosan. Its slope was calculated by linearization and is equal to 27.24. In red, glucose biosensor immobilized by GTA. Its slope was calculated by linearization and is equal to 28.39.

Few questions about the interaction between GOx and surface still open. For example: how much GOx is immobilized in the surface from the solution? Or, how the change in pH solution during the GOx immobilization can change the quality of the final biosensor?

New experiments are necessary to answer these questions. For example, to know how much GOx was immobilized on the surface of the sensor it is necessary to perform the Bradford method. This is an experiment not performed to this work, though.

To answer what is the influence of changing the pH of the immobilization solution, new immobilizations need to be done and compared to the presented data. This is another experiment not performed in this work.

2.4 – Chapter Conclusion

In this chapter was presented two different micro/nanostructured glucose sensors. They were designed to make glucose measurements in solutions. Moreover, they have a real potential to become a continuous glucose sensor.

The main difference between the two sensors is the GOx immobilization technique: one used GTA and the other chitosan. The GTA glucose sensor presented a detection range between 3mM and 15mM of glucose in solution. The chitosan glucose sensor presented a detection range between 1mM and 5mM of glucose in solution.

Recent FET devices have reported glucose concentration range of 0mM to 25mM [131], 20μM to 100μM [136] and between 1nM to 100mM [137]. Moreover, the biosensors reported in this work can be considered having a high affinity with glucose as shown by K_m^{app} values found (0.161 mM for chitosan and 0.157mM for GTA).

Chapter 3 –

Glucose sensor:

intracellular Measurement

3.1 Introduction

Nanopipettes are tiny pipettes with pore diameter at nanometer scale. These devices can be made of quartz capillary glass. The capillary heated by a laser beam get soft and the two opposite ends of the capillary are pulled apart (at controlled conditions) to form nanopipettes.

Being so small, one can use these nanopipettes to penetrate cell bio-layer with such a small injury the cell is kept alive during and after the interrogation. This, by itself, is already a great advantage for nanopipettes when used as described. Other kinds of interrogation of cell physiology as patch clamp[138], for instance, are very precise and can sense very small signals. Nevertheless, the cell suffers such a great injury on this technique, it can't survive after the experiment.

Nanopipettes were already used to image a cell as a scanning ion conductance microscopy technique (SCIM)[139–141], make detection of proteins[142], carbohydrate[143] and DNA molecules[144]. Further than that, nanopipettes were already used in a procedure named "nano-biopsy"[145] which consists on going inside a single cell and take a sample of its cytoplasm and another procedure named injection which consists on injecting a solution with different molecules (such as DNA[139] or tRNA[146] for example) inside a cell.

Interrogation at such level can bring a more detailed comprehension of how the cell machinery works. It is known that sugar levels need to be fixed at a specific range in the human blood so its physiological functions can be kept equilibrated.[147] Besides glucose is one of the most important biomolecules at cell physiology which the path we still not fully comprehending. This is exactly the path used for several cancer treatments to attack the cells though.

For a fuller comprehension on glucose path it is necessary a tool at the dimension of a few microns or nanometric scale. Sensors at those dimensions are very few. Bigger sensors are more common. Nevertheless, although some of them

presenting interesting sensitivities and potential to be miniaturized, they do not demonstrate good answers at cell or blood environment[148–152].

In this chapter, a nanopipette is shown as a tool for single cell interrogation. More specifically, the nanopipette is shown as a glucose biosensor. To demonstrate its use, three different types of cells were used and free glucose concentration inside single cells will be presented.

3.2 Material and Methods

The nano-biosensor presented in this work makes use GOx from *Aspergilus Niger* as well. D-glucose was purchased from Sigma. An important factor showed in Figure 7 but not yet commented is the recycle path that GOx needs in order to catalyze the reaction of another D-glucose molecule.

To oxides glucose, GOx molecule needs to suffer reduction. At such a step, GOx cofactor **FAD** is transformed on its reduced form **FADH2**. If the cofactor does not go back to its previous form, GOx is unable to catalyze another glucose molecule. The cofactor recycling process is made through its oxidation. To accomplish this task it is necessary that another molecule suffer chemical reduction. So, Oxygen is reduced when it is used in Oxygen Peroxide molecule (see Figure 7). The problem with this natural reaction is that oxygen can be consumed really fast and becomes a limiting factor for the entire reaction. To avoid such problem we added 10mM Ferrocene (Purchased from Sigma) in 100mM Phosphate 100mM KCl Buffer solution. The ferrocene just plays the role of the Oxygen molecule in the recycling process of FAD, not modifying any final molecules of interest.

Notice that the Ferrocene used for nanopipettes wasn't necessary for the EGFET platform once this other system uses a huge volume of solution compared to the area of the biosensor. In this case, the amount of oxygen in solution is more than sufficient to perform the experiment.

All this chain reaction does not affect the FTO sensors, though. This is because the electrolyte solution for FTO samples has a high volume compared to electrolyte solution used inside a nanopipette. At this high volume the Oxygen quantity is more than necessary to perform the entire experiment.

As already shown in previous work, the main nanopipette's region that modifies its current rectification is the very end of its tip. [153] Charges accumulated on nanopipette's tip are placed on a very small space. The tiny space between the charge carriers makes the electric field very high in this nanopipette's region. Such a high electric field shields the new carriers of a specific sign originating nanopipettes rectification pattern. [143,153]

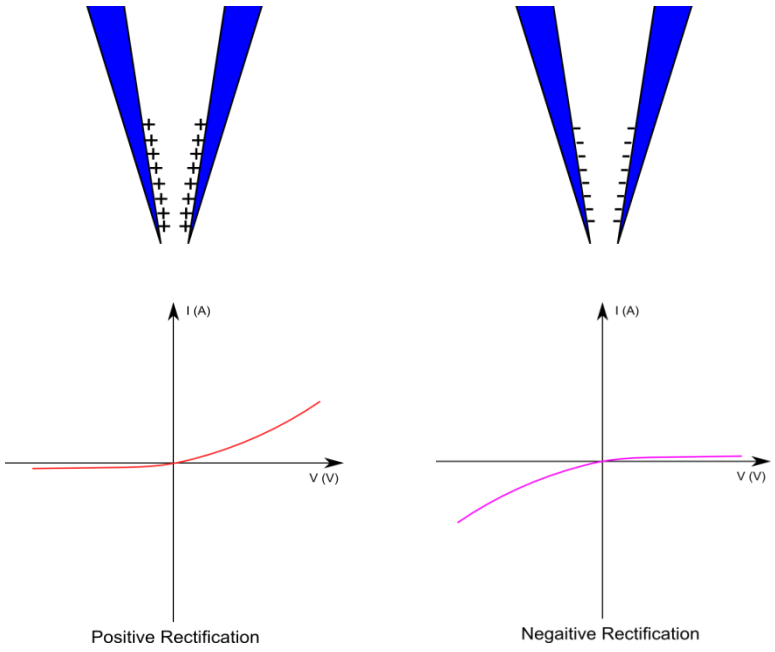

Figure 20 – Pipette's charge and its consequent current rectification pattern.

Figure 20 shows the rectification pattern for each one of the charges sign accumulated on inner nanopipette's walls. As already discussed elsewhere [153,154], the electric potential is responsible for current-voltage response. Moreover, it was shown the intern charges of the nanopipette walls play a very important role in the electrical potential and consequently in nanopipette response.

The nanopipettes were produced pulling apart quartz capillary glass of 0.7mm inner diameter and 1.0 outside diameter (bought from Sutter) at a P-2000 pulling machine (from Sutter). The pore size is around 120nm in diameter.

As a standard procedure for all experiments, 5 minutes before any run, cell plate was rinsed with PBS and the media to fresh filtered media. This plate would then go back to the incubator and left to rest.

For experiments, three different cell lines were used. One is normal cell **Human Fibroblasts** and two breast cancer cell lines: **MDA-MB-231** and **MCF7**. All cells were cultivated in normal DMEM cell media in the presence of glucose (25mM), 10% Fetal Bovine Serum and antibiotics (Penicillin and streptomycin). Part of the experiments used the same normal DMEM media. Another part of experiments used glucose free DMEM media with 10% Fetal Bovine Serum and antibiotics.

To image the cells an inverted microscope Olympus IX 70 was used with an eyepiece camera (AM4023X Dino-Eye) attached to it. The nanopipette was fixed in a holder (Axon Instruments, Union City, CA) which contained a measurement Ag/AgCl electrode connected to it. The holder was connected to an Axopatch 200B amplifier (Axon Instruments). The amplifier was set to current-clamp (clamped at 1nA) mode with a signal filter at 1kHz bandwidth. The signal was further digitized by an Axon Instruments Digidata 1320A. The data were then recorded by a LabView 9.0 home-made software.

3.2.1 Nanopipette Functionalization

Pulled Nanopipettes were functionalized with the steps as follows (see Figure 21 (a)):

i. **First Poly-l-lysine (PLL - 0.1% solution purchased from Sigma) is attached to the inner walls of nanopipette, as previous work described.** [154] **Nanopipettes were back filled with 0.1% Poly-l-lysine solution and spun for 30 seconds to ensure solution reached the tip. The nanopipettes were then baked at 120ºC for 90 minutes.**

ii. **Next step is to attach Glutaraldehyde (GTA - 25% solution from Sigma) to the walls. To do that the purchased GTA was diluted in water to a 10% GTA solution. Nanopipettes were then backfilled with this solution and spun for 30 seconds. The nanopipettes were then left to rest at room temperature for 90 minutes, followed by water rinse (back filling the pipettes with water, spinning for 30 seconds and then aspirating the excess with a vacuum pump).**

iii. **The final step consists of putting the GOx on the walls. A solution of 6mg/ml was then prepared with 100mM phosphate + 100mM KCl Buffer pH7.4. Nanopipettes were backfilled with this solution and left to rest at room temperature for 3 hours or in the fridge overnight. To finalize the nanopipettes were rinsed with water again.**

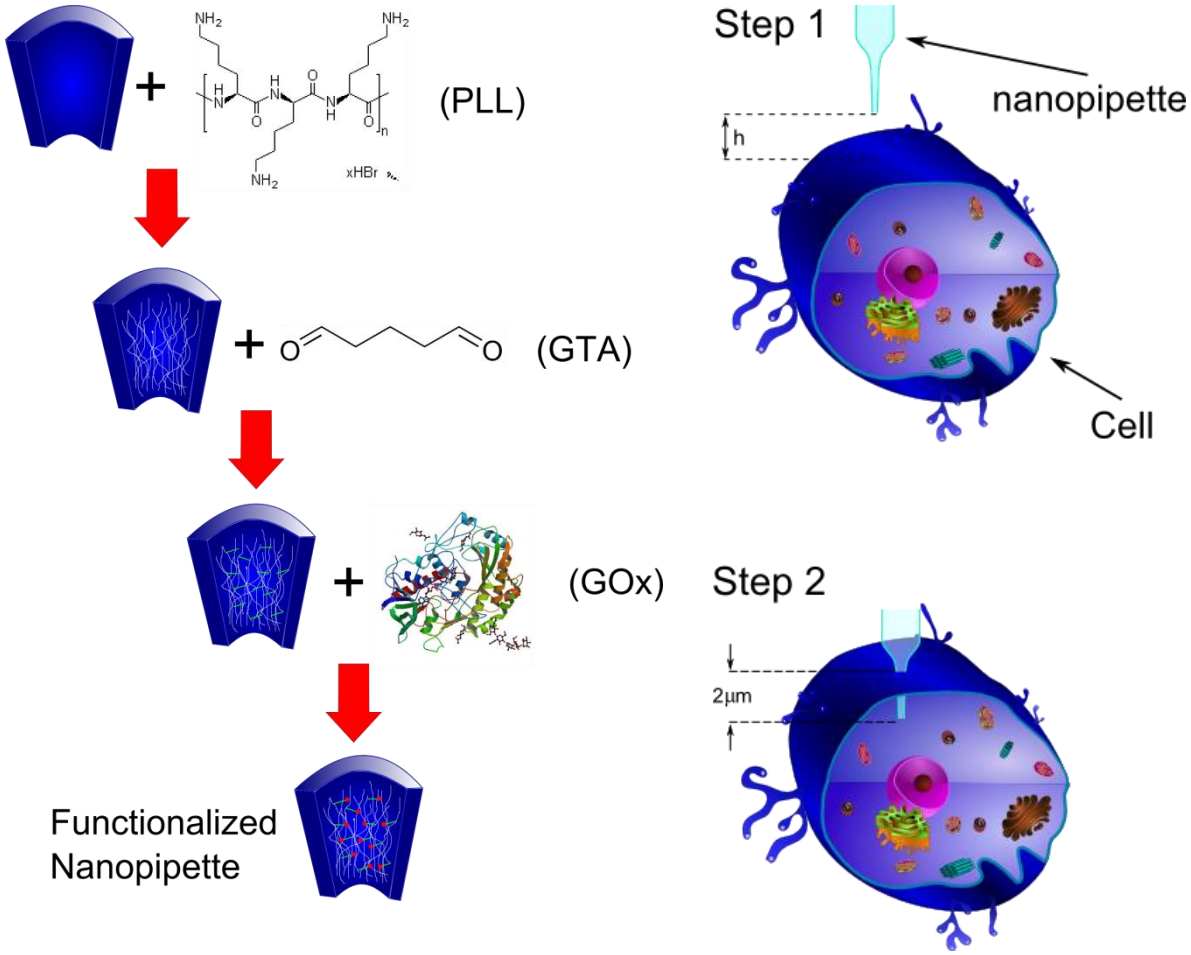

a) **b)**

Figure 21 – Nanopipettes preparation and cell experimentation. A) Nanopipette functionalization process; B) Signal Acquisition by a nanopipette.

Figure 21 (b) shows a very simple schematic of measurements made. On the top of the figure is possible to see a nanopipette outside the cell. This represents an extracellular measurement made in cell media with living cells present. Bellow, it is possible to see the nanopipette tip already inside a single cell. In both scenarios cell media (outside) was changed: part of the experiments was done in glucose free cell media and another part of experiments were done in normal cell media (25mM glucose).

3.2.2 The experiment

The entire experiment consists on start the measurements outside the single cell at a certain distance **h** (as can be seen on top part of Figure 21-B) from it. The nanopipette travels and then the entire distance h plus a pre-defined distance of 2 micrometers, reaching then the interior of the target cell. The nanopipette is kept inside the target cell for a pre-defined time of 60 seconds. After this time, the nanopipette gets back to the previous place at a distance h from the cell. This entire nanopipette withdraw is recorded too. As consequence of such an experiment one can expect to find a signal similar to Figure 22bellow.

All signals acquired during experiment consist on current vs. potential pair. So, the response can be directly associated to the pipette impedance. To understand the signal one needs to keep in mind that the reference electrode is always kept outside the cell at the cell media environment. Based on this reference the impedance inside a single cell is greater than outside. Likewise, once the current is clamped, the

potential inside a single cell needs to be greater than outside too, as one can see in Figure 22.

There are two different events that are characterized by signal pattern. First, if the nanopipette doesn't penetrate the cell its signal does not present any change. Second, in case nanopipette breaks, the current signal would suddenly increase dramatically and irreversibly, indicating the pore is too big.

To find an optimal insertion depth a batch of experiments was done and the best distance of 2 micrometers was defined to be the best choice (data not presented).

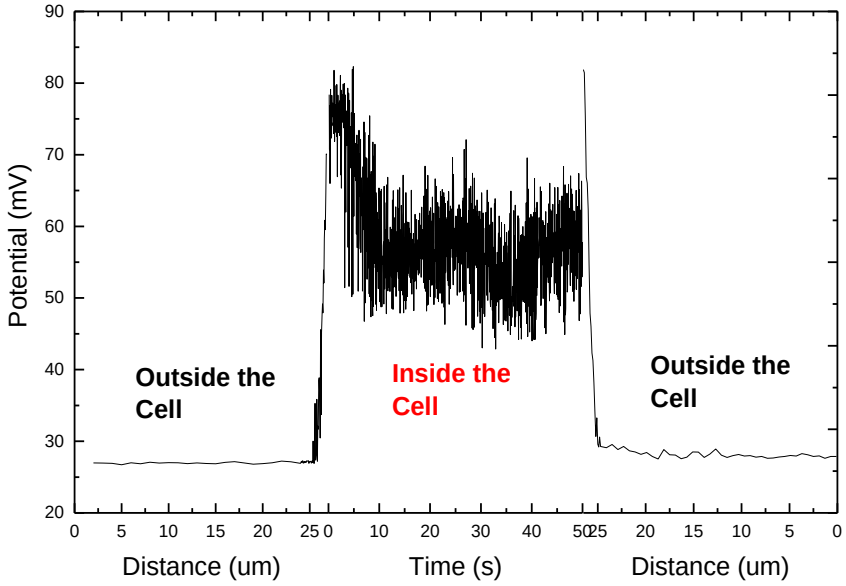

Figure 22 – Complete course of a pipette during a cell measurement

There is no consensus on the value of free glucose concentration inside a single cell. Different groups and techniques were employed to attempt to resolve this trouble. The only agreement, though, is that this concentration is very low when it is not negligible [155–158]. Some articles claim about a different intracellular glucose concentration range at a maximum of 2mM[159], 3mM[160] or even more [161] at special or odd occasions.

3.3 Results and Discussion

A functionalized nanopipette was tested on buffer solution with different glucose concentrations (Figure 23).

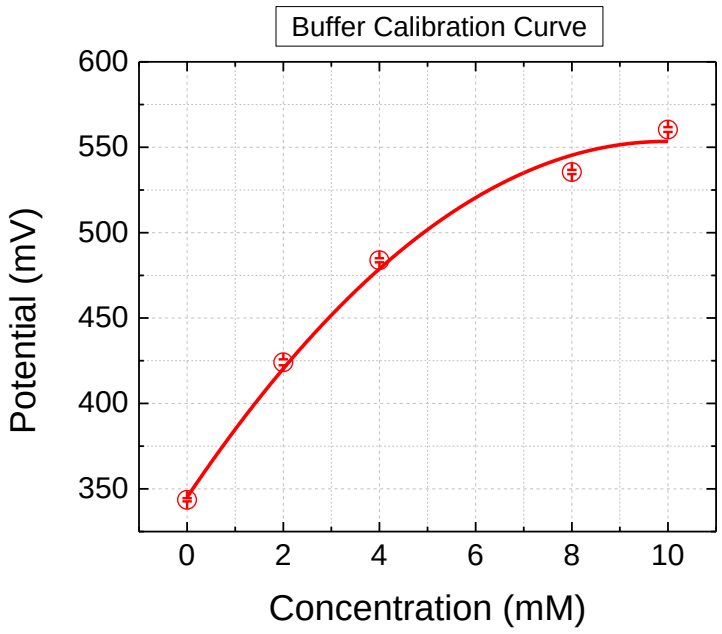

Figure 23 – Calibration curve for a functionalized nanopipette in buffer solution.

The range of most interest is, initially, one that included the majority of values previously reported for intracellular glucose concentration (until 5mM). At phosphate buffer nanopipette presented a reliable range from 0 to 10mM of glucose concentrations. The error bars on graph refers to the standard deviation of data. The fitting was performed with a second order polynomial equation and the R2 for such curve is 0.99107.

The same analysis was tested with a non-functionalized nanopipette (what we call **bare nanopipette**). This nanopipette didn't show a response as function of the

glucose concentration as see in Figure 24. According with both tests in buffer solution one can conclude that GOx was successfully functionalized at pipette tip and it presented the expected behavior on presence of glucose.

Despite the success in using nanopipettes on buffer solution we still require to prove nanopipettes can work in cell media. Thus a functionalized nanopipette was used to build a calibration curve on cell media (DMEM). The outcome of this experiment is shown in Figure 25.

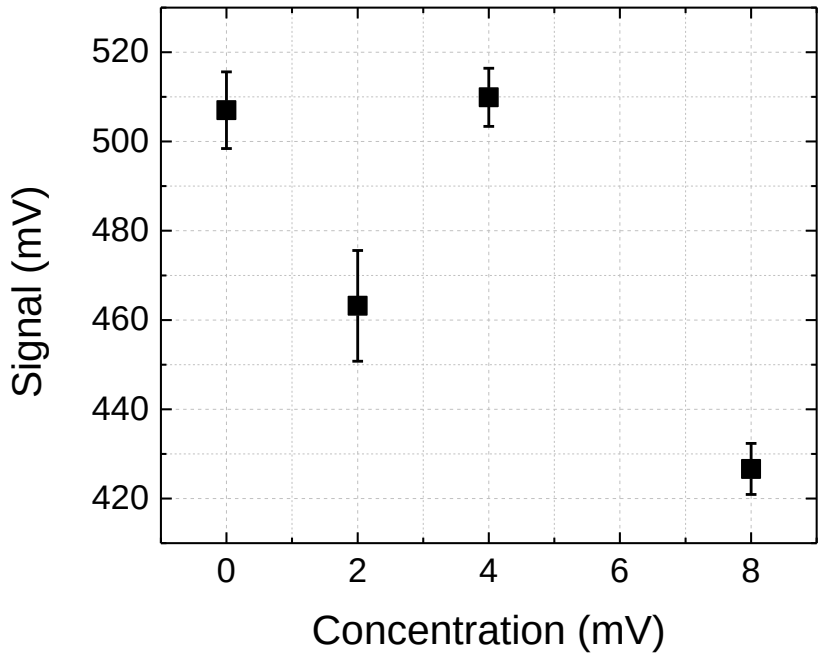

Figure 24 – Calibration curve for a not-functionalized ("naked") nanopipette in buffer solution.

As one can see in Figure 25, the signal range is quite smaller than the calibration curve in buffer solution (see Figure 23). This can be explained by the conductivity of environment where the pipette is inserted. The cell media has a less conductivity than buffer solution. However, biosensor behaves similarly in both cases.

The fitting equation used for the data in Figure 25 is a second order polynomial equation again, but the detection limit is smaller for cell media at the concentration of 8mM. The R^2 for such fitting is 0.99958.

An important detail that should be noticed is that functionalized pipette used to collect data of Figure 25 was used, before its functionalization, to collect data from Figure 24. So, as one can find out, this is another prove the functionalization works as planned.

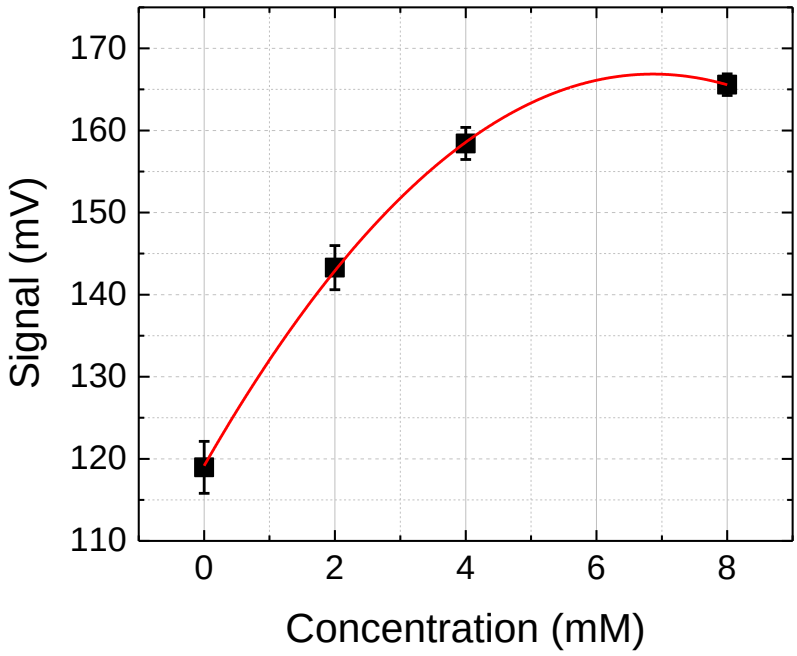

Figure 25 – Calibration curve for a functionalized nanopipette in Cell Media.

One final test was used to prove bare pipettes cannot sense glucose. In this experiment naked pipettes were used to sense 3 different fibroblast cells. A direct comparison of signal inside and outside cells was made and the result is shown in Figure 26. In this graph different symbol shape represents different cells. Fully painted symbols represent signal outside a cell. On the other hand, empty symbols represent signal inside the cell. The error bars shown represent the standard deviation.

It is quite clear the lack of patterns of response of a naked nanopipette in Figure 26. This is consequence, again, of bare nanopipette insensibility to the environment. Figure 26 yet suggests there is no appreciable ion difference (in charge quantities) between inside and outside a single cell. This is because such a nanopipette does not recognize any specifically molecule and its signal is similar in both cases. Moreover, the nanopipette signal depends on the charges present in the media, what suggests intra and extracellular media are similar to this question.

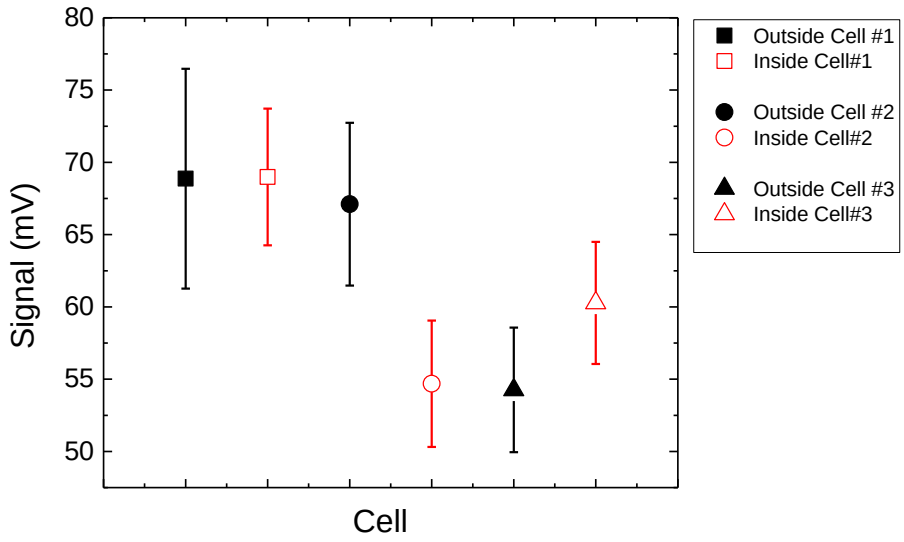

Figure 26 – Cell Measurements with a bare pipette.

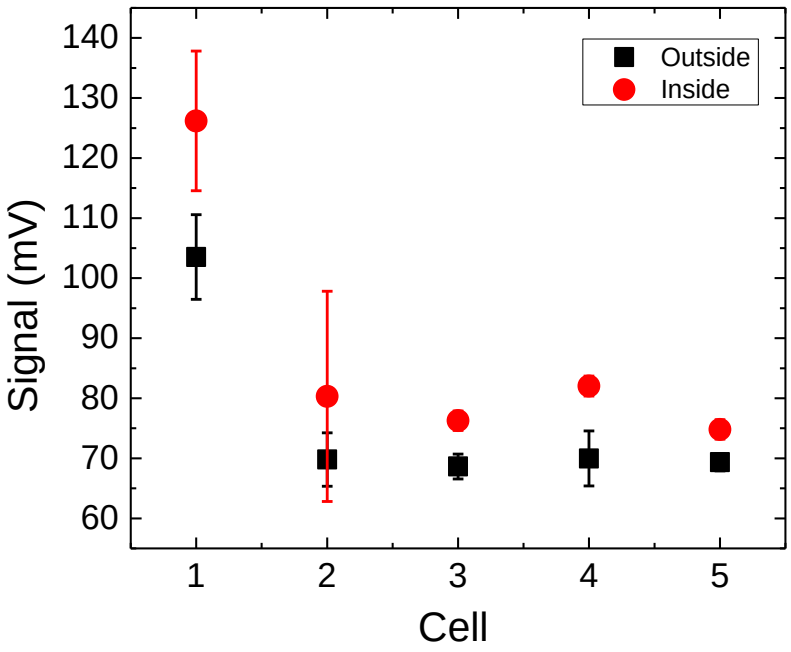

Figure 27 – Cell measurement with a functionalized pipette.

Figure 27 shows the result of the same experiment that resulted in Figure 26 but now with a functionalized nanopipette. It is possible to notice a pattern behavior present in this figure. The signal from intracellular media is always bigger than extracellular media. Analyzing both Figures (24 and 25) is possible to conclude that a functionalized nanopipette is sensitive to changes in media – inside and outside the cell. This can be explained by the fact that the diameter of the hollowed channel inside the pipette is smaller on functionalized nanopipette than in bared nanopipette. Being smaller the pipette should present a bigger impedance and consequently even a small change in ion concentration would be sensed. The bigger impedance of functionalized pipette is shown indirectly in Figure 27. If Figure 27 and Figure 26 are compared, it should be noticed that for intracellular measurements the potential applied is greater, which is a consequence of higher impedance.

In Figure 28 is possible to see a nanopipette in action. These pictures were taken during a real measurement of two fibroblast cell. On Figure 28 (a) and (d) nanopipette approaches the target cell number 1 and 2 respectively. Figure 28 (b) and (e) nanopipette is acquiring data from inside a single cell (number 1 and 2 respectively). In Figure 28 (c) and (f) nanopipette already finished its measurement

and is away from the cells. The circle inside both figures indicates the region where the pipette has penetrated the cell. Note it is not possible to find out any hole or wound on the cell membrane in both cases. This is a strong argument together with the cell normal life observation after the measurement towards the affirmation this technique does not hurt the cell significantly because the small size of the nanopipette.

A direct comparison between intracellular signals from different cell types can reveal interesting understanding about their behavior. Figure 29 shows an intracellular signal collected during 60 seconds inside six cells of fibroblasts (in red) and another six cells of MDA-MB-231 (in black). All twelve cells used in this experiment were measured using the same nanopipette. Two interesting characteristics should appeal ones attention on this figure: the signals do not cross one to each other, and signals coming from fibroblasts are more uniform than signals from MD-MB-231.

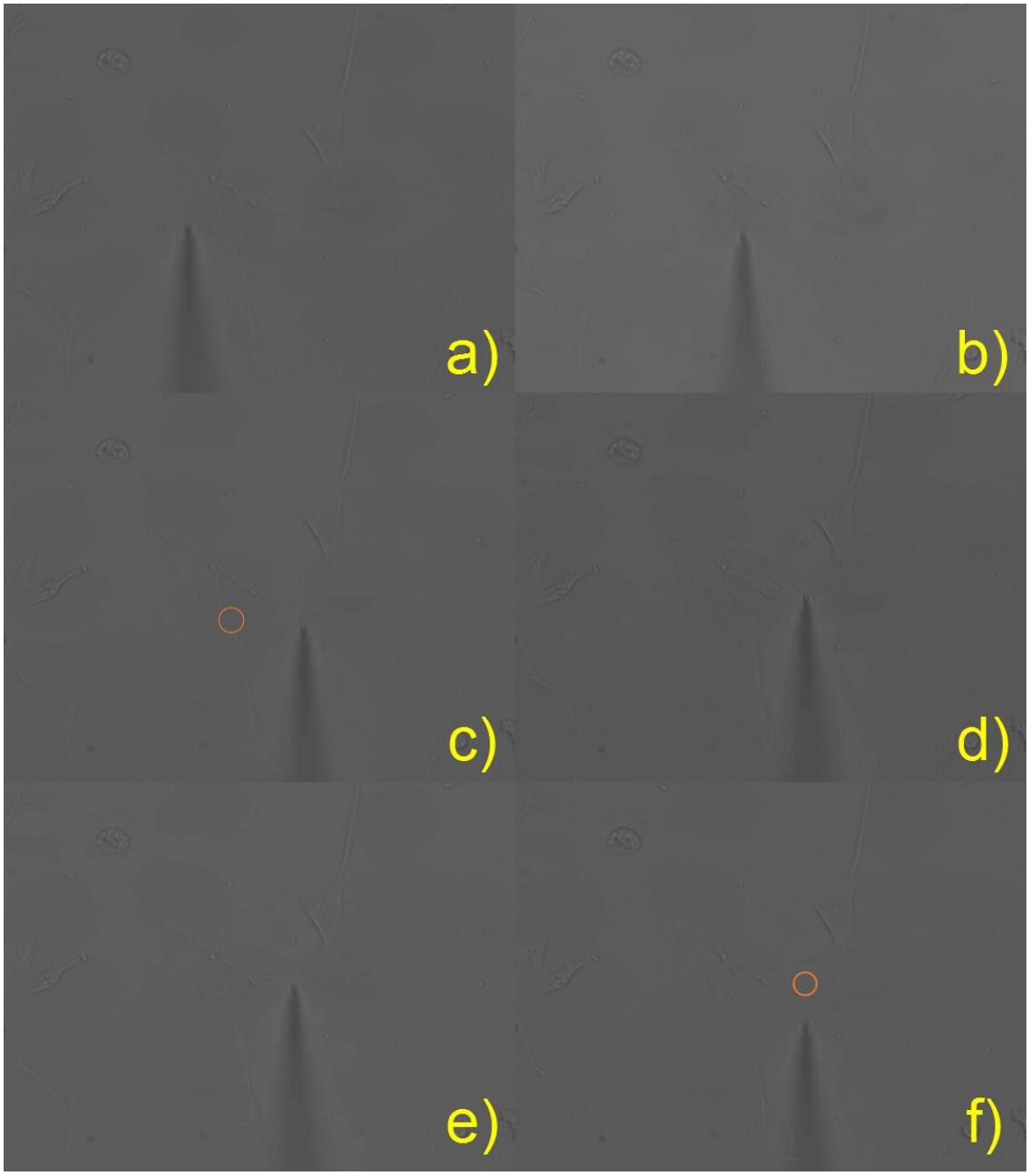

Figure 28 – Optical Microscopy of nanopipettes penetrating fibroblast cells. a) approaching cell number 1; b) Nanopipette inserted to cell number 1 during measurement; c) nanopipette away from cell number 1; d) approaching cell number 2; e) Nanopipette inserted to cell number 2 during measurement; f) nanopipette away from cell number 2;

The fact that the signals do not cross with each other will be further discussed. Keeping the same measurement parameters for all cells, fibroblasts have shown much more close results than MDA-MB-231. The more dispersive behavior of MDA-MB-231 cells in this experiment can be explained by the fact that cancer cells as

MDA-MB-231 are more heterogeneous than normal cells (as fibroblasts for instance). It is well known cancer cells mutate themselves very fast, random and in an uncontrollable way besides consuming a bigger quantity of glucose due to it. This generates a very heterogeneous population when compared to normal cells. One can even go deeper and claim that such heterogeneity is one of the keys to understand the cancer cells' resistance and further recurrence of some kinds of cancers during and after the treatment protocols been applied.

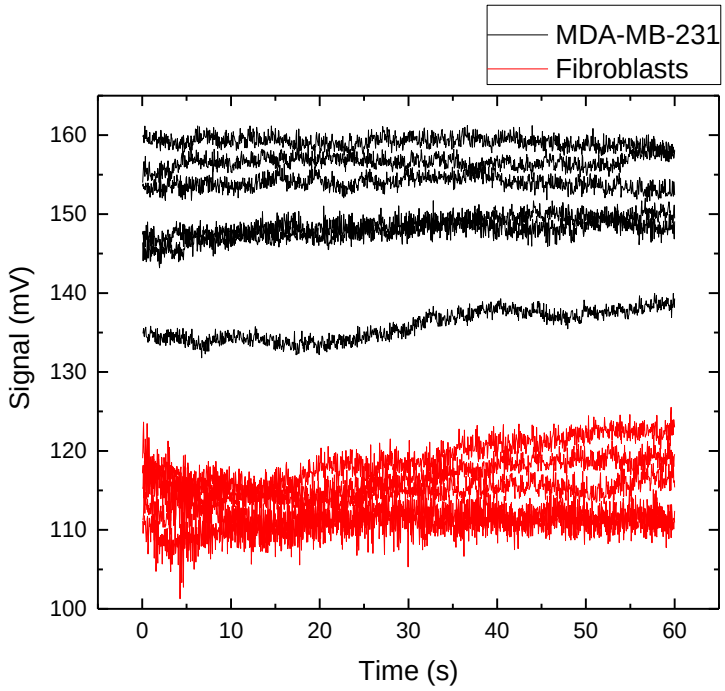

Figure 29 – Signal difference between six individual cells from two different cell lines: human fibroblasts and MDA-MB-231.

On the other hand, fully functional cell machinery – as occurs in normal cells – keeps the similarity among individual cells. When a normal cell figure out a harmful mutation, its normal reaction is try to fix it. If it cannot fix the problem the cell achieve cell's death pathway and kills the abnormal cell. This chain of reaction guarantees a more homogeneous and healthy population and consequently a less

glucose consumption which explain why normal cells present a clustered set of response to the experiment in addition to a smaller signal after all.

In a direct comparison between intracellular signal of different cell lines would be natural to expect – with the ideas presented until now – that more aggressive cell lines present a bigger signal than less aggressive cancers and even normal cells. Such comparison is shown in Figure 30.

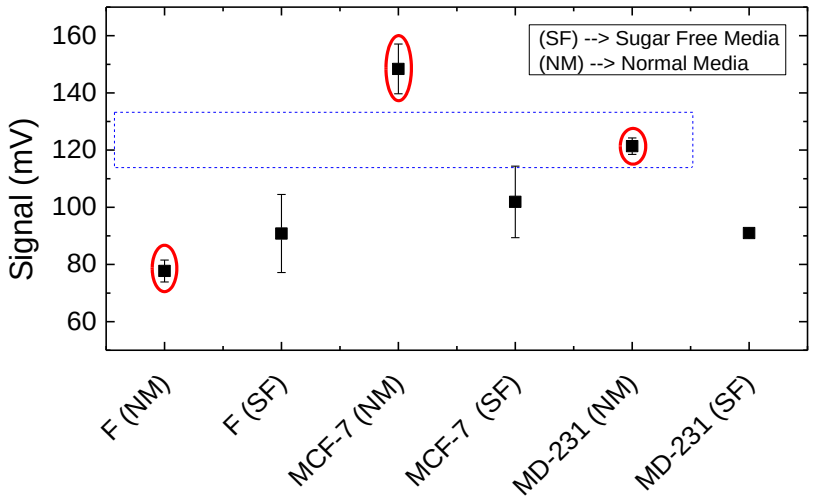

Figure 30 – Inside signal comparison between different cell types and different media. This figure has the followed legend: NM = Normal Media; SF = Media Glucose Free (Sugar Free); F = Human Fibroblasts; MCF-7 = Cancer Cell line MCF-7; MD-231 = Cancer Cell line MDA-MB-231.

Figure 30 shows the average signal of groups of five cells each. There are three different cell lines that were used on this experiment: human fibroblasts (representing normal cells); MCF-7 (cancer cell line); MDA-MB-231 (very aggressive cancer cell line). For each of these cell lines two groups of cells generated two experiments: one when the cell was in normal cell media and another one when the cell was in glucose free media.

Once in glucose free media, the three different cell lines didn't show big differences between their signals. This can be explained by the fact that cells need to keep homeostasis by burning glucose. If there is no more glucose in media to supply the cell, all free glucose there was inside the cells as stock, now would be consumed

or ready to be consumed at phosphorylated form. The GOx does not recognize glucose-6-phosphate by itself [162,163]. The phosphorylated form of glucose is exactly the type of glucose most common inside cells[158] and the form of glucose needed for cell respiration[164]. Thus, one can assume that the five minutes cells were left to rest before experiment begin were enough for cells, of all lines used, to consume their stored free glucose. Some improvements on functionalization process can lead the nanopipettes to sense glucose-6-phosphate in the future.

Another possible analysis can be made considering each cell line separately for two different media used: normal cell media and glucose free media (see Figure 30). Hence, is possible to observe that Human Fibroblasts did not express significant difference between their signals for different media. Once there is glucose free media considered on this discussion and intracellular signals for both media are not significantly different, this suggests that glucose concentration inside Human Fibroblasts is really low. If a comparison between the signal of fibroblasts in Figure 30 and bare nanopipettes in Figure 27 is made, it should be noticed that there is no significant difference as well. This should corroborate the result of a small concentration of intracellular glucose.

Analyzing cell line MCF-7 is possible to see an expressive signal difference between normal media and glucose free media. This difference suggests there is a significant concentration of free glucose inside this cell line. It is not possible to quantify such concentration by this figure, but is possible to assure its intracellular free glucose concentration is higher than fibroblasts' intracellular free glucose concentration. This exactly same discussion can be extended to explain the signal from MDA-MB-231.

Comparing data of all cell lines in normal media, a different pattern is found. As said before, it is believed the concentration of free glucose would be directly linked with cell activity. This would lead us to a small glucose concentration in normal cells and greater concentration for cancer cells. Among cancer cells, glucose concentration was expected to be bigger as bigger was their aggressiveness. Nevertheless, this idea was not completely confirmed by data. As shown in Figure 30, cancer cells have a bigger signal than normal cells but, regarding aggressiveness,

most aggressive cancer cell line MDA-MB-231 has a smaller signal than MCF-7. This response pattern was confirmed by the same experiment made with other functionalized nanopipette as shown in Figure 31.

Basically, there are two explanations that should be investigated in the future to elucidate this phenomenon. First relies on cancer cell physiology: more aggressive cell is, greater should be its power supply. The power supply is glucose-6-phosphate and not glucose free form. Unfortunately, as already said, our sensor is not able to sense such form of glucose. A second possible explanation relies on the sensor's response components. In this case the sensor's response is a function of more than just one factor. Actually, two factors would compose the major part of response: free glucose concentration and ion concentration. It was already suggested that the number of ion channels increases with the aggressiveness of cancer cell[165,166]. If the pipette is immersed in an environment where the number of ions is big, its impedance will be low and consequently its potential will decrease.

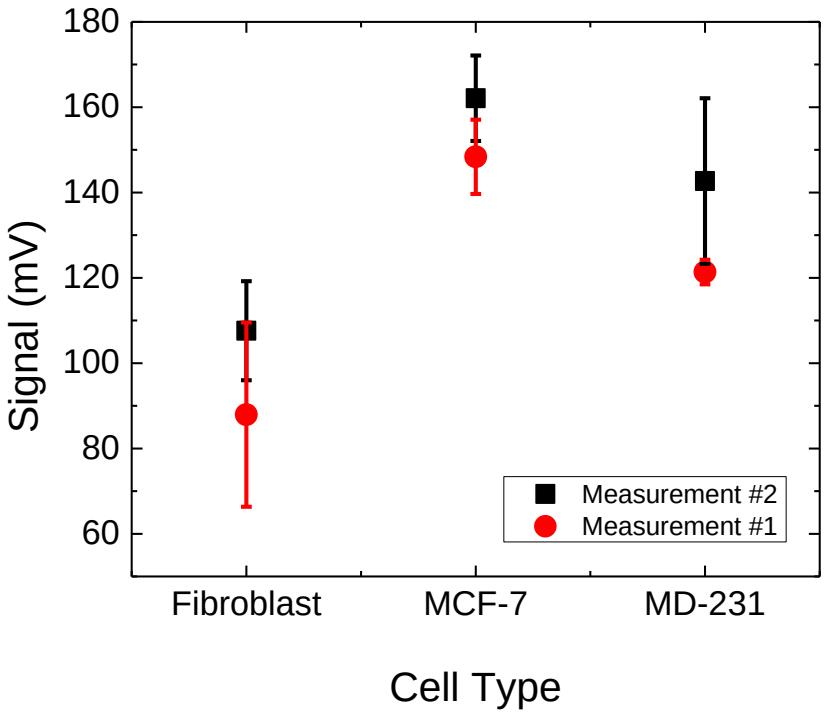

Figure 31 – Response of two different pipettes to the three different cell lines.

It is not trivial to quantitatively determine glucose concentration with a functionalized nanopipette due to production issues. It is very hard to reproduce exact same physical characteristics to different nanopipettes. Besides, even a little change in any physical parameter will have a big influence at the nanopipette response in the end. On the top of that, do not forget the biological differences between individual cells. Thus, is quite hard to establish a common reference value for all cells and nanopipettes.

An alternative suggestion for this issue is to compare signal variation for all cells and calibration curve. When in glucose free media (see Figure 30), all cell lines shown, approximately, same response. Once in normal media, same cells presented their own fluctuations. So, the system proposed here is as follows*: i) It is going to be made a percentage comparison between signals from cell of the same line in both media (normal and glucose free); ii) glucose free media is assumed to be the reference signal (0%).* In summary such variation represents how much, in percentage, signal for cells in normal media is different than signal for glucose free media. Following, the calibration curve shown in Figure 26 is shown in percentage variation instead of potential. The reference value of this curve (0%) is 0mM of glucose. The result of this analysis is shown in Figure 32.

In this figure, error bars represent the error progression to calculate each point. The curve is the fitting representation of a polynomial equation of second order. According to the signal and error bars, one can inquire, quantitatively, a range for free glucose concentration to each cell type. Thus, one can affirm that for fibroblasts the intracellular concentration of free glucose is a value between 0 and 2.8mM; for MCF-7 the sugar concentration is greater than 4.7 mM; for MDA-MB-231 the concentration is between 3.6 and 4.5 mM.

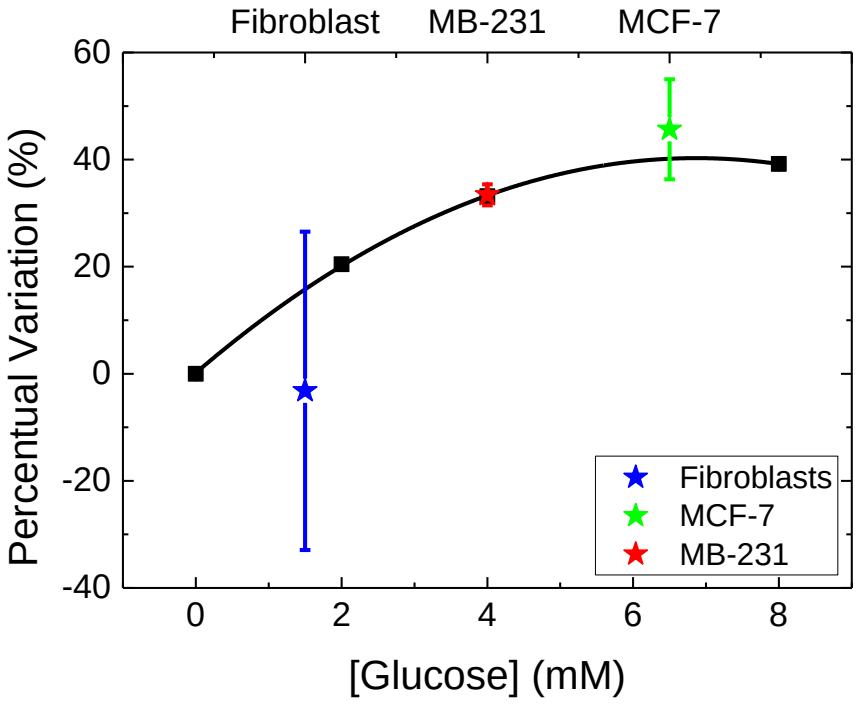

Figure 32 – Calibration Curve and Cell types' percentage variation

3.4 – Chapter Conclusion

In this chapter it was demonstrated the use of quartz glass nanopipettes for glucose detection. The glucose sensor was successfully applied to sense free glucose inside single cells. Its glucose sensing range is between 1mM and 8mM. Moreover, it was possible to distinguish different cell lines, two cancer cell lines and normal human Fibroblasts.

In an attempt to quantitatively differentiate the glucose concentration inside the cell lines, it was pointed a glucose concentration between 0 and 2.8mM for human Fibroblasts; concentration is greater than 4.7 mM for MCF-7; concentration is between 3.6 and 4.5 mM for MDA-MB-231.

Chapter 4 –

Conclusions

In chapter 2 was described micro/nano-structured biosensor based on an FTO conductive thin film substrate. These biosensors were built by an enzyme (glucose oxidase - GOx) immobilization. Two different methods for enzyme immobilization were described in the same chapter: one using glutaraldehyde (GTA) as immobilization molecule and another using chitosan immobilization matrix.

The biosensors were able to measure different glucose concentration on different ranges depending on the immobilization method adopted. The chitosan method presented a smaller range and smaller sensibility to glucose compared to the biosensors built by the GTA immobilization method. The main difference between the two sensors is the GOx immobilization technique: one used GTA and the other chitosan. The GTA glucose sensor presented a detection range between 3mM and 15mM of glucose in solution. The chitosan glucose sensor presented a detection range between 1mM and 5mM of glucose in solution.

Moreover, biosensors built by GTA method presented a range that includes the entire therapeutic range of human blood glucose concentration. Although chitosan sensors shown a smaller detection range, its range maybe could be used as future sensor intracellular glucose detection, once, as seen in chapter 3, intracellular glucose concentration seems to be always smaller 5mM.

Both extracellular biosensors shown good affinity with glucose as suggested by the K_m^{app} values (0.161 mM for chitosan and 0.157mM for GTA).

In the entire chapter 3, it was described a new nanopipette sensor capable of making intracellular glucose measurements. The sensor is small enough to keep the cell alive and viable during and after the experiments. The glucose sensor was successfully applied to sense free glucose inside single cells. Its glucose sensing range is between 1mM and 8mM. Moreover, it was possible to distinguish different cell lines, two cancer cell lines and normal human Fibroblasts.

Moreover, it was possible to detect significant differences in glucose concentration between normal and cancer cells and even assess the value of these concentrations. The found values are similar to previous values already published in

scientific literature (glucose concentration between 0 and 2.8mM for human Fibroblasts; concentration is greater than 4.7 mM for MCF-7; concentration is between 3.6 and 4.5 mM for MDA-MB-231).

Chapter 5 –

References

[1] S.M. Gapstur, P.H. Gann, W. Lowe, K. Liu, L. Colangelo, A. Dyer, Abnormal glucose metabolism and pancreatic cancer mortality, Jama-J. Am. Med. Assoc. 283 (2000) 2552–2558. doi:10.1001/jama.283.19.2552.

[2] L. Mosconi, Brain glucose metabolism in the early and specific diagnosis of Alzheimer's disease, Eur. J. Nucl. Med. Mol. Imaging. 32 (2005) 486–510. doi:10.1007/s00259-005-1762-7.

[3] J.N. Keller, Z. Pang, J.W. Geddes, J.G. Begley, A. Germeyer, G. Waeg, et al., Impairment of Glucose and Glutamate Transport and Induction of Mitochondrial Oxidative Stress and Dysfunction in Synaptosomes by Amyloid β-Peptide: Role of the Lipid Peroxidation Product 4-Hydroxynonenal, J. Neurochem. 69 (1997) 273–284. doi:10.1046/j.1471-4159.1997.69010273.x.

[4] R.E. Schoen, C.M. Tangen, L.H. Kuller, G.L. Burke, M. Cushman, R.P. Tracy, et al., Increased Blood Glucose and Insulin, Body Size, and Incident Colorectal Cancer, J. Natl. Cancer Inst. 91 (1999) 1147–1154. doi:10.1093/jnci/91.13.1147.

[5] S. Craft, G. Stennis Watson, Insulin and neurodegenerative disease: shared and specific mechanisms, Lancet Neurol. 3 (2004) 169–178. doi:10.1016/S1474-4422(04)00681-7.

[6] WHO | Raised fasting blood glucose, WHO. (n.d.). http://www.who.int/gho/ncd/risk_factors/blood_glucose_prevalence_text/en/ (accessed January 23, 2015).

[7] WHO | Diabetes, WHO. (n.d.). http://www.who.int/mediacentre/factsheets/fs312/en/ (accessed January 23, 2015).

[8] G.L. Semenza, Targeting HIF-1 for cancer therapy, Nat. Rev. Cancer. 3 (2003) 721–732. doi:10.1038/nrc1187.

[9] R.A. Gatenby, R.J. Gillies, Why do cancers have high aerobic glycolysis?, Nat. Rev. Cancer. 4 (2004) 891–899. doi:10.1038/nrc1478.

[10] R.J. DeBerardinis, J.J. Lum, G. Hatzivassiliou, C.B. Thompson, The biology of cancer: Metabolic reprogramming fuels cell growth and proliferation, Cell Metab. 7 (2008) 11–20. doi:10.1016/j.cmet.2007.10.002.

[11] R.J. Shaw, L.C. Cantley, Ras, PI(3)K and mTOR signalling controls tumour cell growth, Nature. 441 (2006) 424–430. doi:10.1038/nature04869.

[12] J. Wang, Glucose Biosensors: 40 Years of Advances and Challenges, Electroanalysis. 13 (2001) 983-988. doi: 10.1002/1521-4109(200108)13:12<983::AID-ELAN983>3.0.CO;2-

[13] P. Bergveld, Development of an Ion-Sensitive Solid-State Device for Neurophysiological Measurements, Ieee Trans. Biomed. Eng. BM17 (1970) 70–&. doi:10.1109/TBME.1970.4502688.

[14] P. Cobben, R. Egberink, J. Bomer, P. Bergveld, W. Verboom, D. Reinhoudt, Transduction of Selective Recognition of Heavy-Metal Ions by Chemically Modified Field-Effect Transistors (chemfets), J. Am. Chem. Soc. 114 (1992) 10573–10582. doi:10.1021/ja00052a063.

[15] L.T. Yin, J.C. Chou, W.Y. Chung, T.P. Sun, S.K. Hsiung, Separate structure extended gate H+-ion sensitive field effect transistor on a glass substrate, Sens. Actuators B-Chem. 71 (2000) 106–111. doi:10.1016/S0925-4005(00)00613-4.

[16] M.J. Schoning, A. Poghossian, Recent advances in biologically sensitive field-effect transistors (BioFETs), Analyst. 127 (2002) 1137–1151. doi:10.1039/b204444g.

[17] T. Matsuo, M. Esashi, Methods of Isfet Fabrication, Sens. Actuators. 1 (1981) 77–96. doi:10.1016/0250-6874(81)80006-6.
[18] J. van der spiegel, I. Lauks, P. Chan, D. Babic, The extended gate chemically sensitive field effect transistor as multi-species microprobe, Sens. Actuators. 4 (1983) 291–298. doi:10.1016/0250-6874(83)85035-5.
[19] L.L. Chi, J.C. Chou, W.Y. Chung, T.P. Sun, S.K. Hsiung, Study on extended gate field effect transistor with tin oxide sensing membrane, Mater. Chem. Phys. 63 (2000) 19–23. doi:10.1016/S0254-0584(99)00184-4.
[20] P.D. Batista, M. Mulato, ZnO extended-gate field-effect transistors as pH sensors, Appl. Phys. Lett. 87 (2005) 143508. doi:10.1063/1.2084319.
[21] P.D. Batista, M. Mulato, C.F. de O. Graeff, F.J.R. Fernandez, F. das C. Marques, SnO2 extended gate field-effect transistor as pH sensor, Braz. J. Phys. 36 (2006) 478–481. doi:10.1590/S0103-97332006000300066.
[22] E.M. Guerra, G.R. Silva, M. Mulato, Extended gate field effect transistor using V2O5 xerogel sensing membrane by sol–gel method, Solid State Sci. 11 (2009) 456–460. doi:10.1016/j.solidstatesciences.2008.07.014.
[23] E.M. Guerra, M. Mulato, Synthesis and characterization of vanadium oxide/hexadecylamine membrane and its application as pH-EGFET sensor, J. Sol-Gel Sci. Technol. 52 (2009) 315–320. doi:10.1007/s10971-009-2062-7.
[24] P.D. Batista, M. Mulato, Polycrystalline fluorine-doped tin oxide as sensoring thin film in EGFET pH sensor, J. Mater. Sci. 45 (2010) 5478–5481. doi:10.1007/s10853-010-4603-4.
[25] E.J. Guidelli, E.M. Guerra, M. Mulato, Ion sensing properties of vanadium/tungsten mixed oxides, Mater. Chem. Phys. 125 (2011) 833–837. doi:10.1016/j.matchemphys.2010.09.040.
[26] É.J. Guidelli, E.M. Guerra, M. Mulato, Vanadium and Titanium Mixed Oxide Films: Synthesis, Characterization and Application as Ion Sensor, J. Electrochem. Soc. 159 (2012) J217–J222. doi:10.1149/2.053206jes.
[27] E.J. Guidelli, E.M. Guerra, M. Mulato, V2O5/WO3 Mixed Oxide Films as pH-EGFET Sensor: Sequential Re-Usage and Fabrication Volume Analysis, Ecs J. Solid State Sci. Technol. 1 (2012) N39–N44. doi:10.1149/2.007203jss.
[28] M.P. da Silva, J.C. Fernandes, N.B. de Figueiredo, M. Congiu, M. Mulato, C.F. de O. Graeff, Melanin as an active layer in biosensors, AIP Adv. 4 (2014) 037120. doi:10.1063/1.4869638.
[29] N.C.S. Vieira, A. Figueiredo, A.D. Faceto, A.A.A. de Queiroz, V. Zucolotto, F.E.G. Guimarães, Dendrimers/TiO2 nanoparticles layer-by-layer films as extended gate FET for pH detection, Sens. Actuators B Chem. 169 (2012) 397–400. doi:10.1016/j.snb.2012.01.003.
[30] L.-T. Yin, J.-C. Chou, W.-Y. Chung, T.-P. Sun, K.-P. Hsiung, S.-K. Hsiung, Glucose ENFET doped with MnO2 powder, Sens. Actuators B Chem. 76 (2001) 187–192. doi:10.1016/S0925-4005(01)00629-3.
[31] J.-C. Chou, J.-L. Chiang, C.-L. Wu, pH and Procaine Sensing Characteristics of Extended-Gate Field-Effect Transistor Based on Indium Tin Oxide Glass, Jpn. J. Appl. Phys. 44 (2005) 4838. doi:10.1143/JJAP.44.4838.
[32] J.-C. Chou, J.-H. Li, T.-S. Lee, Preparation and Characteristics of Screen-Printed Calcium Ion Sensor, Biomed. Eng.-Appl. Basis Commun. 21 (2009) 381–384. doi:10.4015/S1016237209001490.

[33] N.C.S. Vieira, A. Figueiredo, A.A.A. de Queiroz, V. Zucolotto, F.E.G. Guimarães, Self-Assembled Films of Dendrimers and Metallophthalocyanines as FET-Based Glucose Biosensors, Sensors. 11 (2011) 9442–9449. doi:10.3390/s111009442.

[34] Y.-L. Chin, J.-C. Chou, Z.-C. Lei, T.-P. Sun, W.-Y. Chung, S.-K. Hsiung, Titanium Nitride Membrane Application to Extended Gate Field Effect Transistor pH Sensor Using VLSI Technology, Jpn. J. Appl. Phys. 40 (2001) 6311. doi:10.1143/JJAP.40.6311.

[35] C.-W. Pan, J.-C. Chou, I.-K. Kao, T.-P. Sun, S.-K. Hsiung, Using polypyrrole as the contrast pH detector to fabricate a whole solid-state pH sensing device, IEEE Sens. J. 3 (2003) 164–170. doi:10.1109/JSEN.2002.807300.

[36] N.C. Vieira, W. Avansi, A. Figueiredo, C. Ribeiro, V.R. Mastelaro, F.E. Guimarães, Ion-sensing properties of 1D vanadium pentoxide nanostructures, Nanoscale Res. Lett. 7 (2012) 310. doi:10.1186/1556-276X-7-310.

[37] L.-L. Chi, L.-T. Yin, J.-C. Chou, W.-Y. Chung, T.-P. Sun, K.-P. Hsiung, et al., Study on separative structure of EnFET to detect acetylcholine, Sens. Actuators B Chem. 71 (2000) 68–72. doi:10.1016/S0925-4005(00)00606-7.

[38] D. Welch, J.B. Christen, Real-time feedback control of pH within microfluidics using integrated sensing and actuation, Lab. Chip. 14 (2014) 1191–1197. doi:10.1039/C3LC51205C.

[39] N.C.S. Vieira, E.G.R. Fernandes, A.D. Faceto, V. Zucolotto, F.E.G. Guimarães, Nanostructured polyaniline thin films as pH sensing membranes in FET-based devices, Sens. Actuators B Chem. 160 (2011) 312–317. doi:10.1016/j.snb.2011.07.054.

[40] C.-P. Chen, A. Ganguly, C.-Y. Lu, T.-Y. Chen, C.-C. Kuo, R.-S. Chen, et al., Ultrasensitive in Situ Label-Free DNA Detection Using a GaN Nanowire-Based Extended-Gate Field-Effect-Transistor Sensor, Anal. Chem. 83 (2011) 1938–1943. doi:10.1021/ac102489y.

[41] T. Mikolajick, R. Kühnhold, H. Ryssel, The pH-sensing properties of tantalum pentoxide films fabricated by metal organic low pressure chemical vapor deposition, Sens. Actuators B Chem. 44 (1997) 262–267. doi:10.1016/S0925-4005(97)00166-4.

[42] T. Minami, T. Minamiki, Y. Hashima, D. Yokoyama, T. Sekine, K. Fukuda, et al., An extended-gate type organic field effect transistor functionalised by phenylboronic acid for saccharide detection in water, Chem. Commun. 50 (2014) 15613–15615. doi:10.1039/C4CC07498J.

[43] L. Maiolo, S. Mirabella, F. Maita, A. Alberti, A. Minotti, V. Strano, et al., Flexible pH sensors based on polysilicon thin film transistors and ZnO nanowalls, Appl. Phys. Lett. 105 (2014) 093501. doi:10.1063/1.4894805.

[44] T. Minamiki, T. Minami, R. Kurita, O. Niwa, S. Wakida, K. Fukuda, et al., A Label-Free Immunosensor for IgG Based on an Extended-Gate Type Organic Field Effect Transistor, Materials. 7 (2014) 6843–6852. doi:10.3390/ma7096843.

[45] C.-H. Hsieh, W.-C. Hung, P.-H. Chen, I.-Y. Huang, High-performance extended gate field-effect-transistor-based dissolved carbon dioxide sensing system with a packaged microreference electrode, J. Micro-Nanolithography Mems Moems. 13 (2014) 033017. doi:10.1117/1.JMM.13.3.033017.

[46] T. Minamiki, T. Minami, R. Kurita, O. Niwa, S. Wakida, K. Fukuda, et al., Accurate and reproducible detection of proteins in water using an extended-gate type

organic transistor biosensor, Appl. Phys. Lett. 104 (2014) 243703. doi:10.1063/1.4883739.

[47] T.K. Truong, T.N.T. Nguyen, T.Q. Trung, I.Y. Sohn, D.-J. Kim, J.-H. Jung, et al., Reduced graphene oxide field-effect transistor with indium tin oxide extended gate for proton sensing, Curr. Appl. Phys. 14 (2014) 738–743. doi:10.1016/j.cap.2014.03.007.

[48] C.-H. Kao, H. Chen, L.-T. Kuo, J.-C. Wang, Y.-T. Chen, Y.-C. Chu, et al., Multi-analyte biosensors on a CF4 plasma treated Nb2O5-based membrane with an extended gate field effect transistor structure, Sens. Actuators B Chem. 194 (2014) 419–426. doi:10.1016/j.snb.2013.12.056.

[49] C.H. Kao, H. Chen, C.-Y. Huang, Effects of Ti addition and annealing on high-k Gd2O3 sensing membranes on polycrystalline silicon for extended-gate field-effect transistor applications, Appl. Surf. Sci. 286 (2013) 328–333. doi:10.1016/j.apsusc.2013.09.080.

[50] T.-E. Bae, W.-J. Cho, Enhanced Sensing Properties of Fully Depleted Silicon-on-Insulator-Based Extended-Gate Field-Effect Transistor with Dual-Gate Operation, Appl. Phys. Express. 6 (2013) 127001. doi:10.7567/APEX.6.127001.

[51] H. Anan, M. Kamahori, Y. Ishige, K. Nakazato, Redox-potential sensor array based on extended-gate field-effect transistors with ω-ferrocenylalkanethiol-modified gold electrodes, Sens. Actuators B Chem. 187 (2013) 254–261. doi:10.1016/j.snb.2012.11.016.

[52] J.V. Pinto, R. Branquinho, P. Barquinha, E. Alves, R. Martins, E. Fortunato, Extended-Gate ISFETs Based on Sputtered Amorphous Oxides, J. Disp. Technol. 9 (2013) 729–734. doi:10.1109/JDT.2012.2227298.

[53] I.-Y. Huang, C.-H. Hsieh, W.-C. Chang, Development of a low-hysteresis and high-linearity extended gate field-effect transistor-based chloride ion-sensitive microsensor, J. Micro-Nanolithography Mems Moems. 12 (2013) 023016. doi:10.1117/1.JMM.12.2.023016.

[54] Z. Cao, Z.-L. Xiao, L. Zhang, D.-M. Luo, M. Kamahori, M. Shimoda, Molecule counting with alkanethiol and DNA immobilized on gold microplates for extended gate FET, Mater. Sci. Eng. C. 33 (2013) 1481–1490. doi:10.1016/j.msec.2012.12.050.

[55] T.N.T. Nguyen, Y.G. Seol, N.-E. Lee, Organic field-effect transistor with extended indium tin oxide gate structure for selective pH sensing, Org. Electron. 12 (2011) 1815–1821. doi:10.1016/j.orgel.2011.07.009.

[56] I. Kwon, H.-H. Lee, J. Choi, J.-K. Shin, S.-H. Seo, S.-W. Choi, et al., Extended-Gate Metal Oxide Semiconductor Field Effect Transistor-Based Biosensor for Detection of Deoxynivalenol, Jpn. J. Appl. Phys. 50 (2011) 06GL08. doi:10.1143/JJAP.50.06GL08.

[57] Y. Ishige, S. Takeda, M. Kamahori, Direct detection of enzyme-catalyzed products by FET sensor with ferrocene-modified electrode, Biosens. Bioelectron. 26 (2010) 1366–1372. doi:10.1016/j.bios.2010.07.053.

[58] P. Estrela, D. Paul, Q. Song, L.K.J. Stadler, L. Wang, E. Huq, et al., Label-Free Sub-picomolar Protein Detection with Field-Effect Transistors, Anal. Chem. 82 (2010) 3531–3536. doi:10.1021/ac902554v.

[59] Y. Ishige, M. Shimoda, M. Kamahori, Extended-gate FET-based enzyme sensor with ferrocenyl-alkanethiol modified gold sensing electrode, Biosens. Bioelectron. 24 (2009) 1096–1102. doi:10.1016/j.bios.2008.06.012.

[60] M. Kamahori, Y. Ishige, M. Shimoda, Detection of DNA hybridization and extension reactions by an extended-gate field-effect transistor: Characterizations of immobilized DNA–probes and role of applying a superimposed high-frequency voltage onto a reference electrode, Biosens. Bioelectron. 23 (2008) 1046–1054. doi:10.1016/j.bios.2007.10.013.

[61] M. Kamahori, Y. Ishige, M. Shimoda, Enzyme Immunoassay Using a Reusable Extended-gate Field-Effect-Transistor Sensor with a Ferrocenylalkanethiol-modified Gold Electrode, Anal. Sci. 24 (2008) 1073–1079. doi:10.2116/analsci.24.1073.

[62] M. Kamahori, Y. Ishige, M. Shimoda, A novel enzyme immunoassay based on potentiometric measurement of molecular adsorption events by an extended-gate field-effect transistor sensor, Biosens. Bioelectron. 22 (2007) 3080–3085. doi:10.1016/j.bios.2007.01.011.

[63] M. Kamahori, Y. Ishige, M. Shimoda, DNA Detection by an Extended-Gate FET Sensor with a High-Frequency Voltage Superimposed onto a Reference Electrode, Anal. Sci. 23 (2007) 75–79. doi:10.2116/analsci.23.75.

[64] D.-S. Kim, J.-E. Park, J.-K. Shin, P.K. Kim, G. Lim, S. Shoji, An extended gate FET-based biosensor integrated with a Si microfluidic channel for detection of protein complexes, Sens. Actuators B Chem. 117 (2006) 488–494. doi:10.1016/j.snb.2006.01.018.

[65] Y. Ishige, M. Shimoda, M. Kamahori, Immobilization of DNA Probes onto Gold Surface and its Application to Fully Electric Detection of DNA Hybridization using Field-Effect Transistor Sensor, Jpn. J. Appl. Phys. 45 (2006) 3776. doi:10.1143/JJAP.45.3776.

[66] J. Bausells, J. Carrabina, A. Errachid, A. Merlos, Ion-sensitive field-effect transistors fabricated in a commercial CMOS technology, Sens. Actuators B Chem. 57 (1999) 56–62. doi:10.1016/S0925-4005(99)00135-5.

[67] S.M. Sze, K.K. Ng, Physics of Semiconductor Devices, 3 edition, Wiley-Interscience, Hoboken, N.J, 2006.

[68] A.J. Bard, L.R. Faulkner, Electrochemical Methods: Fundamentals and Applications, 2nd Edition, Wiley, 2000.

[69] J.O. Bockris, A.K.N. Reddy, M.E. Gamboa-Aldeco, Modern Electrochemistry 2A: Fundamentals of Electrodics, 2nd edition, Springer, New York, 2001.

[70] H.D. Young, R.A. Freedman, University Physics with Modern Physics Technology Update Plus MasteringPhysics with eText -- Access Card Package, 13 edition, Addison-Wesley, 2013.

[71] C.-E. Lue, I.-S. Wang, C.-H. Huang, Y.-T. Shiao, H.-C. Wang, C.-M. Yang, et al., pH sensing reliability of flexible ITO/PET electrodes on EGFETs prepared by a roll-to-roll process, Microelectron. Reliab. 52 (2012) 1651–1654. doi:10.1016/j.microrel.2011.10.026.

[72] Y.-S. Chien, W.-L. Tsai, I.-C. Lee, J.-C. Chou, H.-C. Cheng, A Novel pH Sensor of Extended-Gate Field-Effect Transistors With Laser-Irradiated Carbon-Nanotube Network, IEEE Electron Device Lett. 33 (2012) 1622–1624. doi:10.1109/LED.2012.2213794.

[73] S.-Y. Yang, C.-W. Chen, J.-C. Chou, Investigation on the sensitivity of TiO2:Ru pH sensor by Taguchi design of experiment, Solid-State Electron. 77 (2012) 82–86. doi:10.1016/j.sse.2012.05.024.

[74] S.-P. Chang, C.-W. Li, K.-J. Chen, S.-J. Chang, C.-L. Hsu, T.-J. Hsueh, et al., ZnO-Nanowire-Based Extended-Gate Field-Effect-Transistor pH Sensors Prepared on Glass Substrate, Sci. Adv. Mater. 4 (2012) 1174–1178. doi:10.1166/sam.2012.1410.

[75] B.-R. Huang, J.-C. Lin, Y.-K. Yang, ZnO/Silicon Nanowire Hybrids Extended-Gate Field-Effect Transistors as pH Sensors, J. Electrochem. Soc. 160 (2013) B78–B82. doi:10.1149/2.110306jes.

[76] J.-L. Wang, P.-Y. Yang, T.-Y. Hsieh, C.-C. Hwang, M.-H. Juang, pH-Sensing Characteristics of Hydrothermal Al-Doped ZnO Nanostructures, J. Nanomater. 2013 (2013) e152079. doi:10.1155/2013/152079.

[77] H.-H. Li, C.-E. Yang, C.-C. Kei, C.-Y. Su, W.-S. Dai, J.-K. Tseng, et al., Coaxial-structured ZnO/silicon nanowires extended-gate field-effect transistor as pH sensor, Thin Solid Films. 529 (2013) 173–176. doi:10.1016/j.tsf.2012.05.045.

[78] J.-C. Lin, B.-R. Huang, Y.-K. Yang, IGZO nanoparticle-modified silicon nanowires as extended-gate field-effect transistor pH sensors, Sens. Actuators B Chem. 184 (2013) 27–32. doi:10.1016/j.snb.2013.04.060.

[79] W.-L. Tsai, B.-T. Huang, P.-Y. Yang, K.-Y. Wang, C. Hsiao, H.-C. Cheng, Oxygen Plasma Functionalized Multiwalled Carbon Nanotube Thin Film as A pH Sensing Membrane of Extended-Gate Field-Effect Transistor, IEEE Electron Device Lett. 34 (2013) 1307–1309. doi:10.1109/LED.2013.2278214.

[80] P.D. Batista, An embedded measurement system for the electrical characterization of EGFET as a pH sensor, Meas. Sci. Technol. 25 (2014) 027001. doi:10.1088/0957-0233/25/2/027001.

[81] A. Das, D.H. Ko, C.-H. Chen, L.-B. Chang, C.-S. Lai, F.-C. Chu, et al., Highly sensitive palladium oxide thin film extended gate FETs as pH sensor, Sens. Actuators B Chem. 205 (2014) 199–205. doi:10.1016/j.snb.2014.08.057.

[82] C.L. Li, B.R. Huang, S. Chattopadhyay, K.H. Chen, L.C. Chen, Amorphous boron carbon nitride as a pH sensor, Appl. Phys. Lett. 84 (2004) 2676–2678. doi:10.1063/1.1691195.

[83] J.-F. Hsu, B.-R. Huang, C.-S. Huang, H.-L. Chen, Silicon Nanowires as pH Sensor, Jpn. J. Appl. Phys. 44 (2005) 2626. doi:10.1143/JJAP.44.2626.

[84] E.G.R. Fernandes, N.C.S. Vieira, A.A.A. de Queiroz, F.E.G. Guimaraes, V. Zucolotto, Immobilization of Poly(propylene imine) Dendrimer/Nickel Phtalocyanine as Nanostructured Multilayer Films To Be Used as Gate Membranes for SEGFET pH Sensors, J. Phys. Chem. C. 114 (2010) 6478–6483. doi:10.1021/jp9106052.

[85] S.-P. Chang, T.-H. Yang, Sensing Performance of EGFET pH Sensors with CuO Nanowires Fabricated on Glass Substrate, Int. J. Electrochem. Sci. 7 (2012) 5020–5027.

[86] Y.-S. Chiu, C.-Y. Tseng, C.-T. Lee, Nanostructured EGFET pH Sensors With Surface-Passivated ZnO Thin-Film and Nanorod Array, IEEE Sens. J. 12 (2012) 930–934. doi:10.1109/JSEN.2011.2162317.

[87] P.-Y. Yang, J.-L. Wang, P.-C. Chiu, J.-C. Chou, C.-W. Chen, H.-H. Li, et al., pH Sensing Characteristics of Extended-Gate Field-Effect Transistor Based on Al-Doped ZnO Nanostructures Hydrothermally Synthesized at Low Temperatures, IEEE Electron Device Lett. 32 (2011) 1603–1605. doi:10.1109/LED.2011.2164230.

[88] B.-R. Huang, T.-C. Lin, Leaf-like carbon nanotube/nickel composite membrane extended-gate field-effect transistors as pH sensor, Appl. Phys. Lett. 99 (2011) 023108. doi:10.1063/1.3610554.
[89] L.-T. Yin, Y.-T. Lin, Y.-C. Leu, C.-Y. Hu, Enzyme immobilization on nitrocellulose film for pH-EGFET type biosensors, Sens. Actuators B Chem. 148 (2010) 207–213. doi:10.1016/j.snb.2010.04.042.
[90] J.-L. Lin, Y.-M. Chu, S.-H. Hsaio, Y.-L. Chin, T.-P. Sun, Structures of Anodized Aluminum Oxide Extended-Gate Field-Effect Transistors on pH Sensors, Jpn. J. Appl. Phys. 45 (2006) 7999. doi:10.1143/JJAP.45.7999.
[91] S.-P. Chang, K.-J. Chen, Beta-Gallium Oxide Nanowire Extended Gate Field Effect Transistor pH Sensors Prepared Using Furnace-Oxidized Gallium Nitride Thin Films, Nanosci. Nanotechnol. Lett. 6 (2014) 914–917. doi:10.1166/nnl.2014.1848.
[92] R.E.G. van Hal, J.C.T. Eijkel, P. Bergveld, A general model to describe the electrostatic potential at electrolyte oxide interfaces, Adv. Colloid Interface Sci. 69 (1996) 31–62. doi:10.1016/S0001-8686(96)00307-7.
[93] P. Bergveld, A. Sibbald, Analytical and Biomedical Applications of Ion-selective Field-effect Transistors, Elsevier, 1988.
[94] J.-Q. Wang, J.-C. Chou, T.-P. Sun, S.-K. Hsiung, G.-B. Hsiung, pH-based potentiometrical flow injection biosensor for urea, Sens. Actuators B Chem. 91 (2003) 5–10. doi:10.1016/S0925-4005(03)00160-6.
[95] J.-C. Chen, J.-C. Chou, T.-P. Sun, S.-K. Hsiung, Portable urea biosensor based on the extended-gate field effect transistor, Sens. Actuators B Chem. 91 (2003) 180–186. doi:10.1016/S0925-4005(03)00161-8.
[96] M.H. Asif, O. Nur, M. Willander, B. Danielsson, Selective calcium ion detection with functionalized ZnO nanorods-extended gate MOSFET, Biosens. Bioelectron. 24 (2009) 3379–3382. doi:10.1016/j.bios.2009.04.011.
[97] C.-P. Chen, A. Ganguly, C.-Y. Lu, T.-Y. Chen, C.-C. Kuo, R.-S. Chen, et al., Ultrasensitive in Situ Label-Free DNA Detection Using a GaN Nanowire-Based Extended-Gate Field-Effect-Transistor Sensor, Anal. Chem. 83 (2011) 1938–1943. doi:10.1021/ac102489y.
[98] A. Matsumoto, H. Matsumoto, Y. Maeda, Y. Miyahara, Simple and robust strategy for potentiometric detection of glucose using fluorinated phenylboronic acid self-assembled monolayer, Biochim. Biophys. Acta BBA - Gen. Subj. 1830 (2013) 4359–4364. doi:10.1016/j.bbagen.2013.03.004.
[99] T. Goda, Y. Miyahara, Detection of Microenvironmental Changes Induced by Protein Adsorption onto Self-Assembled Monolayers using an Extended Gate-Field Effect Transistor, Anal. Chem. 82 (2010) 1803–1810. doi:10.1021/ac902401y.
[100] C.-G. Ahn, A. Kim, C.W. Park, C.S. Ah, J.-H. Yang, T.-Y. Kim, et al., Modified ion sensitive field effect transistor sensors having an extended gate on a thick dielectric, Appl. Phys. Lett. 96 (2010) 203702. doi:10.1063/1.3431296.
[101] T. Goda, Y. Miyahara, Label-free and reagent-less protein biosensing using aptamer-modified extended-gate field-effect transistors, Biosens. Bioelectron. 45 (2013) 89–94. doi:10.1016/j.bios.2013.01.053.
[102] W. Guan, X. Duan, M.A. Reed, Highly specific and sensitive non-enzymatic determination of uric acid in serum and urine by extended gate field effect

transistor sensors, Biosens. Bioelectron. 51 (2014) 225–231. doi:10.1016/j.bios.2013.07.061.
[103] B. Cho, H.-H. Lee, J.-K. Shin, M. Murata, K. Ohuchida, M. Hashizume, DETECTION OF PANCREATIC CANCER CELLS (SUIT-2) USING AN FET-BASED BIOSENSOR WITH AN EXTENDED Au GATE, Biomed. Eng.-Appl. Basis Commun. 24 (2012) 131–137. doi:10.4015/S1016237212500196.
[104] T. Goda, Y. Miyahara, A hairpin DNA aptamer coupled with groove binders as a smart switch for a field-effect transistor biosensor, Biosens. Bioelectron. 32 (2012) 244–249. doi:10.1016/j.bios.2011.12.022.
[105] H.-Y. Hsu, C.-Y. Wu, H.-C. Lee, J.-L. Lin, Y.-L. Chin, T.-P. Sun, Sodium and Potassium Sensors Based on Separated Extended Gate Field Effect Transistor, Biomed. Eng.-Appl. Basis Commun. 21 (2009) 441–444. doi:10.4015/S1016237209001593.
[106] P.C. Yao, M.C. Lee, J.L. Chiang, Annealing Effect of Sol-Gel TiO2 Thin Film on pH-EGFET Sensor, in: 2014 Int. Symp. Comput. Consum. Control IS3C, 2014: pp. 577–580. doi:10.1109/IS3C.2014.157.
[107] D. s. Koktysh, X. Liang, B.-G. Yun, I. Pastoriza-Santos, R. l. Matts, M. Giersig, et al., Biomaterials by Design: Layer-By-Layer Assembled Ion-Selective and Biocompatible Films of TiO2 Nanoshells for Neurochemical Monitoring, Adv. Funct. Mater. 12 (2002) 255–265. doi:10.1002/1616-3028(20020418)12:4<255::AID-ADFM255>3.0.CO;2-1.
[108] Z. Li, R. Yang, M. Yu, F. Bai, C. Li, Z.L. Wang, Cellular Level Biocompatibility and Biosafety of ZnO Nanowires, J. Phys. Chem. C. 112 (2008) 20114–20117. doi:10.1021/jp808878p.
[109] R. Wu, X. Chen, J. Hu, Synthesis, characterization, and biosensing application of ZnO/SnO2 heterostructured nanomaterials, J. Solid State Electrochem. 16 (2012) 1975–1982. doi:10.1007/s10008-011-1590-6.
[110] R. He, L. Zhao, Y. Liu, N. Zhang, B. Cheng, Z. He, et al., Biocompatible TiO2 nanoparticle-based cell immunoassay for circulating tumor cells capture and identification from cancer patients, Biomed. Microdevices. 15 (2013) 617–626. doi:10.1007/s10544-013-9781-9.
[111] J.-M. Jang, S.-J. Park, G. Choi, T.-Y. Kwon, K.-H. Kim, Chemical state and ultra-fine structure analysis of biocompatible TiO2 nanotube-type oxide film formed on titanium substrate, Met. Mater. Int. 14 (2008) 457–463. doi:10.3365/met.mat.2008.08.457.
[112] Z. Cao, L.X. Sun, T. Zhou, Y.F. Luo, J.L. Zeng, S. Long, et al., Investigation on Electronic Signals for Detection of Target DNA Molecule Based on Extended Gate FET Sensing Chip, Adv. Mater. Res. 236-238 (2011) 1923–1926. doi:10.4028/www.scientific.net/AMR.236-238.1923.
[113] C.-H. Hsieh, P.-H. Chen, R.-H. Chen, I.-Y. Huang, Development of EGFET-based microsensors with high-sensitivity and high-linearity for dissolved oxygen and carbon dioxide detection, in: 2013 Transducers Eurosensors XXVII 17th Int. Conf. Solid-State Sens. Actuators Microsyst. TRANSDUCERS EUROSENSORS XXVII, 2013: pp. 2051–2054. doi:10.1109/Transducers.2013.6627202.
[114] D.-S. Kim, D.-I. Han, J.-E. Park, J.-K. Shin, P. Choi, J.-H. Lee, et al., An extended gate field effect transistor based protein sensor integrated with a Si micro-fluidic channel, in: 13th Int. Conf. Solid-State Sens. Actuators Microsyst. 2005

Dig. Tech. Pap. TRANSDUCERS 05, 2005: pp. 2011–2014 Vol. 2. doi:10.1109/SENSOR.2005.1497496.
[115] J.-C. Chou, C.-Y. Lin, Sensing Properties and Stability Analysis of Miniaturized Dual-Mode Uric Acid Biosensor Based on TiO2 Extended Gate Field Effect Transistor, Sens. Lett. 6 (2008) 929–932. doi:10.1166/sl.2008.532.
[116] C.-T. Lee, Y.-S. Chiu, S.-C. Ho, Y.-J. Lee, Investigation of a Photoelectrochemical Passivated ZnO-Based Glucose Biosensor, Sensors. 11 (2011) 4648–4655. doi:10.3390/s110504648.
[117] P.-Y. Lee, S.-P. Chang, P.-J. Kuo, E.-H. Hsu, S.-J. Chang, S.-C. Shei, Sensing Performance of EGFET pH Sensors with CZTSe Nanoparticles Fabricated on Glass Substrates, Int. J. Electrochem. Sci. 8 (2013) 3866–3875.
[118] L.-L. Chi, J.-C. Chou, W.-Y. Chung, T.-P. Sun, S.-K. Hsiung, Study on extended gate field effect transistor with tin oxide sensing membrane, Mater. Chem. Phys. 63 (2000) 19–23. doi:10.1016/S0254-0584(99)00184-4.
[119] B. Liu, R. Hu, J. Deng, Studies on a potentiometric urea biosensor based on an ammonia electrode and urease, immobilized on a γ-aluminum oxide matrix, Anal. Chim. Acta. 341 (1997) 161–169. doi:10.1016/S0003-2670(96)00553-3.
[120] S.M. Usman Ali, O. Nur, M. Willander, B. Danielsson, A fast and sensitive potentiometric glucose microsensor based on glucose oxidase coated ZnO nanowires grown on a thin silver wire, Sens. Actuators B Chem. 145 (2010) 869–874. doi:10.1016/j.snb.2009.12.072.
[121] H.H. Afify, R.S. Momtaz, W.A. Badawy, S.A. Nasser, Some physical properties of fluorine-doped SnO2 films prepared by spray pyrolysis, J. Mater. Sci. Mater. Electron. 2 (1991) 40–45. doi:10.1007/BF00695003.
[122] T. Minami, New n-Type Transparent Conducting Oxides, MRS Bull. 25 (2000) 38–44. doi:10.1557/mrs2000.149.
[123] R.G. Gordon, Criteria for Choosing Transparent Conductors, MRS Bull. 25 (2000) 52–57. doi:10.1557/mrs2000.151.
[124] J. Brophy, Basic Electronics for Scientists, 5th edition, McGraw-Hill Companies, New York, 1990.
[125] R. A. S. Nascimento, Análise dos procedimentos de medida de dispositivos EGFET, Ribeirão Preto – SP Brazil, 2010.
[126] A.D.A. 1701 N.B.S. Alex, ria, V. 22311 1-800-Diabetes, Checking Your Blood Glucose, Am. Diabetes Assoc. (n.d.). http://www.diabetes.org/living-with-diabetes/treatment-and-care/blood-glucose-control/checking-your-blood-glucose.html (accessed August 4, 2014).
[127] D.L. Nelson, M.M. Cox, Lehninger Principles of Biochemistry, Sixth Edition edition, W.H. Freeman, New York, 2012.
[128] J. Kiernan, Formaldehyde, formalin, paraformaldehyde and glutaraldehyde: What they are and what they do., Microsc. Today. 00-1 pp. 8-12 (2000). (n.d.). http://publish.uwo.ca/~jkiernan/formglut.htm (accessed May 28, 2015).
[129] I. Migneault, C. Dartiguenave, M.J. Bertrand, K.C. Waldron, Glutaraldehyde: behavior in aqueous solution, reaction with proteins, and application to enzyme crosslinking, Biotechniques. 37 (2004) 790–+.
[130] H. Wang, X. Wang, X. Zhang, X. Qin, Z. Zhao, Z. Miao, et al., A novel glucose biosensor based on the immobilization of glucose oxidase onto gold nanoparticles-modified Pb nanowires, Biosens. Bioelectron. 25 (2009) 142–146. doi:10.1016/j.bios.2009.06.022.

[131] C.-T. Lee, Y.-S. Chiu, Photoelectrochemical passivated ZnO-based nanorod structured glucose biosensors using gate-recessed AlGaN/GaN ion-sensitive field-effect-transistors, Sens. Actuators B Chem. 210 (2015) 756–761. doi:10.1016/j.snb.2015.01.042.
[132] F.R. Shu, G.S. Wilson, Rotating ring-disk enzyme electrode for surface catalysis studies, Anal. Chem. 48 (1976) 1679–1686. doi:10.1021/ac50006a014.
[133] Y. Zou, C. Xiang, L.-X. Sun, F. Xu, Glucose biosensor based on electrodeposition of platinum nanoparticles onto carbon nanotubes and immobilizing enzyme with chitosan-SiO2 sol–gel, Biosens. Bioelectron. 23 (2008) 1010–1016. doi:10.1016/j.bios.2007.10.009.
[134] X. Chu, D. Duan, G. Shen, R. Yu, Amperometric glucose biosensor based on electrodeposition of platinum nanoparticles onto covalently immobilized carbon nanotube electrode, Talanta. 71 (2007) 2040–2047. doi:10.1016/j.talanta.2006.09.013.
[135] G.K. Kouassi, J. Irudayaraj, G. McCarty, Activity of glucose oxidase functionalized onto magnetic nanoparticles, Biomagn. Res. Technol. 3 (2005) 1. doi:10.1186/1477-044X-3-1.
[136] J. Qi, H. Zhang, Z. Ji, M. Xu, Y. Zhang, ZnO nano-array-based EGFET biosensor for glucose detection, Appl. Phys. A. 119 (2015) 807–811. doi:10.1007/s00339-015-9122-3.
[137] J.W. Park, C. Lee, J. Jang, High-performance field-effect transistor-type glucose biosensor based on nanohybrids of carboxylated polypyrrole nanotube wrapped graphene sheet transducer, Sens. Actuators B Chem. 208 (2015) 532–537. doi:10.1016/j.snb.2014.11.085.
[138] O.P. Hamill, A. Marty, E. Neher, B. Sakmann, F.J. Sigworth, Improved patch-clamp techniques for high-resolution current recording from cells and cell-free membrane patches, Pflüg. Arch. Eur. J. Physiol. 391 (1981) 85–100.
[139] D. Klenerman, Y. Korchev, Potential biomedical applications of the scanned nanopipette, Nanomed. 1 (2006) 107–114. doi:10.2217/17435889.1.1.107.
[140] C.-C. Chen, Y. Zhou, L.A. Baker, Scanning Ion Conductance Microscopy, Annu. Rev. Anal. Chem. 5 (2012) 207–228. doi:10.1146/annurev-anchem-062011-143203.
[141] L. Ying, A. Bruckbauer, D. Zhou, J. Gorelik, A. Shevchuk, M. Lab, et al., The scanned nanopipette: a new tool for high resolution bioimaging and controlled deposition of biomolecules, Phys. Chem. Chem. Phys. PCCP. 7 (2005) 2859–2866. doi:10.1039/b506743j.
[142] W. Li, N.A.W. Bell, S. Hernández-Ainsa, V.V. Thacker, A.M. Thackray, R. Bujdoso, et al., Single Protein Molecule Detection by Glass Nanopores, ACS Nano. 7 (2013) 4129–4134. doi:10.1021/nn4004567.
[143] B. Vilozny, A.L. Wollenberg, P. Actis, D. Hwang, B. Singaram, N. Pourmand, Carbohydrate-actuated nanofluidic diode: switchable current rectification in a nanopipette, Nanoscale. 5 (2013) 9214–9221. doi:10.1039/C3NR02105J.
[144] M. Karhanek, J.T. Kemp, N. Pourmand, R.W. Davis, C.D. Webb, Single DNA Molecule Detection Using Nanopipettes and Nanoparticles, Nano Lett. 5 (2005) 403–407. doi:10.1021/nl0480464.
[145] P. Actis, M.M. Maalouf, H.J. Kim, A. Lohith, B. Vilozny, R.A. Seger, et al., Compartmental Genomics in Living Cells Revealed by Single-Cell Nanobiopsy, ACS Nano. 8 (2014) 546–553. doi:10.1021/nn405097u.

[146] S.E. Anderson, H.H. Bau, Electrical detection of cellular penetration during microinjection with carbon nanopipettes, Nanotechnology. 25 (2014) 245102. doi:10.1088/0957-4484/25/24/245102.
[147] F.M. Matschinsky, Glucokinase as Glucose Sensor and Metabolic Signal Generator in Pancreatic β-Cells and Hepatocytes, Diabetes. 39 (1990) 647–652. doi:10.2337/diab.39.6.647.
[148] L.-C. Jiang, W.-D. Zhang, A highly sensitive nonenzymatic glucose sensor based on CuO nanoparticles-modified carbon nanotube electrode, Biosens. Bioelectron. 25 (2010) 1402–1407. doi:10.1016/j.bios.2009.10.038.
[149] F. Teng, X. Wang, C. Shen, S. Li, A micro glucose sensor based on direct prototyping mesoporous carbon electrode, Microsyst. Technol. (2014) 1–7. doi:10.1007/s00542-014-2159-y.
[150] L.-M. Lu, L. Zhang, F.-L. Qu, H.-X. Lu, X.-B. Zhang, Z.-S. Wu, et al., A nano-Ni based ultrasensitive nonenzymatic electrochemical sensor for glucose: Enhancing sensitivity through a nanowire array strategy, Biosens. Bioelectron. 25 (2009) 218–223. doi:10.1016/j.bios.2009.06.041.
[151] S.G. Ansari, Z.A. Ansari, R. Wahab, Y.-S. Kim, G. Khang, H.-S. Shin, Glucose sensor based on nano-baskets of tin oxide templated in porous alumina by plasma enhanced CVD, Biosens. Bioelectron. 23 (2008) 1838–1842. doi:10.1016/j.bios.2008.02.022.
[152] S. Zhao, Y.-B. Zheng, S.-L. Cai, Y.-H. Weng, S.-H. Cao, J.-L. Yang, et al., Sugar-stimulated robust nanodevice: 4-Carboxyphenylboronic acid modified single glass conical nanopores, Electrochem. Commun. 36 (2013) 71–74. doi:10.1016/j.elecom.2013.09.009.
[153] J. Liu, D. Wang, M. Kvetny, W. Brown, Y. Li, G. Wang, Quantification of Steady-State Ion Transport through Single Conical Nanopores and a Nonuniform Distribution of Surface Charges, Langmuir. 29 (2013) 8743–8752. doi:10.1021/la4009009.
[154] S. Umehara, N. Pourmand, C.D. Webb, R.W. Davis, K. Yasuda, M. Karhanek, Current Rectification with Poly-l-Lysine-Coated Quartz Nanopipettes, Nano Lett. 6 (2006) 2486–2492. doi:10.1021/nl061681k.
[155] W. de Koning, K. van Dam, A method for the determination of changes of glycolytic metabolites in yeast on a subsecond time scale using extraction at neutral pH, Anal. Biochem. 204 (1992) 118–123. doi:10.1016/0003-2697(92)90149-2.
[156] L. Zhang, F. Su, S. Buizer, X. Kong, F. Lee, K. Day, et al., A polymer-based ratiometric intracellular glucose sensor, Chem. Commun. 50 (2014) 6920. doi:10.1039/c4cc01110d.
[157] M. Rizzi, U. Theobald, E. Querfurth, T. Rohrhirsch, M. Baltes, M. Reuss, In vivo investigations of glucose transport in Saccharomyces cerevisiae, Biotechnol. Bioeng. 49 (1996) 316–327. doi:10.1002/(SICI)1097-0290(19960205)49:3<316::AID-BIT10>3.0.CO;2-C.
[158] M. Neves, J. Francois, On the Mechanism by Which a Heat-Shock Induces Trehalose Accumulation in Saccharomyces-Cerevisiae, Biochem. J. 288 (1992) 859–864.
[159] D. Clifton, R.B. Walsh, D.G. Fraenkel, Functional studies of yeast glucokinase., J. Bacteriol. 175 (1993) 3289–3294.

[160] B. Teusink, J.A. Diderich, H.V. Westerhoff, K. van Dam, M.C. Walsh, Intracellular Glucose Concentration in Derepressed Yeast Cells Consuming Glucose Is High Enough To Reduce the Glucose Transport Rate by 50%, J. Bacteriol. 180 (1998) 556–562.
[161] A. Behjousiar, C. Kontoravdi, K.M. Polizzi, In Situ Monitoring of Intracellular Glucose and Glutamine in CHO Cell Culture, PLoS ONE. 7 (2012) e34512. doi:10.1371/journal.pone.0034512.
[162] G.G. Guilbault, M. Nanjo, A phosphate-selective electrode based on immobilized alkaline phosphatase and glucose oxidase, Anal. Chim. Acta. 78 (1975) 69–80. doi:10.1016/S0003-2670(01)84753-X.
[163] A.S.G. Huggett, D.A. Nixon, USE OF GLUCOSE OXIDASE, PEROXIDASE, AND O-DIANISIDINE IN DETERMINATION OF BLOOD AND URINARY GLUCOSE, The Lancet. 270 (1957) 368–370. doi:10.1016/S0140-6736(57)92595-3.
[164] J. Wilson, T. Hunt, Molecular Biology of the Cell, Fifth Edition: The Problems Book, 5 edition, Garland Science, New York, 2007.
[165] K. Kunzelmann, Ion Channels and Cancer, J. Membr. Biol. 205 (2005) 159–173. doi:10.1007/s00232-005-0781-4.
[166] K. Kunzelmann, Thematic issue: Ion channels and cancer, J. Membr. Biol. 205 (2005) 113–114. doi:10.1007/s00232-005-0775-2.
[167] Protein Data Bank in Europe.
https://www.ebi.ac.uk/pdbe/entry/pdb/1cf3/analysis (Accessed in August 2015)
[168] Otsukaa, I., Yaoitab, M., Nagashimac, S., Higanod, M., Molecular dimensions of dried glucose oxidase on a Au(1 1 1) surface studied by dynamic mode scanning force microscopy. Electrochimica Acta, 50, 25–26, (2005), 4861–4867.

Appendices I –

Chemical Structures

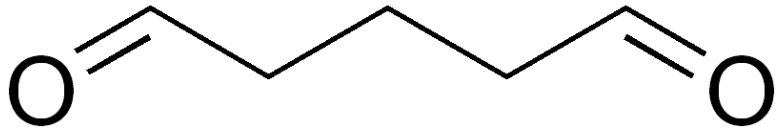

Figure 33 – GTA Molecule – *Glutaraldehyde*

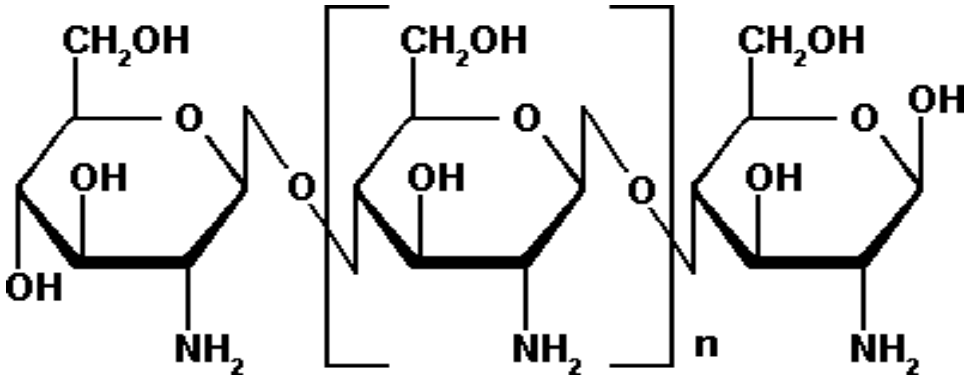

Figure 34 – Chitosan molecule

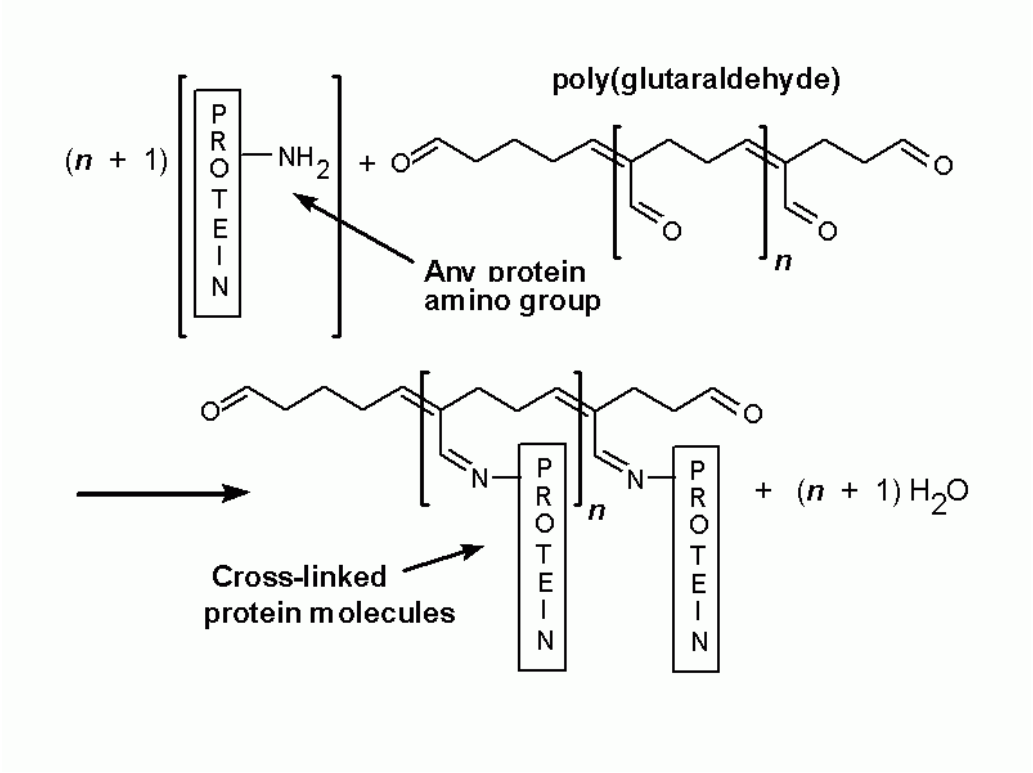

Figure 35 – Peptide bound between poly-glutaraldehyde and lysine group. [128]

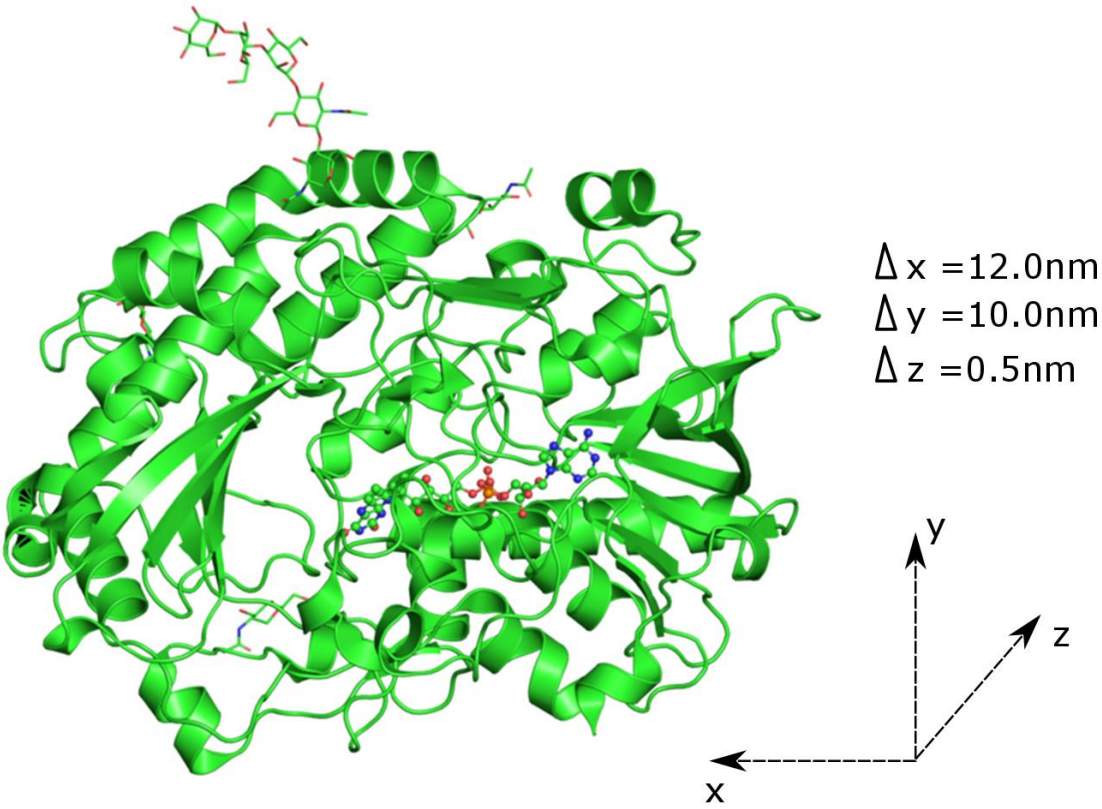

Figure 36 – Glucose Oxidase 3D-structure and size: 0.5 x 12.0 x 10.0 nm. [167, 168]